The Pennsylvania State University

The Graduate School

Department of Aerospace Engineering

REDUCING TRAILING EDGE FLAP DEFLECTION REQUIREMENTS IN PRIMARY CONTROL THROUGH A MOVEABLE HORIZONTAL TAIL

A Thesis in

Aerospace Engineering

by

James Edward Bluman

Submitted in Partial Fulfillment
of the Requirements
for the Degree of

Master of Science

May 2008

The thesis of James Edward Bluman was reviewed and approved* by the following:

Farhan S. Gandhi
Professor of Aerospace Engineering
Thesis Advisor

Edward C. Smith
Professor of Aerospace Engineering

George A. Lesieutre
Professor of Aerospace Engineering
Head of the Department of Aerospace Engineering

*Signatures are on file in the Graduate School

ABSTRACT

Achieving primary control of helicopters through the use of trailing edge flaps holds significant promise in eliminating the swashplate and related controls—a system that is complex, heavy, a significant source of drag, and subject to demanding maintenance requirements. However, the predicted deflections that trailing edge flaps serving in this role must reach to achieve high speed trimmed flight are currently beyond the stroke and authority of current smart-material actuators that could be used. A method of reducing the required trailing edge flap deflections through fixed frame moments input via a moveable horizontal tail is developed and demonstrated to significantly reduce the required trailing edge flap deflections on a UH-60 helicopter.

Expanding on previous work which demonstrated the ability to reduce cyclic pitch requirements in high speed flight through moveable horizontal tail inputs, this study presents a 2-DOF flap-torsion rigid blade trim analysis utilizing linear inflow and advanced UH-60 rotor and fuselage geometry in conjunction with the moveable tail. Parametric studies are performed on the effect of blade root torsional stiffness and rotor blade pitch indexing on the required flap deflections. A moveable horizontal tail is added and demonstrated to reduced required cyclic elevon deflections on a UH-60 with non-dimensional rotating natural frequency (ν_θ) of 2.1 and pitch index (θ_{Pre}) of 20° at a forward speed of 130 knots ($\mu = 0.3$) to deflections with the capability of current actuators (±5°) without prohibitive vehicle attitude and performance penalties.

TABLE OF CONTENTS

LIST OF FIGURES

LIST OF TABLES

LIST OF SYMBOLS

A	main rotor area\
A_{ht}	horizontal tail planform area
D_f	fuselage drag force
D_{ht}	drag on the horizontal tail
$F_{X(HT)}$	Force exerted along the body x-axis by the horizontal tail
$F_{Y(N)}$	Force exerted along the body y-axis by helicopter subsystem "N"
I_θ	sectional moment of inertia about the blade pitch axis
I_x	inertial flap-pitch coupling
I_f	total blade moment of inertia about the blade axis (integrated spanwise)
I_f^*	total blade moment of inertia, non-dimensionalized with respect to I_β
I_x^*	inertial flap-pitch coupling, non-dimensionalized with respect to I_β
I_β	blade flapping moment of inertia
I_{cg}	blade moment of inertia about the blade center of gravity
J	Jacobian matrix
L_f	fuselage lift force
L_{ht}	lift on the horizontal tail
M_x	rotor roll moment (roll left is positive)
M_y	rotor pitch moment (pitch up is positive)
M_β	total blade flapping moment due to aerodynamic forces
M_θ	total blade pitching moment due to aerodynamic forces
M_ζ	total blade lagging moment due to aerodynamic forces
Q	rotor torque

R	Rotor Radius
S_{ht}	Span of horizontal tail
T	rotor thrust
T_{tr}	tail rotor thrust
$T_{1...15}$	Theodorsen Geometric Functions for quasi-steady analysis
TEE	Trailing Edge Elevon
TEF	Trailing Edge Flap (equivalent to TEE)
W	Aircraft weight
X	rotor drag force (oriented toward the tail)
Y	rotor side force (oriented out the right door)

a	blade section lift curve slope
b	semi-chord length
c	chord length
d	distance of quarter chord behind the pitch axis
dr	differential spanwise displacement
c_p	power coefficient
c_t	thrust coefficient
c_q	torque coefficient
c_d	blade section drag coefficient
c_l	blade section lift coefficient
$c_{L\alpha}$	Lift curve slope of the blade section
$c_{L\delta}$	Lift curve slope of the TEF

c_m blade section pitching moment coefficient

e flap and lag hinge offset distance

x_{cg}, y_{cg}, z_{cg} Location of CG with respect to the hub

x_{tr}, y_{tr}, z_{tr} Location of the tail rotor with respect to the hub

x_{ht}, y_{ht}, z_{ht} Location of the horizontal tail with respect to the hub

x_i, y_i, z_i axes of inertial frame

x_h, y_h, z_h hub axes

x_a non-dimensional distance from the blade mid-chord to the pitch axis

x_c non-dimensional distance from the blade mid-chord to the TEF hinge

Δ increment in lift, moment or drag due to TEE deflection

$\Delta\delta_{TOT}$ TEF deflection envelope

$\vec{\theta}$ vector of control inputς

Ω rotor rotational velocity

α blade section angle of attack

α_{wl} fuselage angle of attack (nose down is positive)

α_{Sx} shaft incidence angle (forward tilt is positive)

β blade flapping, alternatively Glauert's compressibility factor

β_0 blade coning angle

β_{1c} longitudinal flapping angle

β_{1s} lateral flapping angle

ψ azimuth position

δ	trailing edge flap deflection
δ_{MAX}	maximum deflection the TEF must make over all airspeeds
δ_0	trailing edge flap collective deflection
δ_1	amplitude of one-per-revolution trailing edge flap deflection
δ_{1c}	trailing edge flap lateral deflection
δ_{1s}	trailing edge flap longitudinal deflection
ε_{coll}	Horizontal Tail Collective Inputs
ε_{diff}	Horizontal Tail Differential Inputs
φ_f	fuselage roll angle (positive roll right)
φ_{TR}	tail rotor cant angle
γ	lock number
γ_{TR}	tail rotor cant angle
η_{ht}	horizontal tail offset angle between the freestream and the body axis
κ	induced power coefficient
λ	main rotor inflow (non-dimensional)
λ_{tr}	tail rotor inflow (non-dimensional)
μ	advance ratio
ρ	air density
σ	rotor solidity
θ	blade geometric pitch angle
θ_0	blade collective pitch
θ_{1c}	blade lateral cyclic pitch
θ_{1s}	blade longitudinal cyclic pitch

θ_{tr}	tail rotor collection pitch
θ_{tw}	blade twist rate
θ_{75}	blade pitch at 75% radial location on the blade
ω	rotational velocity
ξ_ζ	blade lagging damp ratio
ξ_θ	blade pitch damp ratio
χ	main rotor wake skew angle used to calculate linear inflow distribution
χ_{ht}	free stream angle on the horizontal tail modified by main rotor wake
υ_θ	blade pitch natural frequency (non-dimensional in per revolution)
υ_β	blade flapping natural frequency (non-dimensional in per revolution)
υ_ζ	blade flapping natural frequency (non-dimensional in per revolution)
ζ	blade lagging angle

$()^*$	derivative with respect to azimuth (ψ)
$()^{\cdot}$	derivative with respect to time (t)

ACKNOWLEDGEMENTS

Many thanks are in order as I consider all of the great men and women who have helped me along the way. First I would like to thank my advisor, Dr. Gandhi, for his pivotal role in my entire graduate education thus far. His ideas and enthusiasm first attracted me to the idea of pursuing a degree associated with rotorcraft, and his mentorship and guidance through both coursework and research has been outstanding. I appreciate his patience with my many questions and the significant leeway he gave me in exploring various topics throughout the project. I would also like to thank Dr. Smith for his critical input at several key points in this effort as well as his leadership of the Center.

I would like to thank many of the other researchers who helped me via phone call or by providing just the right resource at the right time. The assistance of Dr. Yeo and Dr. Datta was extremely helpful, and I appreciate Jaye Falls' input and discussion on the various topics that we are both grappling with. I also want to thank many of my fellow students at Penn State who have helped me tremendously: Jason Steiner, James Erwin, Chris Duling, Eui Sung Bae, and Olivier Leon. I don't know what I would have done without you guys, and I wish you all the best in the future.

Lastly, I would like to thank my wife, Kelly, and my boys, Daniel and Joshua, for excelling in the most important things in life, and for putting up with some odd work hours. You make it all worth it.

"What shall it profit a man that he should gain the whole world and yet forfeit his soul?" --Jesus of Nazareth

Chapter 1

Introduction

Helicopters have secured their niche in the worldwide aviation community due to their undeniable usefulness in a wide variety of roles. Their unique ability to land vertically from both improved and unimproved landing surfaces and to fly from hover to in excess of 150 knots has ensured their continued use for the foreseeable future. However, due to their inherent complexity, helicopter development has always been somewhat slower than that of fixed-wing aircraft. In particular, the method of primary control for helicopters has changed little since its first utilization by helicopter pioneers in the 1930s [1, 2].

Helicopter control is provided by tilting the rotor via a swashplate-based system which transfers pilot input from the non-rotating frame to the rotating frame where the rotor blades produce thrust and control forces. This system of push-pull rods, hydraulic boost, and rotating components has been reliably used for the last 60 years. Nonetheless, it has several drawbacks. This flight-critical system is subject to high maintenance requirements since it experiences large cyclic loading. Additionally, it is a source of significant aerodynamic drag and weight. If the swashplate and its associated controls could be replaced by a more efficient system, these deficiencies could be reduced or eliminated. The rotating frame control technique with the most apparent potential is the trailing edge flap. In this design, flap deflections would provide the necessary pitch

control on the blade to control the helicopter. These flaps can also serve in other functions such as vibration or noise control.

In the last ten years, several researchers have focused on how to achieve primary control of rotorcraft via trailing edge flaps in the rotating frame (Figure 1-1). Although the general concept has been demonstrated to be feasible, research to date indicates that the deflections and moments required of trailing edge flaps exceed either the stroke or authority of current smart-material actuators that are small enough to fit inside an airfoil. Since a mechanism has yet to be discovered that would reduce the required deflections to the acceptable levels, other options need to be explored. The purpose of this study is to determine to what extent inputting forces and moments in the fixed frame via horizontal tail inputs is able to reduce the required flap deflections to a suitable level. Of note, since various researchers have adopted different terminology for this topic, both "trailing edge flaps (TEFs)" and "trailing edge elevons (TEEs)" will be used interchangeably in this study.

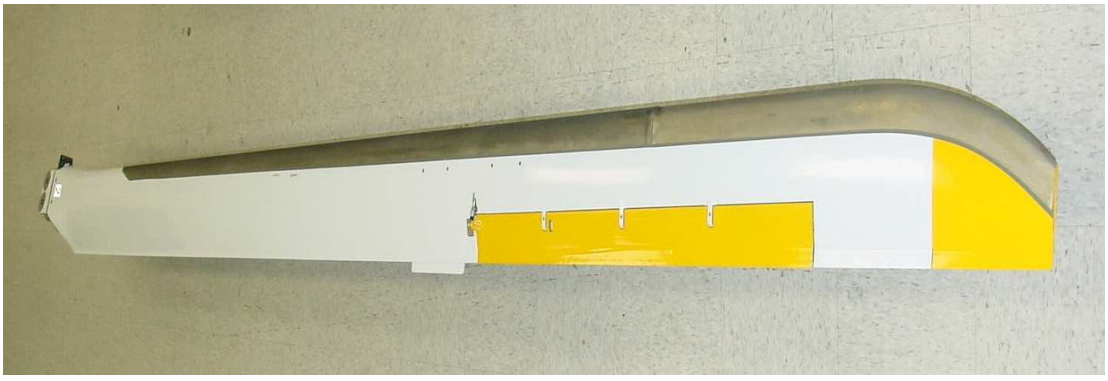

Figure 1-1: Trailing Edge Flap System Developed by Boeing [3]

1.1 Background and Motivation

1.1.1 Swashplate Control Technology

Helicopter control is achieved by tilting the thrust of the main rotor and by applying a net force and moment on the helicopter through collective and cyclic control of the rotor blade pitch. Currently, almost all helicopters in service utilize a swashplate and pitch links in order to provide this cyclic and collective pitch variation to the blade roots. The swashplate moves up and down as a unit in order to apply collective pitch to the blades (increasing or decreasing the pitch on all the blades simultaneously). When the pilot applies directional cyclic, the swashplate system tilts. The upper swashplate rotates on the lower, stationary swashplate in this tilted orientation and provides cyclically varying pitch commands to the blade root via a highly rigid pitch-change link at a rate of once-per-revolution (1/rev).

This system, although robust, has experienced only incremental development since its first implementation in the 1930s. Hydraulics have been added and often automated flight control systems are placed in the loop to provide improved handling qualities, but virtually the only means of controlling the blade pitch across the industry has been via the swashplate. This system includes multiple mechanical linkages that transfer pilot cyclic and collective inputs under the seats, up onto the roof, through hydraulic boost to the swashplate. The swashplate itself consists of rotating and non-rotating plates which must rotate on their interface at cyclic rates of 5-10 Hz while carrying heavy loads (Figure 1-2). Since this system is the only means of controlling the

aircraft, it is critical to flight safety. A structural failure of any of the mechanical components would almost certainly lead to a crash, and in most heavy aircraft, the failure of the hydraulic system would also cause the helicopter to crash.

1.1.2 Shortcomings in the Swashplate System.

Because large cyclically varying loads are developed each time a blade passes through the varied aerodynamic environment that exists in a rotor in translational flight, these loads are carried by the blade and passed to the hub and pitch links. As such, all of the components in the swashplate system must withstand high cyclic loads. The entire system requires frequent inspections and heavy maintenance, and most of the components are subject to strict component-change requirements to prevent fatigue failures. Additionally, after any maintenance on the rotor system, the entire system must be inspected, placed in track and balance, and checked for proper autorotational RPM [4]. These maintenance requirements contribute significantly to the operating cost and logistical burden of the helicopter.

In addition to the maintenance issues inherent in swashplate designs, the standard control system requires heavy, bulky components that contribute to overall vehicle weight and drag. Most of the hydraulic systems reside on the cabin roof under a fairing, which increases the flat plate drag of the fuselage. The exposed rotating linkages and their associated blunt bodies cause flow separation in forward flight and are a large source of parasite drag at high airspeed (Figure 1-2).

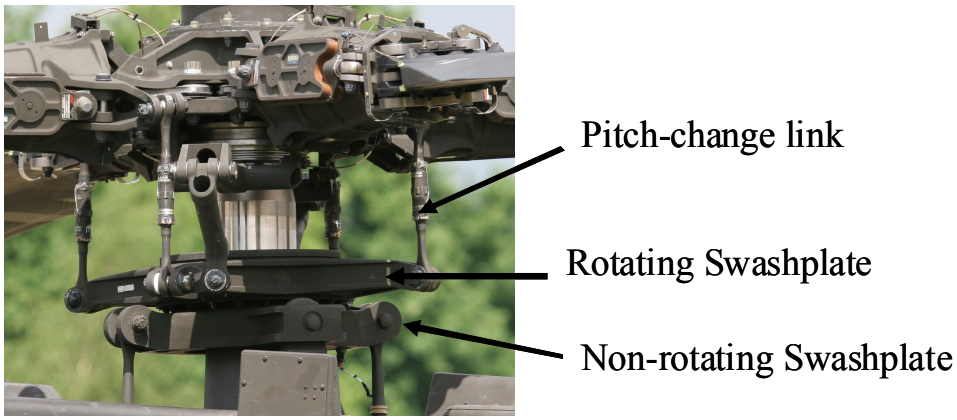

Figure 1-2: Swashplate and Linkages [5]

Finally, applying higher harmonic control or individual blade control technology to a swashplate requires adding new parts to the system and increasing its complexity. Placing such inputs into the rotating frame has been shown to be an effective technique to reduce vibratory cyclic blade and hub loads [6, 7]. These techniques promise to increase the service life of blades and control linkages, as well as reduce the overall vibrations that are transferred to the fuselage. Trailing edge flaps that are actuated by smart-material actuators, however, require no additional hardware to implement either IBC or HHC techniques since these inputs can easily be superimposed on top of the 1/rev inputs required fro primary control.

1.1.3 Advantages of Trailing Edge Flaps

The most obvious advantage of eliminating the swashplate in favor of rotating frame controls such as trailing edge flaps is the immediate realization of weight savings, drag penalty, and maintenance costs. If all of the push-pull rods, gears, hydraulic hoses,

pumps, filters, and servos, swashplates, and pitch-change links could be eliminated, the weight savings would result in a higher payload capability for any given design. If all of these components were removed, they would not need to be inspected, lubricated, replaced, and serviced. The number of parts and tools required to support each airframe would be reduced. Naturally, some of these will be offset by the size, weight, and service requirements of a TEE system, but it is expected that the TEE systems would have significant advantage in each of these areas: it should much lighter, require reduced control loads, have improved parasite drag characteristics, and should require fewer parts to inspect, lubricate, and replace.

Many of these advantages arise from the fact that the trailing edge elevons are acting in the rotating frame in a region of high dynamic pressure. As such, they do not need to resist the large forces and moments that the blade must produce to control the helicopter. On the contrary, TEFs function elegantly by harnessing these forces and moments to control blade pitch. As such, they are not affected by the same scaling difficulties of standard swashplate systems. Finally, their ability to introduce higher harmonic inputs into the rotating frame promises to reduce many main rotor vibrations at the source—further eliminating the need for heavy control systems required to carry these kinds of loads.

1.1.4 **Problems with Trailing Edge Elevons**

Of course, if trailing edge elevons didn't have their drawbacks, they would already be in use. First, cyclically controlling blade pitch in the rotating frame requires

actuators that can fit inside a rotor blade and actuate at rates of 5-10 Hz for one-per-revolution primary control (and multiples of that for higher harmonic control). Although smart-material actuators are in development to this end, their stroke and authority is not yet sufficient for primary control applications. Additionally, the TEE design requires the torsional softening of the rotor at a root spring so that the blade is responsive to control inputs. The baseline torsional stiffness of most rotors have dimensionless rotating natural frequencies (ν_θ) with values ranging from just under 4 per revolution (/rev) to more than 5/rev. Several studies have demonstrated the requirement of TEE rotors to have a torsional frequency of approximately 2/rev [8, 9]. But this torsional compliance allows the blade to be responsive to transients and the naturally higher harmonic forcing that exists in forward flight.

In addition to these problems, the practical challenges of transferring power and signals to the rotating frame remain significant. The reliability of the system is a serious concern as is the system's response to a failure. The aerodynamic effect of actuating flaps on an airfoil designed to undergo both pitching and plunging in a time-varying freestream is non-trivial. Stall and stability boundaries may exist that are not fully understood, and it is expected that these boundaries will be significantly influenced by the magnitude of the trailing edge flap deflections required. Finally, although a power savings is expected concerning the flow separation around the mast and hub, the fact that trailing edge elevons are now deflecting into a high dynamic pressure free-stream implies that the design will have a its own power disadvantages, the magnitude of which are an important area of on-going research.

1.1.5 Reducing Trailing Edge Flap Demands by Horizontal Tail Inputs

Clearly, the concept of trailing edge flaps for primary control has many potential advantages, but it also has significant practical and theoretical concerns as outlined in the preceding paragraphs. The introduction of forces and moments in the fixed frame through a moveable horizontal tail can beneficially affect each one of the problems listed above. Although not very useful at low speeds, as airspeed increases, collective and differential inputs to the horizontal tail will yield significant pitching and rolling moments on the airframe. These moments can be used to alleviate the moments that the rotor must develop through blade flapping, and by extension, the magnitude of the trailing edge flap deflections. If a proper tail control angle is chosen, the horizontal tail, should be able to pitch the entire airframe forward enough to provide the propulsive force from the rotor to fly in high speed translational flight. It may be possible to reduce the deflections required of the TEEs to levels that even currently existing actuators are capable of delivering. Additionally, reducing the TEE deflections should relieve blade/elevon stall concerns, manifest stability and power savings, and possibly afford rotors with less torsional softness.

1.2 Literature Survey

Achieving primary helicopter control through the use of trailing edge elevons constitutes an enormous departure from the long-standing and well-established methods of controlling rotor thrust through a swashplate. Any time such an ambitious change to the status quo is undertaken, many different issues must be addressed. This survey will

consider some of the critical modeling and design issues, and report on the current state of technology.

1.2.1 Primary Control through Trailing Edge Flaps

1.2.1.1 Servo-flap Control Technique from Kaman Aerospace

Although interest in primary control through trailing edge elevons has been elevated in the last ten years, one company has utilized a very similar concept for blade pitch control for the last 50 years on all of their production helicopter models. The Kaman corporation's servo-flap concept has proven itself on a number of different aircraft designs including the SH-2 Seasprite (Figure 1-3) which has been in service with the US Navy since 1967 and the K-1200 K-MAX synchropter which received FAA certification in 1994.

Figure 1-3: Kaman's SH-2G Seasprite Helicopter [10]

The servo-flap concept is based on the same physical principles as the trailing edge elevons—namely that an aerodynamic surface controls the blade pitch by imparting a pitching moment to a blade mounted on a torsionally soft hub. Although Kaman helicopters still incorporate a swashplate, they are only required to move the push-pull rod assemblies that control the servo flap, and as such, they are much smaller and lighter than conventional swashplate systems. The servo-flap system rotors also use most of the same design elements that will be required and incorporated into the TEE rotor. The application of each of these features on Kaman's rotors provides a good introduction to their utilization on the TEE rotor. These include pre-pitch, reduced torsional stiffness, size and location of the flap or elevon, and blade response coupling.

In lieu of a rigid pitch-change link connected to the blade, Kaman utilizes a soft root torsional spring. The low torsional stiffness of their root spring restraint allows the blade the significant angular freedom of movement about the root spring that is required to trim and control the helicopter. This stiffness is typically measured in non-dimensional rotating natural frequency, ν_θ (expressed in per-revolutions or /rev), which is primarily a combination of the structural stiffness of the root restraint and the tendency of the propeller moment to force the pitch to zero. Although conventional helicopters' ν_θ are almost always 3.5/rev and higher, Kaman's designs use a ν_θ of 1.3 to 1.5. This softness results in significantly lower control forces because the rotor is controlled by a technique that takes advantage of the large aerodynamic forces near the blade tips instead of having to overcome them (as in the case of conventional swashplate systems) [11]. Another advantage is the blade's increased pitch response makes it more apt to vibration reduction strategies. In fact, all Kaman production helicopters contain an active blade

tracking system which virtually eliminates 1/rev vibrations [12]. One disadvantage of torsionally soft systems is their sensitivity to blade response coupling and potential for aeroelastic instability. Kaman has designed a novel system of mass and stiffness tuning in order to alleviate the detrimental coupling effects and yet retain beneficial coupling [10].

Kaman has designed several unique features into their rotors in order to account for the unique design considerations that a torsionally soft system entails. Since most high-performance airfoils have nose down aerodynamic pitching moments, Kaman pre-pitches their blades from as high as 27° (on the SH-2) to as low as 5° (on the K-MAX). Additionally, Kaman engineers utilize negative pitch-flap (δ_3) coupling in order to enhance rotor flapping for a given pitch input. Their pitch flap coupling is reported to be as high as -37° [12].

All Kaman helicopters position their servo-flaps at the .75R position on the blade. This places them in a region of high enough dynamic pressure so they can develop the necessary pitching moments. Additionally, since the servo-flap is located well behind the trailing edge of the blade (Figure 1-4), the servo-flaps produce 40% more control moment on the blade than if they were embedded in the blade's cross section. And the servo-flap span is typically between 12.5% and 15.8% of the blade span [10]. This relatively small size keeps the control forces low and prevents the inevitable elastic blade bending to have an adverse effect on the structure of the servo flap.

Figure 1-4: Size and Structure of Kaman's Servo-flap Design [10]

Since Kaman's servo-flaps utilize the same mechanism for rotor control through trailing edge flaps, it is worthwhile to elaborate the concept fully at this juncture. In short, the blade pitch is controlled by adjusting the flap angle of attack with respect to the blade. If one starts with a pre-pitched blade and then deflects the flap down (positive δ since the nose is up) a negative pitching moment is produced, which causes the blade to rotate (or twist) nose down against the root restraint. This occurs in both a cyclic and collective sense. As such, with increasing airspeed, one would expect to see an increase in collective flap pitch (imparting a decreasing collective blade pitch) up to the maximum endurance airspeed, and then a steady decrease in collective flap pitch (δ_0) to allow the blade to increase its pitch to the higher values needed for high speed flight. For cyclically controlled blade pitch, the same concept is applied. In forward flight, where lower blade pitch is required on the advancing side and high pitch on the retreating side, the flap is deflected to a large positive value on the advancing side (impelling the blade as a whole to a lower value), and the flap is deflected to it lowest (most negative) value on the retreating side (allowing the blade to return to a higher pitch required for the lower

dynamic pressure on the retreating side). These same physical principles transfer directly to the consideration of trailing edge elevons embedded in the blade cross section.

1.2.1.2 Primary Control Through Embedded Trailing Edge Flaps

The first comprehensive analysis of a primary control mechanism via trailing edge flaps to appear in the published literature was conducted by Shen and Chopra [8, 13, 14, 15, 16, 17, 18, 19]. Their analysis included trim analysis, stability analysis, quasi-steady aerodynamics for the flap and unsteady aerodynamics for the rotor blades, actuator dynamics, as well as maneuvering and autorotation performance. Shen also included a higher harmonic input in order to reduce vibrations [19].

The largest differences between Shen and the work by Kaman are the fact that Shen's rotor uses a TEF embedded in the profile of the blade section and the fact that Shen's TEFs were intended to be operated by a smart material actuator such as a piezo-electric bender instead of the mechanical linkages that are used on Kaman designs. Trailing edge flaps contained within the blade profile present much less drag than external servo-flaps; however, they are also not able to produce as large a pitching moment. Shen performed his analysis on the Boeing MDART rotor, and validated his results against both experimental data from Boeing and CAMRAD II analysis from NASA [13].

Shen adopted the Theodorsen-Garrick formulation [16] for the quasi-steady lift, moment, and hinge moment produced by the trailing edge flaps, and he incorporated UMARC's Leishman-Beddoes unsteady aerodynamic scheme in order to calculate the

aerodynamic forces and moments. He successfully trimmed his MDART rotor through μ=.35 (145 knots) using an aerodynamically balanced flap (Figure 1-5) to reduce the required hinge moment [8].

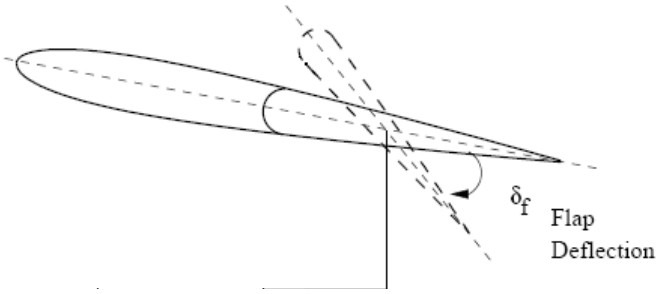

Figure 1-5: Aerodynamically Balanced Flap from Shen [19]

Utilizing the robust capability of UMARC to include flexible blades and free wake analysis, the bulk of Shen's work consisted of a series of parametric studies to identify the optimal configuration with respect to flap hinge moment and flap control authority [18]. As was demonstrated by Orimston [9], a TEE chord of .25 gives the maximum possible Δc_m. However, there is a "plateau region" around .25 chord that allows one to reduce the size of the elevon in order to reduce the actuation power without losing much control authority. In fact, Shen recommends a chord ratio of 0.2 as the optimal compromise between authority and power. The span-wise placement and length of the TEE are also important in maximizing the control authority while minimizing power. As the TEE increases in size from 9%-18% R, the required deflection to rotate the blade understandably decreases. Beyond, 18% however, the deflection decrease is much smaller, and the associated profile power and weight penalties with a larger elevon begin to become significant. Shen also recommends placing the TEE as close to the tip

as possible in order to take advantage of the high dynamic pressure. This will reduce elevon deflections, and keep the TEE actuation power relatively constant [19].

The two most important design parameters that Shen identified were the blade pre-pitch and the blade root spring stiffness (Figure 1-6) [18]. Proper selection of these values can dramatically reduce the TEE deflections that are required to trim the rotor, with an absolute minimum TEE deflection achieved with a pitch index of 14° and $\mu = .2$. However, the blade pitch index angle exhibits different optimum values based on airspeed so a compromise needs to be made in order to accommodate a range of advance ratios. For most practical applications, Shen recommends 16-18°of pre-pitch to allow for more efficient operation at higher speeds [17].

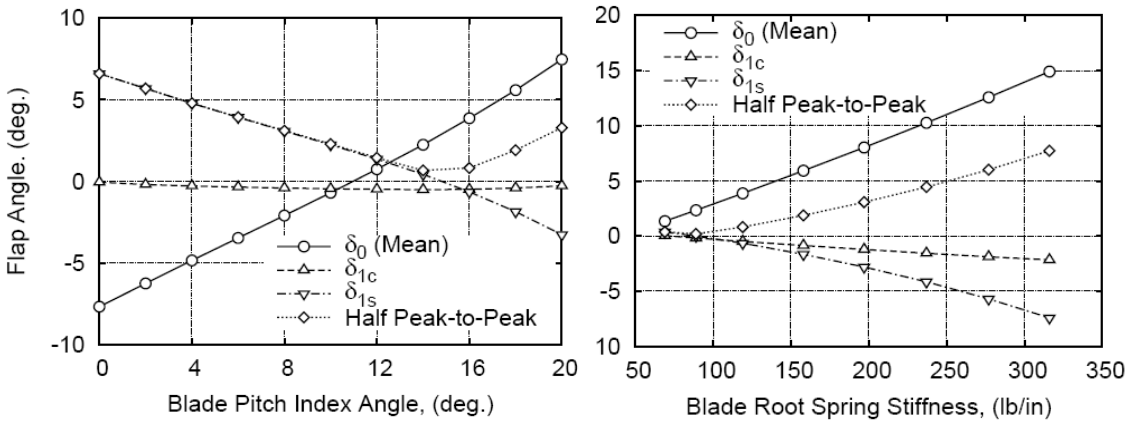

Figure 1-6: Effect of Blade Pitch Index and Root Spring Stiffness on δ at μ=0.20 [8]

However, this value is directly affected by the root spring stiffness. In Shen's study, the minimum torsional natural frequency (tied directly to root spring stiffness) was 1.8 per rev. He discovered, not surprisingly, that this value resulted in the smallest TEE deflections necessary but also commonly uses a value of 2.1 in his analysis [8]. His parametric studies indicated that the optimum arrangement of pitch index, flap size, and

location are summarized in Table 1-1 bases on [18] yielding deflection requirements per Table 1-2 which appears below.

Table 1-1: Optimal Flap Properties for Hinge Moment and Control Authority

Pitch Index	18°	*for μ = .35
	14°	*for μ = .2
Chord-wise size	20%	chord
Length (Spanwise)	18%	Radius
ν_θ	1.8	/rev

Despite all his efforts, Shen's designs [15] still require TEEs to have a deflection range in excess of 15° which is beyond the capability of current smart actuators with hinge moments approaching 2 ft-lbs for trim and 3 ft-lbs for maneuvering flight [14].

Table 1-2: Required TEF Deflections by Pitch Index and Airspeed, MDART

	θ_{Pre} = 16°					θ_{Pre} = 18°			
	δ_0	δ_1	max	min		δ_0	δ_1	max	min
μ = .15	4.8°	1°	5.8°	3.8°	μ = .15	5°	1.5°	6.5°	3.5°
μ = .35	-4°	6°	2°	-10°	μ = .35	-3°	4°	1°	-7°
total deflection req'd across the flight envelope			5.8°	-10°	total deflection req'd across the flight envelope			6.5°	-7°

The next significant body of work to appear in the literature concerning trailing edge flaps as primary control devices was produced by Jaye Falls. Her initial work involved placing tabs on the end of the flap in an attempt to reduce the forces required to actuate the control surfaces [20]. She conducted extensive parametric studies on her flap-tab configurations, and identified an optimal configuration that allowed for trimmed flight in a UH-60 at 155 knots with tab deflections of -5 ±5°. She also conducted

baseline flap-only analyses on the UH-60. Adopting the Theodorsen-Garrick aerodynamic model of the trailing edge flap, she implemented a flap with a chord of 15%, a radial span of 40%, an index angle of 15°, and a torsional frequency of ν_θ=1.992. Using this configuration, she achieved propulsive trim at 155 knots, but with a flap deflection of -15±15° [21]. These results clearly lie well outside the capability of current actuators, and may lie outside the predictive capability of thin airfoil theory upon which Theodorsen-Garrick models are based.

However, one of Falls' more significant contributions to date is the cataloging of various flap drag estimate techniques. Starting with data compiled experimentally on symmetric airfoils in low Reynolds number flows, she published a drag expression that properly predicts the decrement in drag produced by flap deflections that are opposite the airfoil angle of attack in the form of Eq. 1.1 [21].

$$c_d = d_0 + d_2(\alpha+\delta)^2 \qquad 1.1$$

She then refined this result through the inclusion of experimental data on asymmetric airfoil sections in use on modern helicopters (HH-06 and HH-10 airfoils in use on the AH-64 Apache and MDART rotors) at a Mach number of 0.6. Since data on other modern airfoil-flap combinations of interest is so limited, she added CFD analysis to generate her own lift, drag, and moment tables for airfoil-flap combinations like the SC1095 in use on the UH-60. After achieving good correlation between experimental and CFD results for known data sets, she obtained empirical relations that described the drag increment particular to each airfoil. One notable result from this analysis was the fact that the d_0 and d_2 coefficient listed above are remarkably different for each airfoil.

Additionally, the stall point at which the drag increases dramatically is different on different airfoils (4° on the HH-06 and 14° on the SC1095R8 airfoil) [22].

Falls also performed several analyses into the power penalties associated with using trailing edge flaps for primary control. Using her preliminary findings for drag, she predicted an increase in drag due to TEFs equivalent to a flat plate area of 5 square feet for TEFs with a span of .40R and 8 square feet with TEFs of .30%R, the increase due to the larger TEF deflections required with a smaller flap [21]. However, after incorporating the CFD-backed lookup tables, Falls saw a 33% rise in rotor power (compared to baseline swashplated rotor) power as well as trim difficulty at speeds greater than $\mu = .32$. She also experienced significant variations in the amount of flap deflection required based on the inflow models used (linear vs. free wake) [22]. Her work emphasizes the importance of properly predicting the lift, drag, and moment increments available to the flap through CFD. Her work also highlights the large TEF deflections that are required at high speed flight, and her CFD analysis demonstrates the fact that large TEF deflections not only require large actuation power and moments, but they make the blade-flap prone to stall. A summary of her flap configurations and trim controls appears in Table 1-3.

Table 1-3: TEF Configurations and Deflection Requirements as Developed by Falls

Study	Falls 2007*	Falls 2008**
TEF type	plain	plain
Aircraft	UH-60	UH-60
TEF chord length	.15c	.15c
TEF span	.4R	.4R
TEF midpoint location	.75R	.75R
ν_θ	1.9 /rev	1.92 /rev
Pitch index	15°	15°
μ	0.3	0.3
δ_0	~-10°	-7.5°
δ_1 (hpp)	~10°	6.5°

* Theodorsen-Garrick model used for TEFs
**CFD-based tables used for TEFs; free wake

Recognizing the importance of keeping profile power penalties to a minimum in swashplateless rotors, Ormiston presented a study that demonstrated that the elevon's primary role is in pitching the blade rather than directly changing sectional lift. He also examined torsional frequency, pitch indexing, and elevon size and location. His analysis, based on quasi-steady thin airfoil theory, concluded that torsional frequencies in the neighborhood of 2/rev and chord-wise lengths of .25c provided the high level of pitch response needed in a swashplateless design. Figure 1-7 demonstrates the effect of chord-wise length on the pitching moment and lift coefficients generated by the elevon [9].

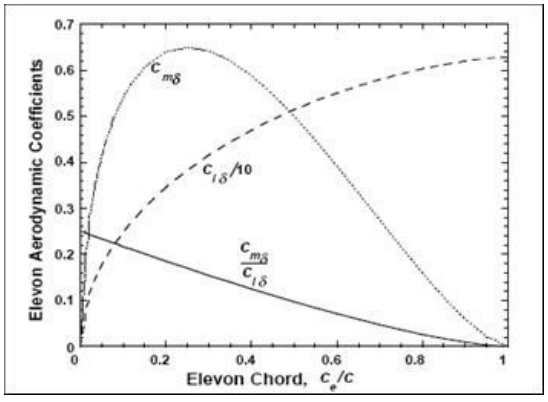

Figure 1-7: TEF Aerodynamic Coefficients Relative to Chord-wise Size [9]

1.2.2 Capabilities of Current Actuators

The actuators that allow for primary control through TEEs need to be reliable, large stroke, high authority, and capable of responding at rates up 10 Hz. Most of the smart material actuators under consideration fall into one of two categories: piezo-electric benders and piezo-electric linear stack actuators. Piezo-electric benders (Figure 1-8) generally do not produce enough force for full-scale rotors, but have been successful in relieving vibrations during TEE wind tunnel tests since they are able to respond with up to 5° deflections at up to 40 Hz as long as the deflecting surface is on the order of 1-5 inches [23].

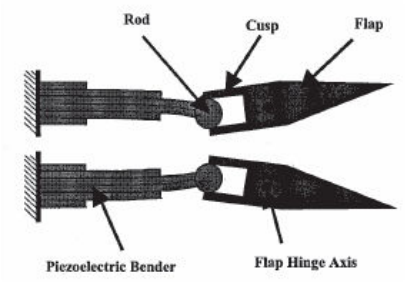

Figure 1-8: Piezo-electric Bender Designed by Koratkar [23]

Piezo stack actuators typically provide much larger forces, but very limited stroke and therefore require some sort of amplification device. Various amplification schemes have been developed. Researchers at Boeing, using a double X-frame amplification device, constructed and tested a full scale MDART rotor with trailing edge flaps and achieve deflections of ±3.5° [24, 25]. Eurocopter built a full scale BK-117 ADASYS rotor with trailing edge flaps and tested it in wind tunnels and flight tests as well, having achieved controlled deflections of a 11% span flap of ±5° [26, 27]. Szefi developed a

novel buckling beam actuation mechanism, presented in Figure 1-9, which achieved up to 6.23° of elevon defection at 20 Hz rate of actuation while producing a moment of 22.43 in-lbs. Analysis indicates that a full-scale version of this device would be able to deflect a 36" elevon 4° while producing 57.6 in-lbs of moment [28]. Although each of these achievements is notable, they all fall short of the deflection requirements for primary control set forth by Shen and Falls.

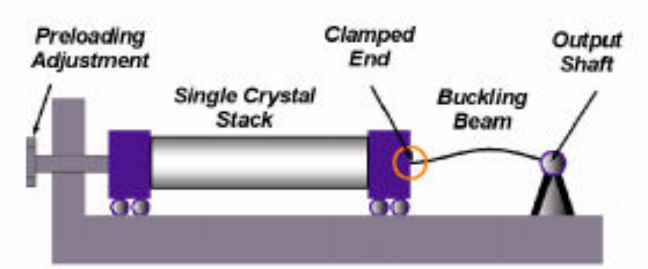

Figure 1-9: Buckling Beam Actuation Device Developed by Szefi [28]

1.2.3 Vibration Reduction Through Trailing Edge Flaps

One of the ancillary benefits of a swashplateless rotor with smart actuators is the ability to use the elevons for more than simply primary control. The most attractive and promising of these roles is that of vibration reduction, and a host of both analytical and experimental studies has been conducted to that end [6, 19, 27, 29, 30, 31, 32, 33]. Reducing these vibrations is important for many reasons--ride comfort for passengers and reduced fatigue wear on the rotor blade, hub, control system, and fuselage. However, all of the vibration reduction strategies to date have utilized two separate systems; a swashplate is used for control inputs and a separate actuator is used for vibration-

reduction inputs. The elegance of using TEFs in primary control is that the same actuators may be used for both primary control and vibration reduction, as Shen and Chopra have already suggested in their analytical studies [15].

1.2.4 Modeling Techniques of the Trailing Edge Flap

The many studies that exist to date on trailing edge flaps each incorporate a slightly different aerodynamic model. Reviewing these differences is useful in demonstrating the range of modeling options available, as well as in choosing the most effective means of modeling for primary control application. Ideally, an aerodynamic model will be able to accurately predict lift, drag, and pitching moment and incorporate the physical effects brought on by compressibility, unsteady aerodynamic effects, and flow separation.

Preliminary treatment of aerodynamically modeling flaps in an unsteady aerodynamic environment was accomplished by Theodorsen [34]. Theodorsen extended the basic thin airfoil theory result in to include unsteady effects. His work included trailing edge flaps and was based on the frequency domain which requires purely sinusoidal motion of the aerodynamic surfaces. He then extended his work to consider aerodynamic balance and flap-tab combinations [35]. However, direct application of Theodorsen's theory to rotorcraft is difficult at best due to the variation in reduced frequency with respect to both ψ and radial position. Additionally, Theodorsen's theory cannot predict drag, separation or compressibility effects. As such, most researchers who choose to employ Theodorsen's results for flapped airfoils modify these results with

experimental values and for compressibility with the standard Glauert factor applied to both C_l, C_m, and C_d [38]. In an extension of Theodorsen's work, Greenberg [36] added a pulsating free stream velocity to the pitching and plunging airfoil analysis by retaining the velocity time derivative terms (which Theodorsen sets to zero) for application to a helicopter rotor. Millott used Greenberg's theory and applied it to a flapped airfoil, enabling its use in rotors with TEEs [28]. His work enables Theodorsen's methodology to be more readily applied to the helicopter rotor, but it is still unable to model compressibility, stall, and drag.

Other researchers have attempted to deal with the shortcomings of some of the classical theories outlined above. Leishman's work in the indicial time domain can capture non-oscillatory motion of both flaps and airfoils, transients due to wind gusts, and can resolve very brief aerodynamic phenomena. As such, these approaches are particularly suited to analyze rotorcraft noise and compressibility effects. Hariharan's primary contribution to the analysis of TEEs is in the treatment of compressible unsteady flow around airfoils with elevons [37]. However, his work is still unsuited to time-varying freestream phenomena. Jose and Baeder have advanced the indicial technique to include time-varying freestream velocities, but they have not yet considered flapped airfoils in this sense [38]. They did, however, demonstrate that for steady-state analyses, time-domain methods are not required because all transients are damped within five system oscillations. Finally, Myrtle and Friedmann [39] developed a rational function approximation of the time-varying freestream, compressible, unsteady loads on a flapped airfoil using Laplace transform methods and correlating the result with experimental data.

Analyses that involve vibration reduction require advanced treatment of unsteady aerodynamics in order to capture lift attenuation and phasing, especially since TEFs designed for vibration reduction actuate at N_b and $N_b \pm 1$ /rev. However, all of the studies conducted to date involving primary control through TEEs (Ormiston, Shen, and Falls) have utilized Theodorsen's quasi-steady theory for the flap and discount the unsteady lift deficiency and phasing effects. In order to properly account for compressibility, drag and separation in these analyses, however, some reliance on experimental data has been appropriate. In summary, although Shen utilized some values of c_l and c_m from experimental data sets, he did not consider drag. On the other hand, Falls' incorporation of CFD-based c_l, c_d, and c_m should account for compressibility and flow separation in her analysis.

1.2.5 Alternative Forms of Swashplateless Control

Although much work has been done on swashplateless control through trailing edge flaps, other researchers have presented alternative forms of helicopter control without the use of a swashplate. Sekula and Gandhi [40] utilized horizontal tail incidence control to reduce rotor cyclic pitch and blade flapping on both a UH-60 and BO-105. They showed that cyclic pitch requirements could be reduced to less than .5° for airspeeds above $\mu = .15$ on a UH-60, albeit at the expense of somewhat large nose down aircraft attitudes (~6.5°).

In a parallel study, Yoshizaki and Gandhi [41] demonstrated swashplateless control of a UAV based on a R-22 scaled helicopter via only CG movement for attitude

control and RPM variation for thrust control. This configuration was able to fly up to speeds of 120 knots with a 7 degree nose down aircraft attitude. Although this high-speed attitude can be reduced somewhat by shaft incidence angle, an unusual hover attitude is realized.

1.3 Problem Statement and Thesis Overview

As can be seen from the review of recent work in this area, there are a significant number of advantages to be realized by placing trailing edge flaps on the rotor blades and using them for primary control. Although this presents a new bevy of challenges to designers, many of these challenges are tied to the large TEF deflections required to trim the helicopter at high speed. These large deflection angles create three main problems:

--Current smart-material actuators lack the capability to meet the stroke and force demands required to trim at high speeds,

--large TEF deflections cause an unacceptably large increase in profile drag and an associated increase in required main rotor power, and

--large required TEF deflections cast significant doubt on the fidelity of current modeling techniques to predict flow separation and other physical phenomena that would impede their use on a rotor.

The objective of the current project is to combine the ideas of moveable horizontal tail control with trailing edge elevons for swashplateless control of the helicopter. The pitching moments introduced by the horizontal tail in high-speed flight reduce the rotor cyclic pitch requirements and consequently relieve cyclic TEF

requirements. Aircraft CG selection may further reduce cyclic elevon requirements over the operational envelope. By simultaneously using on-blade elevons and horizontal tail control, the main goal of this study is to demonstrate that it is possible to accomplish swashplateless primary control of a helicopter by reducing required elevon deflections to levels that are comfortably achieved by piezo-electric actuators and do not result in a large drag penalty. A secondary objective is to use this system to trim in high speed flight without torsionally softening the rotor as much as current designs suggest.

In order to address these objectives, the analytical and simulation model developed for the study will be detailed in Chapter 2. Chapter 3 will present the results and discuss pertinent issues that arise. First, two new parameters will be defined to assist in proper analysis of each configurations in Section 3.1. Validation results for the conventional (swashplated) UH-60 will be detailed in Section 3.2. It will then present baseline result for the swashplateless rotor controlled via trailing edge flaps and compare these results to previous work in the area in Section 3.3 and 3.4. Then, an investigation into the effects of pitch indexing will be presented in Section 3.4 in order to identify its impact on the control inputs required at various airspeeds. Next, a study of torsional stiffness will be reviewed in Section 3.5 to establish the effect of this parameter on TEF deflections as well. Once these two primary issues have been considered, a combination of pitch index and torsional stiffness will be selected on which to base the horizontal tail studies. The horizontal tail studies for the nominal case of θ_{Pre}=16° and for the recommended case will be presented in Sections 3.7.1 and 3.6.2 respectively. As a secondary goal, a rotor that is relatively stiff in torsion will be selected and the horizontal

tail study repeated in an attempt to reduce elevon deflection requirements with a stiff rotor (Section 3.6.3 and 3.7.4). Finally, a summary of the work will be presented as well as several recommendations for future work in Chapter 4. Several appendices include graphical results that may be of interest to other researchers in the area, but they are not necessary for the specific discussion in Chapter 3.

Chapter 2

Model Formulation

The mathematical and physical model developed for this study must accurately predict control inputs in a propulsive trim analysis and identify trends in power. To that end, this model consists of a three degree-of-freedom rigid blade rotor model that is free to flap, lag, and pitch about coincident flap and lag hinges and a torsion bearing. The model is tailored to suit a UH-60A helicopter. Much of the mathematical formulation is based on Shen, Falls, Datta, Chopra, Leishman, and Johnson [14, 25, 26, 38]. Blade response is determined via a coupled flap-lag-torsion time integration solution. Hub forces and moments are summed with the fuselage, horizontal tail, and tail rotor forces to calculate the net forces and moments acting on the helicopter. In order to achieve trim, the control inputs are modified via a forward difference Newton-Raphson scheme to find the control solution that satisfies equilibrium. The aerodynamic model includes look-up tables for the main rotor and horizontal tail and applies Theodorsen's theory for the quasi-steady contribution of the airfoil and trailing edge flap. Drees' linear inflow model is used to calculate the induced velocity with a Prandtl tip loss factor applied.

This chapter will outline the structural and inertial model of the rotor blades and hub. It will then detail the aerodynamic loads arising from the standard blade as well as a blade fitted with trailing edge flaps. The fuselage model will be described to include contributions from the horizontal tail and tail rotor. The flow chart of the program for the conventionally controlled helicopter appears in Figure 2-1 .

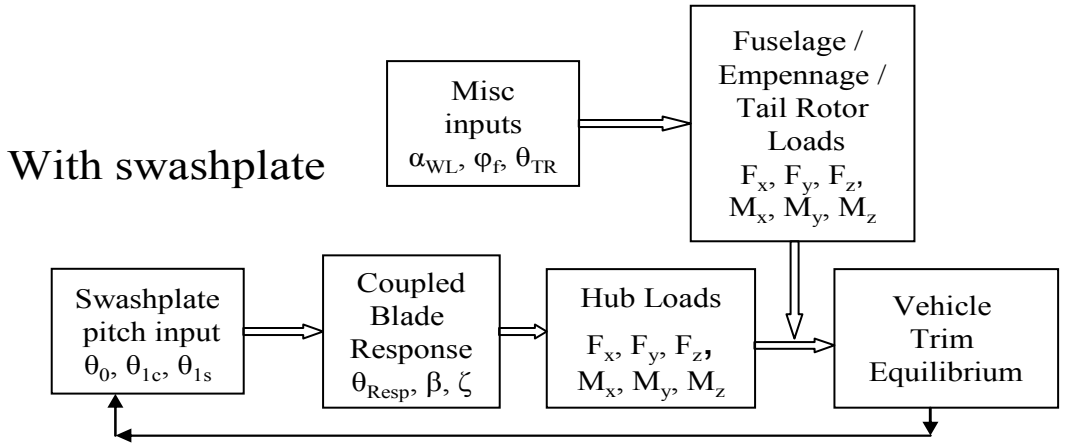

Figure 2-1: Control and Response Flow Chart of Conventional Helicopter

The swashplateless case is run almost identically, but with different control inputs. The same method of achieving trim is used. Once horizontal tail inputs are added as controls, there is no unique solution. However, treating the horizontal tail inputs as a range of fixed values, the same six control inputs can be used to drive the six vehicle forces and moments to equilibrium for each set on horizontal tail inputs (Figure 2-2).

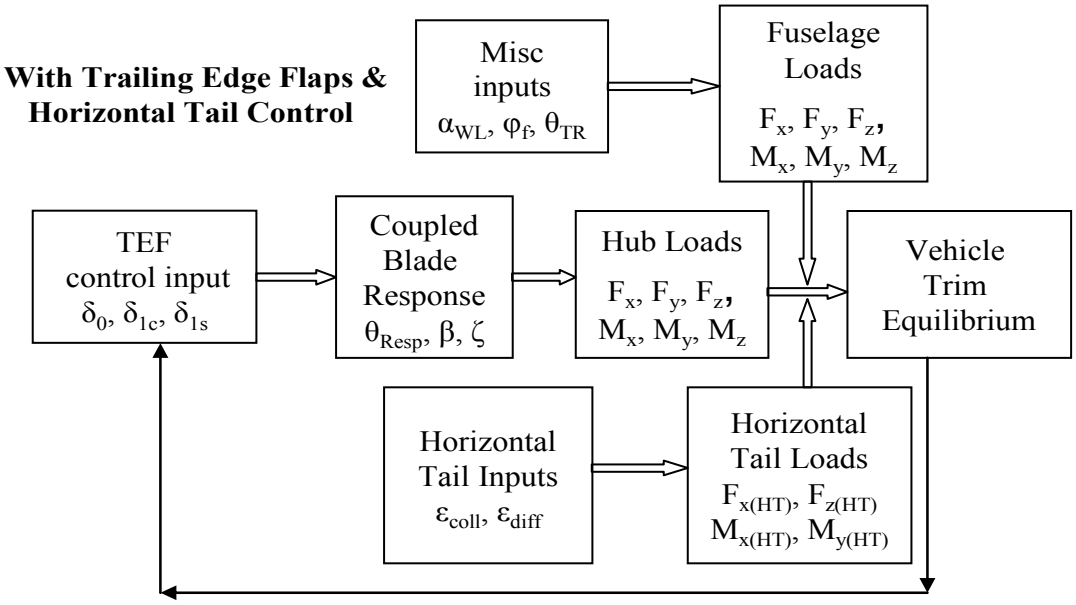

Figure 2-2: Control and Response Flow Chart for Swashplateless Helicopter

2.1 Structural and Inertial Model

The blade and hub structural model for a rigid body free to undergo rotation about a hinge axis out of plane (β), in-plane (ζ), as well as rotation about a pitch axis (θ) can be derived using Newton's method.

2.1.1 Blade Flapping Response

The first degree of freedom to consider is the out of plane, flapping motion of the blade denoted by β. This motion has aerodynamic and inertial contributions as represented in Figure 2-3, and Table 2-1 details the aerodynamic and inertial contributions to the flapping equation of motion:

Table 2-1: Contributors to the Blade Flapping Equations of Motion

Contribution	Differential Force	Moment Arm	Result after Integration
Aerodynamic	$F_{z(areo)}dr$	$(r-e)$	$\int_e^R F_{z(areo)}(r-e)dr = M_\beta$
Inertial (flap)			$I_\beta \ddot{\beta}$
Inertial (pitch)	$mx_I dr\left(-\ddot{\theta}\right)$	$(r-e)$	$-I_x \ddot{\theta}$
Centrifugal	$(mdr)r\Omega^2$	$(r-e)\sin(\beta)$ $-x_I \sin(\theta)$	$\left(I_\beta + eS_\beta\right)\beta\Omega^2 - I_x\theta\Omega^2$
Coriolis	$2mdr\Omega(r-e)\dot{\zeta}$	$(r-e)\sin(\beta)$	$2I_\beta\Omega\dot{\zeta}\beta$

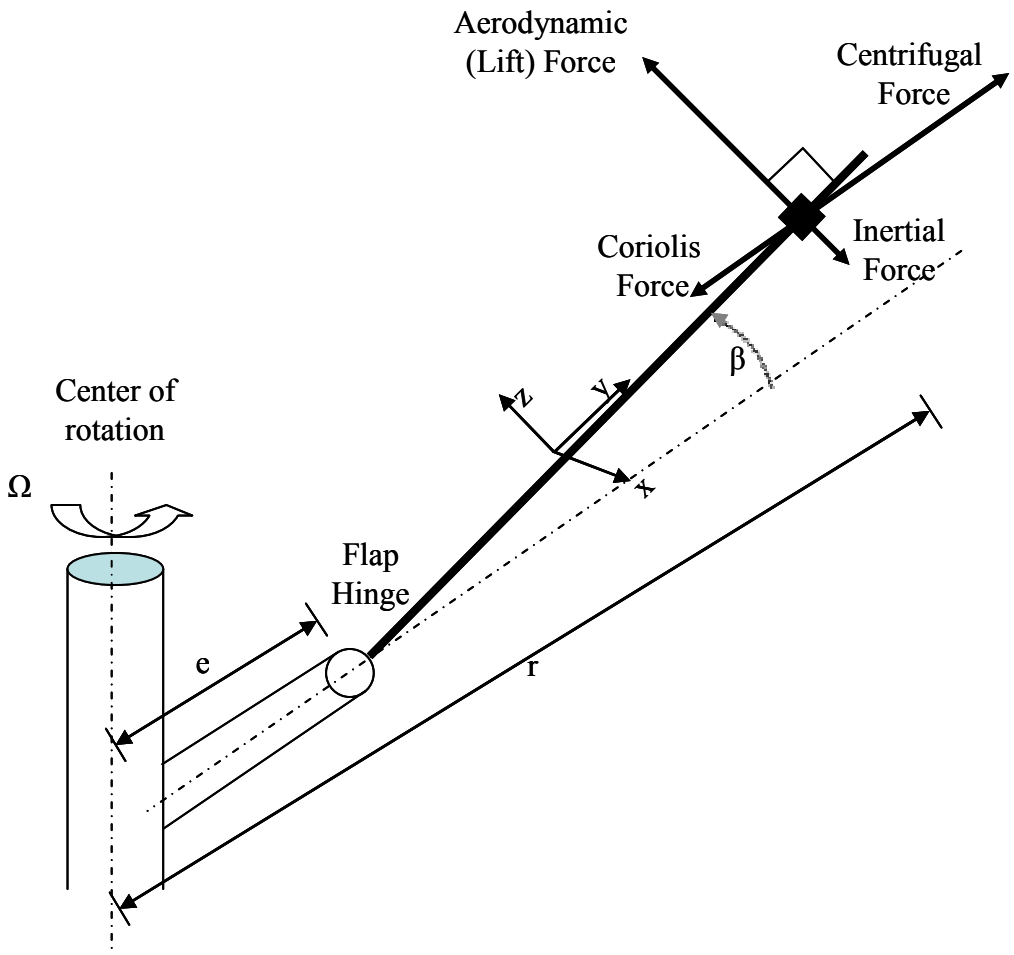

Figure 2-3: Aerodynamic and Inertial Contributions for Flapping Moments

In Table 2-2, $S_\beta = \int_e^R m(r-e)dr$ and the pitch-flap inertial coupling parameter is defined as $I_x = \int_e^R m(r-e)x_I dr$. It is also useful to define the following moments of inertia about the flapping and lagging hinge (assumed to be the same location):

$I_\beta = I_\zeta = \int_e^R m(r-e)^2 dr$ and the moment of inertia about the pitch axis:

$I_f = \int_e^R \left(mx_I^2 + I_{CG}\right)dr$. The inertial contributions of the TEFs are considered small and are not included in this analysis. The aerodynamic forcing term, M_β, includes θ, β, and ζ. Its derivation is deferred to the next section.

The small angle assumption can be applied to some of these terms such that $\sin(\beta) \cong \beta$, $\sin(\zeta) \cong \zeta$, $\sin(\theta) \cong \theta$, $\cos(\beta) \cong \cos(\zeta) \cong \cos(\theta) \cong 1$. Additionally, since the offset of the flap and lag hinge (e) is assumed to be small, the term, $(r - e) \cong r$. Finally, the equations of motion are typically expressed in non-dimensional form using $\dot{\beta} = \Omega \overset{*}{\beta}$, $\ddot{\beta} = \Omega^2 \overset{**}{\beta}$, $\dot{\zeta} = \Omega \overset{*}{\zeta}$, $\ddot{\zeta} = \Omega^2 \overset{**}{\zeta}$, $\dot{\theta} = \Omega \overset{*}{\theta}$, and $\ddot{\theta} = \Omega^2 \overset{**}{\theta}$.

After applying these assumptions and summing the moments about the flapping hinge, a linear second order ODE results (Eq. 2.1) as follows:

$$I_\beta \ddot{\beta} + \left(I_\beta + eS_\beta\right)\beta\Omega^2 - I_x\theta\Omega^2 - 2I_\beta\beta\Omega\dot{\zeta} - I_x\left(\ddot{\theta} + \Omega^2\theta\right) = M_\beta \qquad 2.1$$

After non-dimensionalizing with respect to I_β and Ω^2, Eq. 2.1 becomes Eq. 2.2

$$\overset{**}{\beta} + \nu_\beta^2\beta - 2\beta\overset{*}{\zeta} - I_x^*\left(\overset{**}{\theta} + \theta\right) = \frac{1}{I_\beta\Omega^2}M_\beta \qquad 2.2$$

Where the non-dimensional natural frequency of the flapping motion, ν_β, arises from the hinge offset of the blade (the UH-60 has a fully articulated rotor with no flapping spring) as follows: $\nu_\beta^2 = 1 + \frac{eS_\beta}{I_\beta}$ and $I_x^* = \frac{I_x}{I_\beta}$.

2.1.2 Blade Lag Response

In addition to flapping, the blade is free to move in rigid body rotation about the lag hinge in the plane of the rotor's rotation. This motion is influenced by drag aerodynamic forces and inertial forces as described in Figure 2-4 .

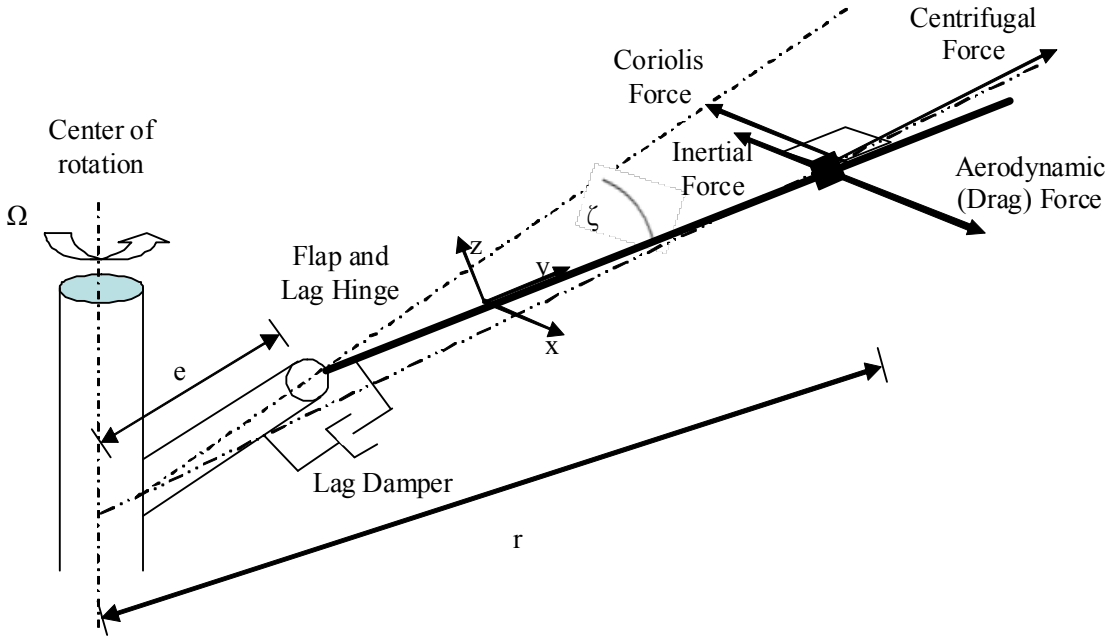

Figure 2-4: Aerodynamic and Inertial Contributions to Blade Lag Moments

Following the same procedure above with the intermediate steps omitted, the lag equation is as follows (Eq. 2.3):

$$\overset{**}{\zeta}+\nu_\zeta^2\zeta+2\nu_\zeta\xi_\zeta\overset{*}{\zeta}+2\beta\overset{*}{\beta}-2\mathrm{I}_x^*\overset{*}{\beta}\theta=\frac{1}{\mathrm{I}_\beta\Omega^2}\mathrm{M}_\zeta \qquad 2.3$$

with $\mathrm{I}_\beta \cong I_\zeta$. Several differences in this equation are apparent. The first is the fact that there is a damper installed on the lag degree of freedom. For the UH-60, the damping force, *c*, is a non-linear function of lagging rate as described in Appendix A, but is

expressed in terms of the appropriate damping ratio, ξ_ζ, such that $2\nu_\zeta\xi_\zeta = \frac{c}{\Omega I_\beta}$.

Additionally, although there is no lagging spring, stiffness in the lagging mode arises from the hinge offset in a similar manner as defined for flapping: $\nu_\zeta^2 = \frac{eS_\zeta}{I_\beta}$ since $I_\beta \cong I_\zeta$.

However, this stiffness is typically an order of magnitude less than that for flapping. Lastly, the aerodynamic moment, M_ζ, arises from the drag forces distributed spanwise along the blade, and it is defined as follows:

$$M_\zeta = \int_e^R F_{X(aero)}(r-e)dr \qquad 2.4$$

The aerodynamic term, $F_{X(aero)}$, is itself a function of θ, β, and ζ. It is derived in Section 2.2.1.

2.1.3 Blade Pitch Response

In a similar fashion to flapping and lag motion, the blade responds in pitch to both aerodynamic and inertial moments generated by the blade's interaction with the freestream and its velocity and acceleration as represented in Figure 2-5 . The components of each term are detailed in Table 2-2 .

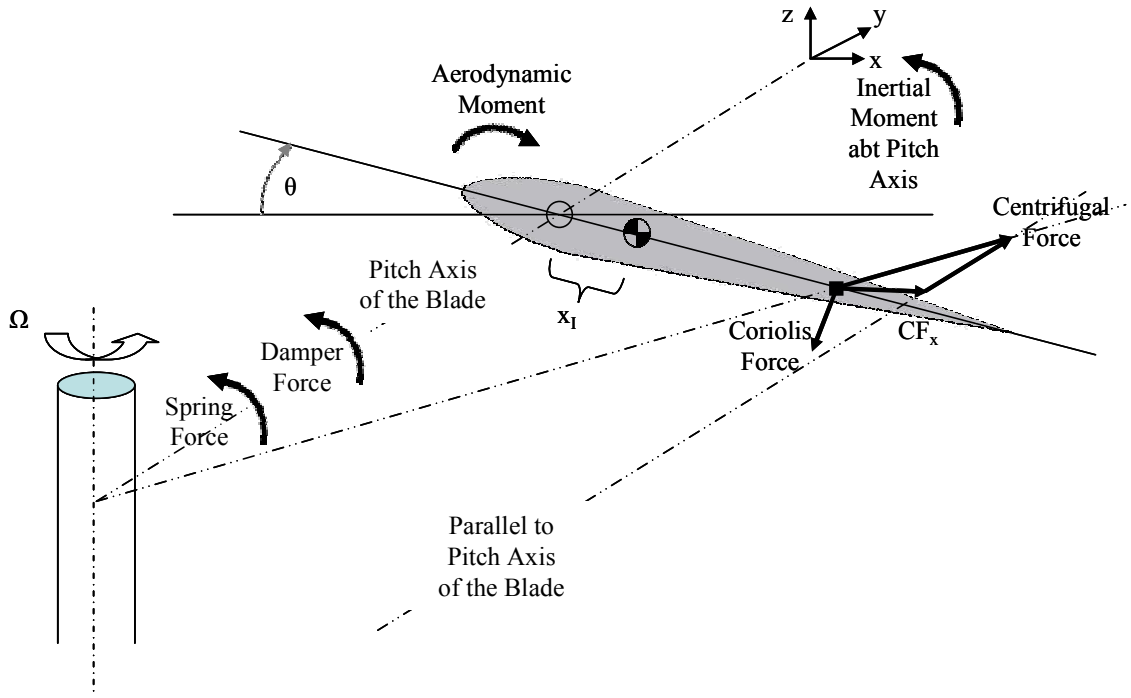

Figure 2-5: Aerodynamic and Inertial Components to the Blade Pitching Moment

Table 2-2: Contributors to the Blade Pitch Equations of Motion

Contribution	Differential Force	Moment Arm	Result after Integration
Aerodynamic			M_θ
Inertial (flapping)	$mdr(r-e)\ddot{\beta}$	x_I	$I_x\ddot{\beta}$
Inertial (pitch)			$I_f\ddot{\theta}$
Centrifugal			$I_f\theta\Omega^2$
Centrifugal (flapping)	$mr\Omega^2 dr\sin(\beta)$	x_I	$-I_\beta\beta\Omega^2$
Coriolis	$2mdr\Omega r\dot{\zeta}\dot{\beta}$	x_I	$2I_x\Omega\dot{\zeta}\dot{\beta}$
Control			$k_\theta(\theta-\theta_{con})$
Pre-pitch			$k_\theta(\theta-\theta_{pre})$
Damping			$2I_f\omega_{\theta 0}\xi_\theta\dot{\theta}$

In this model, either direct swashplate control is used or TEF inputs are used and the blade flies against the root restraint spring with a pitch index. In the case of swashplate control, k_θ refers to the finite stiffness of the pitch change links and swashplate system. In the case of the swashplateless rotor, k_θ refers to the stiffness of the root spring. In the swashplateless rotor, a damper is added. Following Shen's findings and recommendations [3], a value of ξ_θ=16% damping is used. Additional parameters are defined as follows:

$$\omega_{\theta 0}^2 = \frac{k_\theta}{I_f},\ \nu_{\theta 0}^2 = \frac{\omega_{\theta 0}^2}{\Omega^2} \text{ and } \nu_\theta^2 = 1 + \frac{\omega_{\theta 0}^2}{\Omega^2} \qquad 2.5$$

Summing moments about the pitch bearing yields Eq. 2.6 for blades controlled via swashplate inputs and Eq. 2.7 for blades controlled through TEF inputs contained in the M_θ term) and pitch indexed to θ_{Pre}. Both equations have been non-dimensionalized with respect to $I_\beta\Omega^2$.

$$I_f^*\left(\overset{**}{\theta} + \nu_\theta^2\theta + 2\nu_{\theta_0}\xi_\theta\overset{*}{\theta}\right) - I_x^*\left(\overset{**}{\beta} + \beta - 2\beta\overset{*}{\zeta}\right) = \frac{1}{\Omega^2 I_\beta}M_\theta + \nu_{\theta_0}^2\theta_{Con} \qquad 2.6$$

$$I_f^*\left(\overset{**}{\theta} + \nu_\theta^2\theta + 2\nu_{\theta_0}\xi_\theta\overset{*}{\theta}\right) - I_x^*\left(\overset{**}{\beta} + \beta - 2\beta\overset{*}{\zeta}\right) = \frac{1}{\Omega^2 I_\beta}M_\theta + \nu_{\theta_0}^2\theta_{pre} \qquad 2.7$$

2.1.4 Blade Response Summary

Eq. 2.2, Eq. 2.3, and Eq. 2.8 or Eq. 2.9 represent three coupled equations that govern the motion of the rigid blade in the current model. They can be solved via a variety of different numerical solution techniques since the aerodynamic term in each

equation cannot be analytically determined. The consolidated equation containing all the terms is as follows (Eq. 2.10):

$$\begin{bmatrix} 1 & 0 & -I_x^* \\ 0 & 1 & 0 \\ -I_x^* & 0 & I_f^* \end{bmatrix} \begin{bmatrix} \ddot{\beta} \\ \ddot{\zeta} \\ \ddot{\theta} \end{bmatrix} + \begin{bmatrix} 0 & -2\beta & 0 \\ 2\beta & 2\nu_{\zeta 0}\xi_\zeta & -2\beta I_x^* \\ 0 & 2\beta I_x^* & 2I_f^*\nu_{\theta 0}\xi_\theta \end{bmatrix} \begin{bmatrix} \dot{\beta} \\ \dot{\zeta} \\ \dot{\theta} \end{bmatrix} + \begin{bmatrix} \nu_\beta^2 & 0 & -I_x^* \\ 0 & \nu_\zeta^2 & 0 \\ -I_x^* & 0 & \nu_\theta^2 \end{bmatrix} \begin{bmatrix} \beta \\ \zeta \\ \theta \end{bmatrix} = \frac{1}{I_\beta \Omega^2} \begin{bmatrix} M_\beta \\ M_\zeta \\ M_\theta \end{bmatrix} + \begin{bmatrix} 0 \\ 0 \\ I_f^*\nu_{\theta 0}^2\theta_{Con/pre} \end{bmatrix} \quad 2.10$$

where $\begin{bmatrix} M_\beta \\ M_\zeta \\ M_\theta \end{bmatrix}$ each depends on the interaction of the blade with the free stream velocity, the pitching rate and acceleration, and the plunging rate and acceleration. In this study, the coupled equations are solved via time integration (Runge-Kutta) until a steady state solution is reached.

2.1.5 Blade Root and Hub Loads

Once blade response has been determined, the loads that are transmitted across the flap/lag hinge and the pitch bearing can be determined. These loads are calculated by integrating the effect of the aerodynamic forcing along the blade length and subtracting the inertial forces. Note that flapping moments are not transmitted across the flapping hinge. Hub pitch and roll moments arise from the vertical blade root shear force acting at a moment arm (hinge offset) from the hub.

$$S_x = \int_e^R \left(F_{X(aero)} - m\ddot{x} \right) dr \qquad 2.11$$

$$S_Y = -\int_e^R \left(F_{Z(aero)} \sin(\beta) - m\Omega^2 r \right) dr \qquad 2.12$$

$$S_Z = \int_e^R \left(F_{Z(aero)} - m\ddot{z} \right) dr \qquad 2.13$$

$$M_Y = \int_e^R \left(M_{\theta(aero)} - I_\theta \ddot{\theta} \right) dr \qquad 2.14$$

$$M_\varphi = \int_e^R S_{X(aero)} r \sin(\beta) dr \qquad 2.15$$

These blade root shear forces are transmitted across the pitch bearing and flap/lag hinge as hub forces and moments as in Figure 2-6 which have been resolved into their components relative to the hub axis.

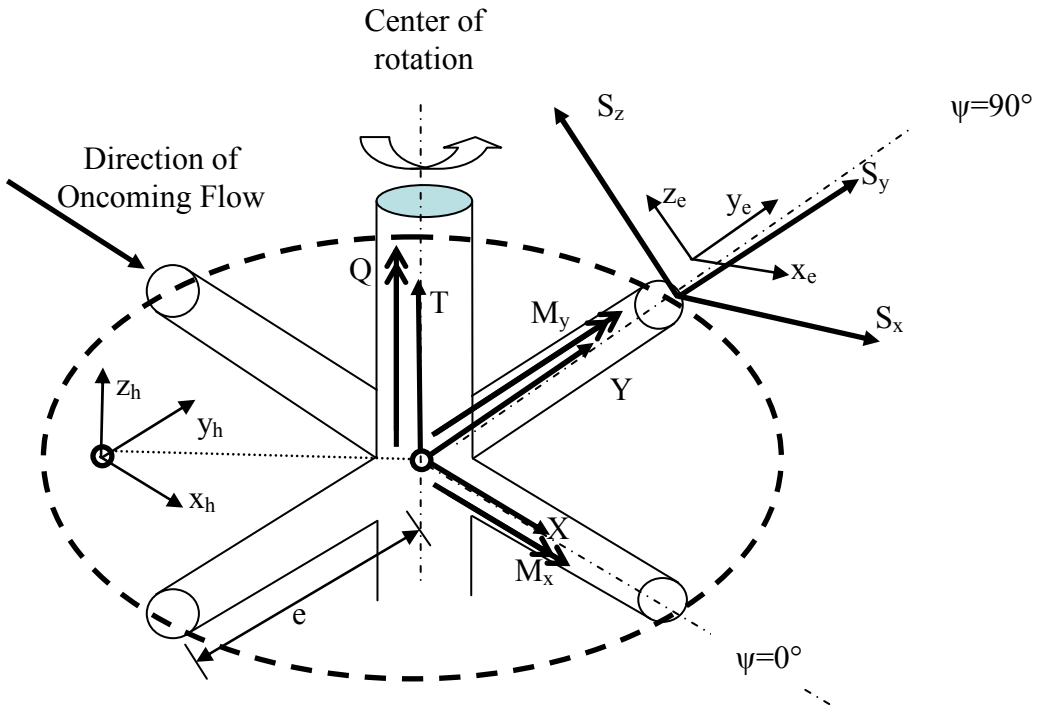

Figure 2-6: Blade Root Shear Loads and Hub Loads

These hub loads are as follows:

$$X = \frac{N_b}{2\pi}\int_0^{2\pi}\left(S_{X(aero)}\sin(\psi) + S_{Y(aero)}\cos(\psi)\right)d\psi \quad 2.16$$

$$Y = \frac{N_b}{2\pi}\int_0^{2\pi}\left(-S_{X(aero)}\cos(\psi) + S_{Y(aero)}\sin(\psi)\right)d\psi \quad 2.17$$

$$T = \frac{N_b}{2\pi}\int_0^{2\pi} S_{Z(aero)}d\psi \quad 2.18$$

$$M_X = \frac{N_b}{2\pi}\int_0^{2\pi}\left(S_{Z(aero)}e\sin(\psi) + \left(M_\theta + M_\varphi\right)\cos(\psi)\right)d\psi \quad 2.19$$

$$M_Y = \frac{N_b}{2\pi}\int_0^{2\pi}\left(-S_{Z(aero)}e\cos(\psi) + \left(M_\theta + M_\varphi\right)\sin(\psi)\right)d\psi \quad 2.20$$

$$Q = \frac{N_b}{2\pi}\int_0^{2\pi} S_{X(aero)}rd\psi \quad 2.21$$

These hub forces and moments are applied to the vehicle as described in Section 2.3.2.

2.2 Aerodynamic Model

The aerodynamic model for this study is based on blade element theory with Theodorsen quasi-steady aerodynamics, linear inflow (Drees' model) and a Prandtl tip loss correction. The current model uses 50 spanwise blade elements and takes a time step every 5° of rotor revolution ($\Delta\psi$=5°).

2.2.1 Base Blade Airloads

Aerodynamic forces arise from the interaction of each airfoil section with the freestream velocity encountered by that blade section at each moment in time given by the classic relations:

$$dL = \tfrac{1}{2}\rho V^2 c C_L dr \qquad 2.22$$

$$dD = \tfrac{1}{2}\rho V^2 c C_D dr \qquad 2.23$$

$$dM = \tfrac{1}{2}\rho V^2 c^2 C_M dr \qquad 2.24$$

In the above equations, the air density (ρ), airfoil chord (c), and blade section (*dr*) are known quantities. The free stream velocity is determined by adding the tangential and perpendicular components as defined below. The aerodynamic coefficients are determined from the angle of attack, pitch and plunge rates, and Mach number of each blade section. The forces arising from pitching and plunging are described in Section 2.2.3. The largest contributor of the aerodynamic coefficients is the angle of attack, which is treated in this section. Lift, drag, and pitching moment are nonlinear functions of the angle of attack and Mach number whose values are strongly affected by flow separation and compressibility effects. These effects are notoriously difficult to model analytically, so wind tunnel test data based on the appropriate airfoil section is used (SC1095 or SC1094R8 as appropriate). This test data is represented by C-81 look-up tables developed and promulgated by the US Army Aeroflightdynamics Directorate [42]. A two-dimensional linear interpolation routine is used to extract data from the tables at angles of attack ranging from $-180° < \alpha < 180°$ and Mach number $0 < M < 1.0$. Thus in order to properly use these tables, an accurate value of α and Mach number is required.

The local freestream velocity at each blade element varies with respect to azimuth (in forward flight), radius, and inflow distribution. Considering a blade section pictured below, u_t is the velocity tangential to the rotor hub consisting of the forward speed of the helicopter, the lagging rate, and the rotation of the rotor; u_p is the velocity perpendicular

to the blade due to flapping angle, flapping rate, and the induced velocity, φ is the inflow angle, and α is the aerodynamic angle of attack. The lift acts perpendicular to the resultant relative wind, V, the drag acts parallel to V, F_z is perpendicular to the hub line, and F_x is parallel to the hub line. θ is the geometric pitch angle which includes the response of the pitch equation of motion and the blade twist. These parameters are outlined in Figure 2-7.

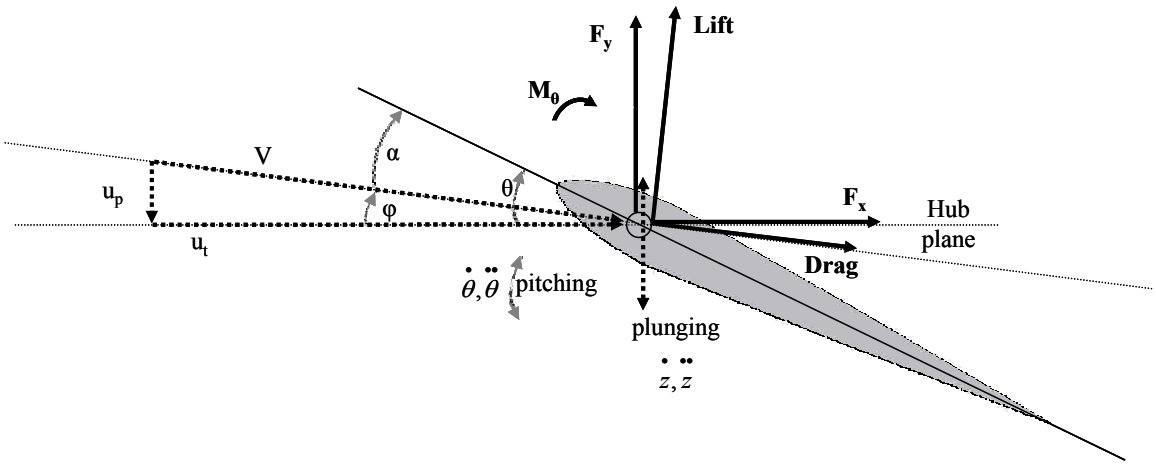

Figure 2-7: Blade Aerodynamic Force Components

The tangential and perpendicular velocities as a result of translational flight, rotor rotation, and blade motion are as follows:

$$u_p = \lambda\Omega R + r\overset{*}{\beta}\Omega\cos(\beta) + (\mu\Omega R)\sin(\beta)\cos(\psi) \qquad 2.25$$

$$u_t = \Omega r + (\mu\Omega R)\sin(\psi) + r\Omega\overset{*}{\zeta}\cos(\zeta) \qquad 2.26$$

and after the small angle assumption is applied to β and ζ

$$u_p = \lambda\Omega R + r\overset{*}{\beta}\Omega + (\mu\Omega R)(\beta)\cos(\psi) \qquad 2.27$$

$$u_t = \Omega r + (\mu\Omega R)\sin(\psi) + r\Omega\overset{*}{\zeta} \qquad 2.28$$

The free stream velocity encountered by the blade is simply $V = \sqrt{u_t^2 + u_p^2}$. The angle of attack is the difference between the geometric pitch angle and the inflow angle: $\alpha = \theta - \phi$ where $\phi = \tan^{-1}\left(u_p / u_t\right)$. θ is a function of azimuth that is given by the solution to the pitch degree of freedom equations of motion which was defined earlier Eq. 2.2. Once the blade section velocity and angle of attack are known, the values of each lift coefficient can be extracted from the appropriate C-81 table as described above. Note that it is possible for u_p to be a negative number in the case of upwash due to flapping angle or flapping rate. In this case the negative sign is retained, and it results in an angle of attack that is larger than the pitch.

One area worth highlighting is the reverse flow region on the retreating side of the rotor disk that develops in forward flight. This region gives rise to unusual blade angles of attack because the flow generally runs form the trailing edge to the leading edge of the airfoil sections in this region. Although the low local dynamic pressure keeps the forces in this area small, this region still must be modeled accurately. In order to do so, the air loads equations are modified to be Eq. 2.29, Eq. 2.30, and Eq. 2.31 [2].

$$dL = \tfrac{1}{2}\rho\left(|u_t|u_t + |u_p|u_p\right)cC_L\,drF \qquad 2.29$$

$$dD = \tfrac{1}{2}\rho\left(|u_t|u_t + |u_p|u_p\right)cC_D\,dr \qquad 2.30$$

$$dM = \tfrac{1}{2}\rho\left(|u_t|u_t + |u_p|u_p\right)c^2C_m\,drF \qquad 2.31$$

Using the equations presented above, the airloads produced by the base blade's orientation and horizontal velocity can be determined. These aerodynamic forces must be converted into the hub frame. As such, they must be rotated through the inflow angle, φ, which is different at every azimuthal station. Therefore, the lift and drag of each blade

section are converted to dF_{Zaero} and dF_{Xaero} prior to being summed along the length of the blade. This manipulation appears in Eq. 2.32 and Eq. 2.33.

$$dF_{Xaero} = dD\cos(\varphi) + dL\sin(\varphi) \tag{2.32}$$

$$dF_{Zaero} = dL\cos(\varphi) - dD\sin(\varphi) \tag{2.33}$$

However, in order to determine these values, an analysis of the rotor inflow must be performed.

2.2.2 Inflow Modeling

The induced velocity of the disk is modeled using Glauert's classic application of momentum theory which treats the rotor as an actuator disk across which the flow is accelerated in order to attain the desired amount of thrust. Using Eq. 2.34

$$\lambda = \mu\tan(\alpha_{hub}) + \frac{C_t}{2\sqrt{\mu^2 + \lambda^2}} \tag{2.34}$$

where λ and μ are u_p, and u_t non-dimensionalized by the rotor tip speed and C_t is the rotor thrust coefficient defined by Eq. 2.35

$$C_t = \frac{T}{\rho V_{tip}^2 A_{disk}} = \frac{T}{\rho(\Omega R)^2(\pi R^2)} \tag{2.35}$$

and α_{hub} is the angle of orientation that the hub makes with the freestream velocity (positive is nose down).

This model has been adapted by Drees to describe the lateral and longitudinal variation in induced flow that occurs across the disk in forward flight. Drees' relation as given in [1] is Eq. 2.36

$$\lambda(r,\psi) = \lambda_{hub}\left(1 + k_x \frac{r}{R}\cos(\psi) + k_y \frac{r}{R}\sin(\psi)\right) \quad 2.36$$

where k_x and k_y are defined as follows:

$$k_x = \frac{4\left(1 - \cos(\chi) - 1.8\mu^2\right)}{3\sin(\chi)} \quad 2.37$$

$$k_y = -2\mu \quad 2.38$$

and $\chi = \tan^{-1}\left(\frac{\mu}{\mu_Z + \lambda}\right)$ is the main rotor wake skew angle.

In addition to the linear variation described above, the inflow varies along the blade length proportional to the circulatory lift that the blade produces such that inflow velocities are typically higher near the blade tip than further inboard. This effect is compounded by the strong tip vortex that exists at the end of the blade. These phenomena result in a significant reduction of lift on the outermost part of the blade, and the lift is reduced to zero at the blade tip. Since this region operates in high dynamic pressure, correctly modeling this effect is important in order to accurately calculate the blade flapping moment and total rotor thrust. Additionally, the UH-60's swept blade tips provide a significant negative pitching moment on the blade, and they introduce aerodynamic coupling between flap and pitch. Since the tip loss effect will strongly affect both of these effects, proper modeling of the tip loss is important. As such, this study uses Prandtl's classic tip loss relation as given in [2]:

$$F = \frac{2}{\pi}\cos^{-1}\left(e^{N_b\left(\frac{x-1}{2\lambda}\right)}\right) \quad 2.39$$

This effect is applied to the Lift and Moment relations as follows:

$$dL = \tfrac{1}{2}\rho\left(|u_t|u_t + |u_p|u_p\right)cC_L\,drF \qquad 2.40$$

$$dM = \tfrac{1}{2}\rho\left(|u_t|u_t + |u_p|u_p\right)c^2C_m\,drF \qquad 2.41$$

2.2.3 Quasi-Steady and Flapped Airfoil Formulation

Although the lift, drag, and moment produced by each blade section due to its angle of attack has already been discussed, forces and moments arising from the blade's vertical and angular velocity and acceleration are also significant. It is convenient to discuss these contributions to the airloads coincident with the treatment of the trailing edge flap effect on the airloads because the TEF motion also contributes to these forces. Of course, the TEF only occupies 20% of the blade span for this study. For the rest of the blade, the terms describing flap contributions are neglected.

These forces are described by thin airfoil potential flow theory and were first detailed by Theodorsen for an airfoil with flaps [34]. This theory can predict the lift and pitch moment caused by circulation and apparent mass effects, but it cannot predict drag due to viscous effects, which is treated later. Theodorsen's work focused primarily on the lift attenuation and delay that was caused by the unsteadiness of the flow. His work was based in the frequency domain, and its applicability is therefore unsuited to helicopters. However, his summary of the circulatory and non-circulatory contributors to lift and pitching moment are pertinent to this study. As such, the forces based on pitch and plunge motions of the flap and airfoil are retained, but the lift deficiency function is neglected (i.e. C(k) = 1).

This theory requires knowledge of the aerodynamic angular position and motion of the blade and the flap. The position and motion of the blade are determined by solving the coupled system of equations Eq. 2.10 described in Section 2.1.4. Although the results of this motion are retained as an explicit relationship between ψ and θ and ψ and $\overset{*}{\theta}$ (via time integration), the motion can be approximated with a Fourier Series representation, from which acceleration can be determined. For the purposes of this study, up to the second harmonic terms in θ are retained such that the velocity and acceleration are given by $\dot{\theta} = \Omega \overset{*}{\theta}$ and Eq. 2.42.

$$\ddot{\theta} \approx \Omega^2 \left(\frac{\overset{*}{\theta}_{\psi+1} - \overset{*}{\theta}_{\psi}}{\Delta\psi} \right) \approx -\Omega^2 \left[\theta_{1c} \cos(\psi) + \theta_{1s} \sin(\psi) + 4\left(\theta_{2c} \cos(2\psi) + \theta_{2s} \sin(2\psi) \right) \right] \quad 2.42$$

In a similar fashion to the pitch of the blade, the flapping position and rate are solved for as explicit functions of azimuth via the Runge-Kutta method. However, the flapping is described to a very accurately degree by a Fourier Series including up to second harmonics. Thus, the blade's plunging motion can be described by $\dot{\beta} = \Omega \overset{*}{\beta}$ and Eq. 2.43

$$\ddot{\beta} \approx \Omega^2 \left(\frac{\overset{*}{\beta}_{\psi+1} - \overset{*}{\beta}_{\psi}}{\Delta\psi} \right) \approx -\Omega^2 \left[\beta_{1c} \cos(\psi) + \beta_{1s} \sin(\psi) + 4\left(\beta_{2c} \cos(2\psi) + \beta_{2s} \sin(2\psi) \right) \right] \quad 2.43$$

For the TEF, the position and motion are control inputs prescribed as a Fourier series including only 0^{th} and 1^{st} harmonics so that

$$\delta(\psi) = \delta_0 + \delta_{1c}\cos(\psi) + \delta_{1s}\sin(\psi) \text{ and } \delta_1 = \sqrt{\delta_{1c}^2 + \delta_{1s}^2} \quad 2.44$$

$$\dot{\delta}(\psi) = \Omega\left(-\delta_{1c}\sin(\psi) + \delta_{1s}\cos(\psi)\right) \quad 2.45$$

$$\ddot{\delta}(\psi) = \Omega^2\left(-\delta_{1c}\cos(\psi) - \delta_{1s}\sin(\psi)\right) \quad 2.46$$

The next critical parameter to define is the flap sizing and chord length. Theodorsen's theory reckons the position of pertinent locations from the semi-chord as pictured in Figure 2-8. The location of the flap is defined by its hinge location (the flap's leading edge and hinge points are coincident for this study) expressed non-dimensionally in semi-chord from the blade mid-point. Therefore, in this section, parameters identified as $x_{n,}$ where n is some location descriptor, are non-dimensional parameters. Parameters such as b (semi-chord), or c (chord) are dimensional quantities. Table 2-3 summarizes the most commonly used parameters and their values in this study based on Figure 2-8.

Table 2-3: Summary of Theodorsen Geometric Parameters

Parameter	Dimensional symbol	Value	Non-dim symbol	Value
Chord length	c	1.73 ft (nominally)		
Semi-chord length	b	0.865 ft		
Location of pitch axis		25%c	x_a	-.5
Location of flap hinge		80%c	x_c	.6

The lift and moment are assumed to act about the ¼-chord of the airfoil. This is coincident with the pitch axis for most of the blade, except where the quarter chord is off-set from the pitch axis as described in [39, 23]. This value becomes significant in the region of the tip sweep. In this region the off-set is accounted for by the moment having additional increment equal to $\Delta dM = dL(d)$ where d takes on negative values when it is

located behind the pitch axis (which it is in the vicinity of the tip sweep resulting in a negative pitching moment).

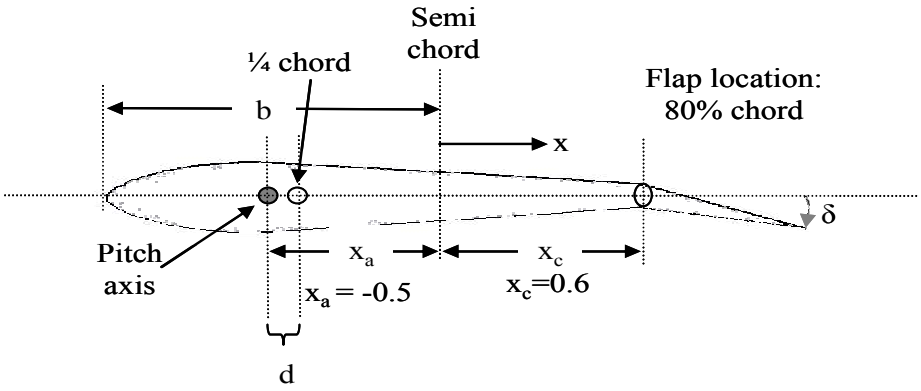

Figure 2-8: Blade Geometric Parameters for Theodorsen Analysis

The last step before describing the lift and moment increments due to the blade and flap motion is to identify the lift curve slope, $C_{L\alpha}$, which potential flow theory predicts to be 2π. The value for the SC1095 airfoil is 5.73, as derived from the linear portion of the SC1095 lift coefficient tables [42].

Armed with these relationships, the increment in lift and pitching moment can be derived. The remaining analysis in this section will consider the non-dimensional c_L, c_D, and c_M. First the lift is expressed in Eq. 2.47 as the combination of contributors from [1]:

1) the base blade;
2) the circulatory contribution from pitching motion of the base blade;
3) the non-circulatory contribution from pitch and plunge of the base blade;
4) the lift increment from the TEE (including angular position, pitch and plunge).

$$c_{L\,TOT} = c_{L\,BASE} + c_{L\,CIRC} + c_{L\,NON-CIRC} + \Delta c_{L\,TEE} \qquad 2.47$$

The total lift coefficient is separated this way for several reasons. First, the lift coefficient produced by the base blade is determined from look-up tables which include compressibility and viscous effects. As stated earlier, the value for angle of attack used in these look up routines already incorporates the changes due to induced velocity, blade flapping motion, $\dot{\beta}$, and the component of freestream velocity normal to the blade chord by virtue of the local flapping angle. Each term can be expanded as follows:

$$c_{L\,CIRC} = C_{L\alpha}\frac{\dot{\alpha}\,b}{V}\left(\tfrac{1}{2} - x_a\right)\frac{1}{\beta} \qquad 2.48$$

This term arise from the pitching motion about the pitch axis of the blade. This motion creates a linear distribution of inflow along the chord, which imparts a parabolic camber to the airfoil. This camber can be represented by an effective angle of attack, which is multiplied by the physical value of $C_{L\alpha}$ to yield the circulatory lift contribution due to pitching. Since this term accounts for circulatory lift, it must be modified by the Glauert factor, β, to capture compressibility effects such that $\beta = \sqrt{1 - M^2}$. The velocity term, V, in this equation and all that follow in this section is the full free-stream velocity given by $V = \sqrt{u_t^2 + u_p^2}$. Note that in each term, all dimensions cancel yielding the non-dimensional lift coefficient. Additionally, note that x_a is typically close to -1/2.

The non-circulatory lift terms arise from the fact that blade must physically displace air up and down as a result of the pitch and plunging velocity and acceleration. The displaced air has inertia, and this inertia imparts reaction forces on the blade in proportion to its motion. These terms are represented as follows.

$$c_{L\,NON-CIRC} = \frac{\pi \dot{\alpha} b}{V} + \frac{\pi \ddot{h} b}{V^2} + \frac{\ddot{\alpha} b^2}{V^2}(-x_a) \qquad 2.49$$

The above relations are used for the entire length of the blade, with $\Delta c_{L\,TEE} = 0$ where appropriate. In the portion of the blade that includes the TEF, the Eq. 2.50 also applies

$$\Delta c_{L\,TEE} = \frac{1}{\beta}\left(c_{L\delta}\delta + \frac{b\dot{\delta}}{V} T_{11} \right) - \frac{b\dot{\delta}}{V} T_4 - \frac{b^2 \ddot{\delta}}{V^2} T_1 \qquad 2.50$$

Thus, the increment in lift produced by the TEE arises from circulatory lift due to its angular deflection and speed (within the first term), and the non-circulatory lift (the last two terms) representing apparent mass effects. The T-functions are geometric functions that describe the location of the flap leading edge and the flap hinge (which are coincident in this study). They are given in Theodorsen's theory and are reproduced at the end of this section [34, 38]. The lift curve slope of the flap is a function of the flap chord-wise length and is given by $c_{L\delta} = 2T_{10}$. Once again, compressibility effects are modeled with the Glauert factor, β, where appropriate.

The airfoil pitching moment about the pitch axis can also be predicted in a similar fashion as given by Eq. 2.51. Its contributions arise from the pressure distribution over the airfoil when its position and motion is included [1]

$$c_{M\,TOT} = c_{M\,BASE} + c_{M\,CIRC} + c_{M\,NON-CIRC} + \Delta c_{M\,TEE} + c_{L\,BASE}\frac{d}{c} \qquad 2.51$$

where d is the offset between the pitch axis and the airfoil section ¼-chord and β is the Glauert compressibility factor. The first four terms give the pitching moment about the airfoil ¼-chord, and the last term accounts for any offset between the quarter chord and

the pitch axis. Again, *d* takes on negative values when the quarter chord is behind the pitch axis. This factor becomes significant in the region of the tip sweep, but appears elsewhere as well due to the trim tab and other such blade irregularities. This correction factor must also be applied to the lift terms that are not included in $C_{L(BASE)}$, as will be explained immediately below. $C_{M(BASE)}$ is determined from the C-81 look-up tables based on angle of attack and Mach number. Each of the remaining terms can be determined as follows:

$$c_{M\,CIRC} = c_{L\,CIRC}\left(x_a + \tfrac{1}{2}\right) \qquad 2.52$$

which simply accounts for the offset between the quarter-chord and the pitch axis multiplied by the lift due to pitching rate that is calculated separately from the other circulatory lift terms. Because x_a is typically very close to -1/2, this term rarely contributes significantly to the sum.

As in the case of lift, the motion of the blade produces apparent mass reaction forces on the blade as detailed in Eq. 2.53 with an appropriate correction for the location of the pitch axis relative to the quarter-chord.

$$c_{M\,NON-CIRC} = -\frac{1}{2V^2}\left[\pi Vb(\tfrac{1}{2} - x_a)\dot{\alpha} + \pi b^2(\tfrac{1}{8} + x_a^2)\ddot{\alpha} - \pi x_a b\ddot{h}\right] \qquad 2.54$$

In addition to the pitching moment produced by the base blade, the position and motion of the TEF produce moments about the pitch axis as given in Eq. 2.55. As before, these terms are divided into circulatory (the first term, modified by the Glauert factor) and non-circulatory components (the second term) where $c_{M\delta} = -\tfrac{1}{2}T_{15}$.

$$\Delta c_{M\,TEE} = \frac{1}{\beta}\left[c_{M\,\delta}\delta + \frac{b\dot{\delta}}{V} T_{11}\left(x_a + \tfrac{1}{2}\right)\right] \\ -\frac{1}{2}\left[\left(T_{10}+T_4\right)\delta + \frac{b}{V}\left(T_1 - T_8 - (x_c - x_a)T_4 + \frac{b}{2}T_{11}\right)\dot{\delta} - \frac{b^2}{V^2}\left(T_7 + (x_c - x_a)T_1\right)\ddot{\delta}\right] \tag{2.56}$$

In summary, the preceding expressions give all of the lift and pitching moment produced by the motion of the airfoil and flap. When possible, real values are used for parameters such as the lift curve slope.

The airfoil profile drag arises from the interaction of viscous shear stresses along the contact between the airfoil and the freestream. As such, potential flow theory cannot predict this phenomenon. The drag produced by the base blade is determined experimentally. These values are used in the analysis per Section 2.2.1. In order to predict the profile drag increment added by the flap deflection, this study relies on an approximation of limited test data. This approximation was analyzed and presented by Falls [22] based on CFD analysis which was validated against experimental results provided by Hassan and Straub [43]. It is reproduced here for reference:

$$c_{D\,TOT} = c_{D\,BASE} + 0.0092 + .2403\left(\alpha + \delta/3\right)^2 \tag{2.57}$$

The profile drag produced by an airfoil varies significantly based on the Mach number and angle of attack. Although Eq. 2.57 offers some flexibility in treating these two phenomena, it does contain an error at all but a few combinations of α, δ, and Mach number. The coefficients in Eq. 2.57 were chosen such that the drag predicted by this equation is always greater than or equal to the limited CFD and test data that is available for comparison. This constitutes the most conservative approach to the problem that could be taken and still consider drag.

This section outlined the various contributions that the position and motion of the airfoil section and flap make on the lift, moment and drag of the blade. The following equations are the geometric constants defined by Theodorsen and used in the quasi-steady analysis of the airfoil-flap combination [34, 38]:

$$T_1 = -\tfrac{1}{3}(2 + x_c^2)\sqrt{1 - x_c^2} + x_c \cos^{-1}(x_c) \tag{2.58}$$

$$T_3 = -\tfrac{1}{8}(1 - x_c^2)(5x_c^2 + 4) + \tfrac{1}{4}x_c(7 + 2x_c^2)\sqrt{1 - x_c^2}\cos^{-1}(x_c) - (\tfrac{1}{8} + x_c^2)(\cos^{-1}(x_c))^2 \tag{2.59}$$

$$T_4 = x_c\sqrt{1 - x_c^2} - \cos^{-1}(x_c) \tag{2.60}$$

$$T_5 = -(1 - x_c^2) + 2x_c\sqrt{1 - x_c^2}\cos^{-1}(x_c) - (\cos^{-1}(x_c))^2 \tag{2.61}$$

$$T_7 = -\tfrac{1}{8}x_c(7 + 2x_c^2)\sqrt{1 - x_c^2}\cos^{-1}(x_c) - (\tfrac{1}{8} + x_c^2)(\cos^{-1}(x_c))^2 \tag{2.62}$$

$$T_8 = -\tfrac{1}{3}(1 - x_c^2)^{3/2} - x_c T_4 \tag{2.63}$$

$$T_9 = \tfrac{1}{2}\left[\tfrac{1}{3}(1 - x_c^2)^{3/2} + x_a T_4\right] \tag{2.64}$$

$$T_{10} = \sqrt{1 - x_c^2} + \cos^{-1}(x_c) \tag{2.65}$$

$$T_{12} = (2 + x_c)\sqrt{1 - x_c^2} - (1 + 2x_c)\cos^{-1}(x_c) \tag{2.66}$$

$$T_{13} = -\tfrac{1}{2}\left[T_7 + (x_c - x_a)T_1\right] \tag{2.67}$$

$$T_{15} = T_4 + T_{10} \tag{2.68}$$

2.3 Helicopter Model

In addition to the rotor forces and moments, the fuselage, tail, and tail rotor also provide forces that contribute to vehicle equilibrium. The forces are summed along with the rotor forces and moments about the rotor hub in the body frame.

2.3.1 Coordinate System Transformations

Because all of the forces and moments are summed in the body frame of reference, a series of coordinate transformations is required to transform each subsystem's forces and moments into the body system. These transformations are as follows:

Rotor forces and moments through the shaft index angle in Eq. 2.69

$$\begin{bmatrix} F_{X\,R} \\ F_{Y\,R} \\ F_{Z\,R} \end{bmatrix} = \begin{bmatrix} \cos(\alpha_{Sx}) & 0 & -\sin(\alpha_{Sx}) \\ 0 & 1 & 0 \\ \sin(\alpha_{Sx}) & 0 & \cos(\alpha_{Sx}) \end{bmatrix} \begin{bmatrix} H \\ Y \\ T \end{bmatrix} \tag{2.69}$$

Horizontal tail forces and moments through the offset angle, η_{HT}, in Eq. 2.70

$$\begin{bmatrix} F_{X\,HT} \\ F_{Y\,HT} \\ F_{Z\,HT} \end{bmatrix} = \begin{bmatrix} \cos(\eta_{HT}) & 0 & \sin(\eta_{HT}) \\ 0 & 1 & 0 \\ -\sin(\eta_{HT}) & 0 & \cos(\eta_{HT}) \end{bmatrix} \begin{bmatrix} D_{HT} \\ 0 \\ L_{HT} \end{bmatrix} \tag{2.70}$$

where $\eta_{HT} = \alpha_{WL} + \chi_{HT}$ represents the angular difference between the freestream and the vehicle pitch attitude. These relationships are detailed more fully in Section 2.3.5 .

Tail Rotor forces through the tail rotor cant angle, γ_{TR}, in Eq. 2.71:

$$\begin{bmatrix} F_{X\,TR} \\ F_{Y\,TR} \\ F_{Z\,TR} \end{bmatrix} = \begin{bmatrix} 1 & 0 & 0 \\ 0 & \cos(\gamma_{TR}) & -\sin(\gamma_{TR}) \\ 0 & \sin(\gamma_{TR}) & \cos(\gamma_{TR}) \end{bmatrix} \begin{bmatrix} 0 \\ 0 \\ T_{TR} \end{bmatrix} \tag{2.71}$$

Fuselage forces consist of both weight and aerodynamic forces. The aerodynamic pitching moment effects on the fuselage are neglected. The aerodynamic side force is also neglected since the vehicle is trimmed with no slide-slip angle. The weight can be resolved into the body axis through two rotations resulting in Eq. 2.72.

$$\begin{bmatrix} F_{XW} \\ F_{YW} \\ F_{ZW} \end{bmatrix} = \begin{bmatrix} -\sin(\alpha_{WL}) \\ \sin(\phi_f)\cos(\alpha_{WL}) \\ -\cos(\phi_f)\cos(\alpha_{WL}) \end{bmatrix} W \qquad 2.72$$

The fuselage aerodynamic forces, which act perpendicular and parallel to the global free stream, are resolved into the body axis through rotation through the vehicle pitch attitude in Eq. 2.73:

$$\begin{bmatrix} F_{Xf} \\ F_{Yf} \\ F_{Zf} \end{bmatrix} = \begin{bmatrix} \cos(\alpha_{WL}) & 0 & \sin(\alpha_{WL}) \\ 0 & 1 & 0 \\ -\sin(\alpha_{WL}) & 0 & \cos(\alpha_{WL}) \end{bmatrix} \begin{bmatrix} D_f \\ 0 \\ L_f \end{bmatrix} + F_W \qquad 2.73$$

Sub-system moments can be transformed via the same series of rotations.

2.3.2 Vehicle Force and Moment Sums

Figure 2-9 and Figure 2-10 outline the orientation of several key dimensions and angles. All dimensions are taken from the hub. Dimensions in the x-direction are positive toward the tail from the hub, in the y-direction are positive out the right door, and in the z-direction, positive if the location is above the hub. Table 2-4 summarizes these dimensions. The pitch attitude of the helicopter, α_{WL}, is positive nose down, and the roll attitude, φ_f, is positive roll right. The vehicle is not flown with any sideslip angle.

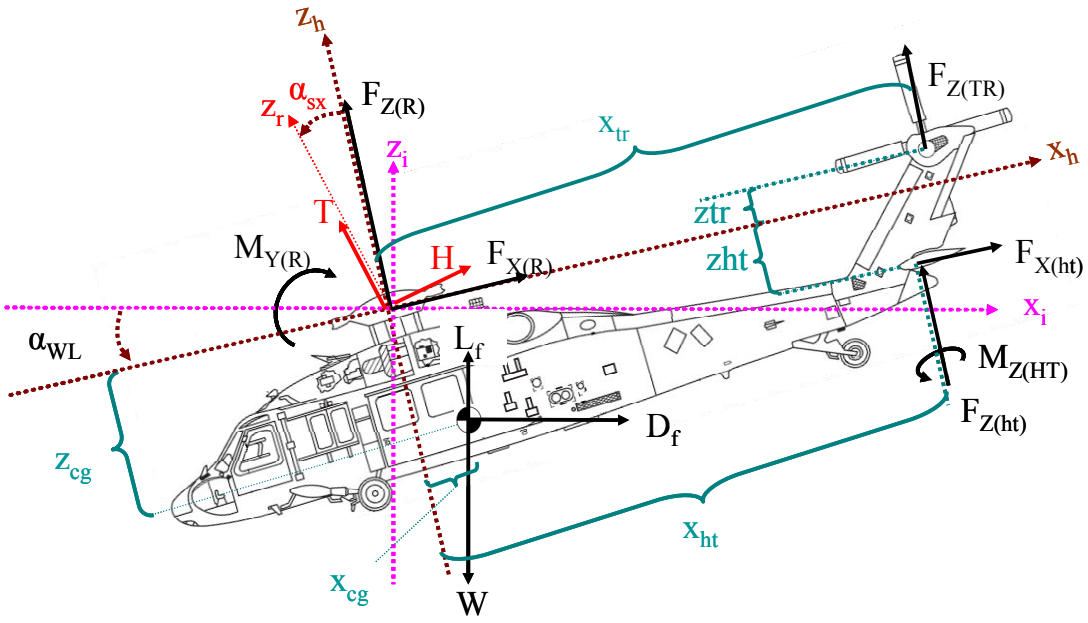

Figure 2-9: Longitudinal Helicopter Forces and Dimensions [44]

Table 2-4: Helicopter Geometric Properties

Helicopter Properties			
Weight	W	18300	lbs
Longitudinal CG Offset	x_{cg}	1.525	ft
Lateral CG Offset	y_{cg}	0	ft
Vertical CG Offset	z_{cg}	-5.825	ft
Lon. Stabilator offset	x_{ht}	29.925	ft
Lat. Stabilator offset	y_{ht}	0	ft
Vert. Stabilator offset	z_{ht}	-5.915	ft
Lon. Tail Rotor offset	x_{tr}	32.565	ft
Lat. Tail Rotor offset	y_{tr}	0	ft
Vert. Tail Rotor offset	z_{tr}	0.805	ft
Forward shaft tilt	α_{SX}	3	deg
Tail Rotor Cant	φ_{TR}	20	deg

distances with respect to the hub

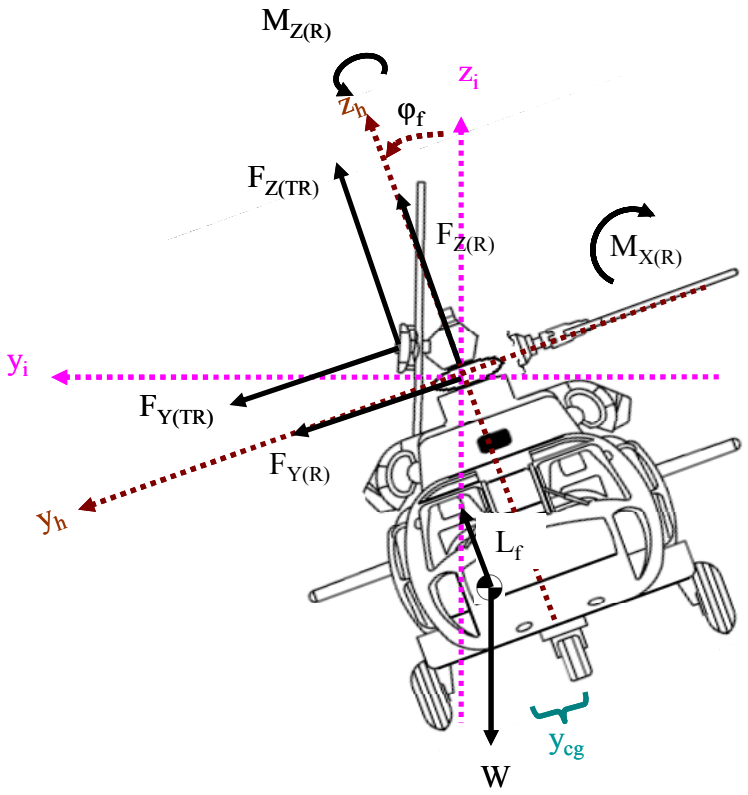

Figure 2-10: Lateral Helicopter Forces and Dimensions

$$\sum F_X = F_{XR} + F_{Xf} + F_{XTR} + F_{XHT} \qquad 2.74$$

$$\sum F_Y = F_{YR} + F_{Yf} + F_{YTR} + F_{YHT} \qquad 2.75$$

$$\sum F_Z = F_{ZR} + F_{Zf} + F_{ZTR} + F_{ZHT} \qquad 2.76$$

Each of the forces described above will generate moments about the hub (except those forces that pass through the hub). In general, this relationship is $\vec{M} = \vec{r} \times \vec{F}$. Because so many components of either the position vector or the force vector are zero, the components of this manipulation will be displayed below.

$$\sum M_X = M_{XR} + M_{XHT} - F_{YTR}\mathrm{z}_{\mathrm{TR}} - F_{Yf}\mathrm{z}_{\mathrm{CG}} \tag{2.77}$$

$$\sum M_Y = M_{YR} + F_{Zf}x_{CG} + F_{Xf}z_{CG} + F_{ZTR}x_{TR} + F_{ZHT}x_{HT} + F_{XHT}z_{HT} \tag{2.78}$$

$$\sum F_Z = M_{ZR} + M_{ZHT} - F_{Yf}x_{CG} - F_{YTR}x_{TR} \tag{2.79}$$

2.3.3 Trim Convergence Procedure

Once these net vehicle loads are known, the control inputs required for trim can be determined iteratively such that the sum of all forces and moments on the vehicle is zero. In this study, the controls are determined through a forward-difference Newton-Raphson method as in Eq. 2.80 . This method uses a (6x6) Jacobian matrix representing the 36 partial derivatives of each net load to a differential control input per Eq. 2.81

$$\vec{\theta}_{n+1} = \vec{\theta}_n - J^{-1}\vec{F}_{Veh} \tag{2.80}$$

$$\vec{\theta} = \begin{Bmatrix} \theta_0 \\ \theta_{1c} \\ \theta_{1s} \\ \alpha_{WL} \\ \phi_f \\ \theta_{TR} \end{Bmatrix}, \ \vec{F}_{Veh} = \begin{Bmatrix} F_{XVeh} \\ F_{YVeh} \\ F_{ZVeh} \\ M_{XVeh} \\ M_{YVeh} \\ M_{ZVeh} \end{Bmatrix}, \text{ and } J = \begin{bmatrix} \frac{\partial F_X}{\partial \theta_0} & \frac{\partial F_X}{\partial \theta_{1c}} & \cdots & \frac{\partial F_X}{\partial \theta_{TR}} \\ \frac{\partial F_Y}{\partial \theta_0} & \frac{\partial F_y}{\partial \theta_{1c}} & & \\ \vdots & & \ddots & \\ \frac{\partial M_Z}{\partial \theta_0} & & & \frac{\partial M_Z}{\partial \theta_{TR}} \end{bmatrix}_{6X6} \tag{2.81}$$

For the swashplateless rotor, the same procedure is used, but with the appropriate control vector and Jacobian, per Eq. 2.82

$$\vec{\delta} = \begin{Bmatrix} \delta_0 \\ \delta_{1c} \\ \delta_{1s} \\ \alpha_{WL} \\ \phi_f \\ \theta_{TR} \end{Bmatrix} \text{ and } J = \begin{bmatrix} \frac{\partial F_X}{\partial \delta_0} & \frac{\partial F_X}{\partial \delta_{1c}} & \cdots & \frac{\partial F_X}{\partial \theta_{TR}} \\ \frac{\partial F_Y}{\partial \delta_0} & \frac{\partial F_y}{\partial \delta_{1c}} & & \\ \vdots & & \ddots & \\ \frac{\partial M_Z}{\partial \delta_0} & & & \frac{\partial M_Z}{\partial \theta_{TR}} \end{bmatrix}_{6X6} \qquad 2.82$$

This procedure is run iteratively until convergence is met. Convergence is typically defined as

$$\left(\%err = \frac{\max(\vec{\theta}_{N+1} - \vec{\theta}_N)}{\vec{\theta}_N} \le Tolerance_{\%err} \right) \cap \left(\max\left(\left| \vec{F} \right| \right) < Tolerance_{Loads} \right) \qquad 2.83$$

Typically $Tolerance_{\%err}$ = 0.1% and $Tolerance_{Loads}$ = 15 (lbs or ft-lbs, which amount to less than .1% of vehicle weight and yield no accelerations in any physical sense). The code flow chart used to model this simulation appears at the end of the chapter in Figure 2-13.

2.3.4 Fuselage and Tail Rotor Model

The fuselage itself is a source of aerodynamic loads and provides a geometric framework upon which the other control and lift producing surfaces are attached. Data taken from wind tunnel tests and detailed in [45] provide the coefficient of lift for the fuselage in a free stream. A least squares regression was performed on this data set yielding Eq. 2.84 for the coefficient of lift (expressed in ft^2):

$$c_{L_f} = 1.0239(-\alpha_{WL})^5 + 12.841(-\alpha_{WL})^4 - 39.558(-\alpha_{WL})^3 - 30.214(-\alpha_{WL})^2 + 106.09(-\alpha_{WL}) \qquad 2.84$$

where α_{WL} is expressed in radians. The negative sign in front of the α_{WL} is required since the angle attack of the fuselage is considered positive nose down. This flat plate lift is multiplied by the freestream dynamic pressure to yield the total lift in lbs:

$$L_f = \tfrac{1}{2}\rho V_\infty^2 c_{L_f} \tag{2.85}$$

The drag of the fuselage was studied by Yeo [46] and his relation was used in this study as follows (although here α_{WL} is expressed in degrees):

$$D_f = \tfrac{1}{2}\rho V_\infty^2 \left(35.14 + .016\left(1.66\alpha_{WL}\right)^2\right) \tag{2.86}$$

Although the fuselage produces a pitching moment, its effect is small and difficult to separate from the empennage effects, which in this study are modeled independently, so this term is omitted. Thus

$$\vec{F}_f = \begin{bmatrix} D_f \\ 0 \\ L_f \end{bmatrix} \tag{2.87}$$

After rotating this force vector through its transformation into the hub frame, these forces can be applied to the body as a whole.

In this model, only tail rotor thrust is considered, and it is calculated using the following closed form solution derived from blade element momentum theory:

$$T_{tr} = \sigma_{tr} a_{tr} \rho \pi \Omega_{tr}^2 R_{tr}^4 \left(\frac{1}{4}\right)\left(\theta_{tr}\left(\frac{2}{3} + \mu_{tr}\right) - \lambda_{tr}\right) \tag{2.88}$$

Tail rotor uniform inflow, λ_{TR}, is calculated using momentum theory using a Newton-Raphson convergence scheme in a similar manner to main rotor inflow. The θ_{TR} term is a control term. All other parameters are given or easily calculable.

2.3.5 Standard Horizontal Tail Scheme

The UH-60 horizontal tail is based on the NACA0014 airfoil. It is rigged to an automatic slewing schedule that keeps it pitched as much as possible into the relative wind as modified by the main rotor wake. The slew schedule, as taken from [47] is represented graphically in Appendix A and is implemented into the code via a piecewise function. Additionally, the main rotor wake creates an offset between the normal orientation of the oncoming flow. This offset is presented in Appendix B, and is represented by χ_{ht} per Figure 2-11, where V_{fus} indicates the freestream velocity seen by the fuselage (generally oriented with the horizon) and V_{ht} is the freestream velocity seen by the horizontal tail.

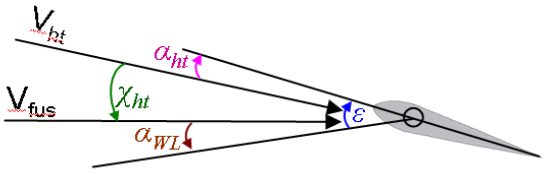

Figure 2-11: Description of α_{ht}

The airloads are generated by the stabilator's interaction with the freestream at a particular angular deflection, α_{ht}. This can be expressed as the sum of the stabilator slew angle, the vehicle angle of attack, and the inflow angle due to the main rotor wake per Eq. 2.89 .

$$\alpha_{ht} = \varepsilon - \alpha_{WL} - \chi_{ht} \tag{2.89}$$

This angle is used to determine the lift and drag via a table look-up based on wind tunnel data for the NACA0012 airfoil as a close approximation to the NACA0014. Since

the airfoil is symmetric, the pitching moments are small and they are neglected. The lift and drag are calculated using these familiar equations

$$L_{HT} = \tfrac{1}{2}\rho V_{\infty}^2 A_{HT} c_{L\,HT} \qquad 2.90$$

$$D_{HT} = \tfrac{1}{2}\rho V_{\infty}^2 A_{HT} c_{D\,HT} \qquad 2.91$$

where A_{HT} is the planform area of the horizontal tail (A_{HT}=45 ft^2 for the UH=60). V_∞ is the freestream velocity as modified by main rotor wake effects. This modification is simply an angular deviation and no attempt is made to increase the free stream velocity due to wake acceleration. The lift and drag forces are then resolved into the hub frame via the transformations given earlier. These transformations require the angular difference between the local flow direction and the aircraft waterline, η_{ht}, given by Eq. 2.92

$$\eta_{HT} = \alpha_{WL} + \chi_{HT} \qquad 2.92$$

2.3.6 Moveable Horizontal Tail Formulation

The moveable horizontal tail utilizes the same stabilator geometry and airfoil of the original UH-60. The only difference is that it is free to move collectively, ε_{coll}, and differentially, ε_{diff}, per Figure 2-12. A positive differential deflection is nose up on the right and nose down on the left (so as to impart a positive roll moment on the helicopter). As such, the aerodynamic angle of attack is evaluated separately for each side as follows:

$$\alpha_{ht} = \varepsilon_{coll} + \varepsilon_{diff} - \alpha_{WL} - \chi_{ht} \qquad 2.93$$

for the right and

$$\alpha_{ht} = \varepsilon_{coll} - \varepsilon_{diff} - \alpha_{WL} - \chi_{ht} \qquad 2.94$$

for the left. Again, in the above equations, χ_{HT} is obtained via table look-up.

The lift and drag of each side of the tail must be determined independently using the Eq. 2.89 and Eq. 2.90. In this case, however, only half of the stabilator's area is considered and each side is evaluated independently. Again, once lift and drag are known, the forces are resolved to the hub frame via the transformation in Eq. 2.68 separately for each side so that the proper moments can be calculated.

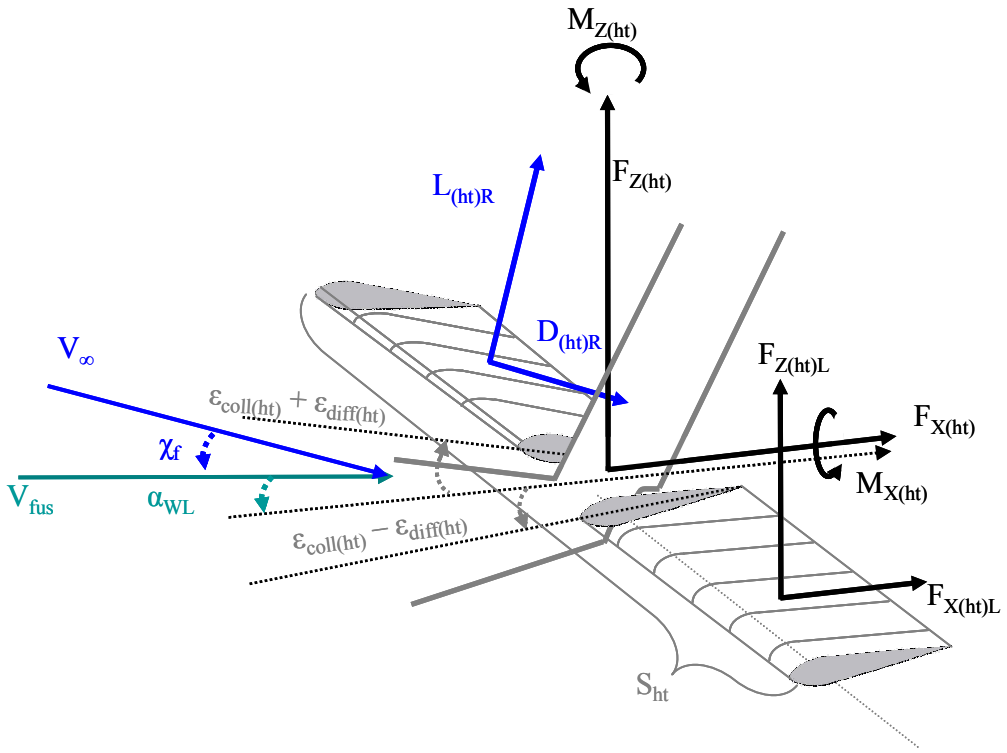

Figure 2-12: Moveable Horizontal Tail Configuration

Because the aerodynamic forces are assumed to act at the mid-span of each side, a difference in lift yields a roll moment, and a difference in drag creates a yaw moment per

Eq. 2.94 and 2.95, where S_{ht} is the span of the stabilator. Of course, the stabilator also provides a pitching moment in forward flight, as given by Eq. 2.97.

$$M_{Y\,HT} = F_{Z\,HT(RIGHT)} \left. S_{ht} \right/ 4 - F_{Z\,HT(LEFT)} \left. S_{ht} \right/ 4 \qquad 2.95$$

$$M_{Z\,HT} = -F_{X\,HT(RIGHT)} \left. S_{ht} \right/ 4 + F_{X\,HT(LEFT)} \left. S_{ht} \right/ 4 \qquad 2.96$$

$$M_{Y\,HT} = \left(F_{Z\,HT(RIGHT)} + F_{Z\,HT(LEFT)}\right) x_{ht} \qquad 2.97$$

2.4 Model Formulation Summary

This chapter has outlined the mathematical model implemented into the computer simulation. It includes a 2- or 3-DOF dynamic rotor model that is attained through coupling the blade response equations with the blade element aerodynamic formulation. These were integrated in time until a steady state response was reached. Blade forces and moments were summed radially and azimuthally to produce hub forces and moments. Additionally, forces generated by all of the other helicopter sub-systems were applied to the hub as well. Trim was reached by finding the control solution that created zero net forces and moments for a given forward airspeed. Figure 2-13 illustrates the flow of the simulation program.

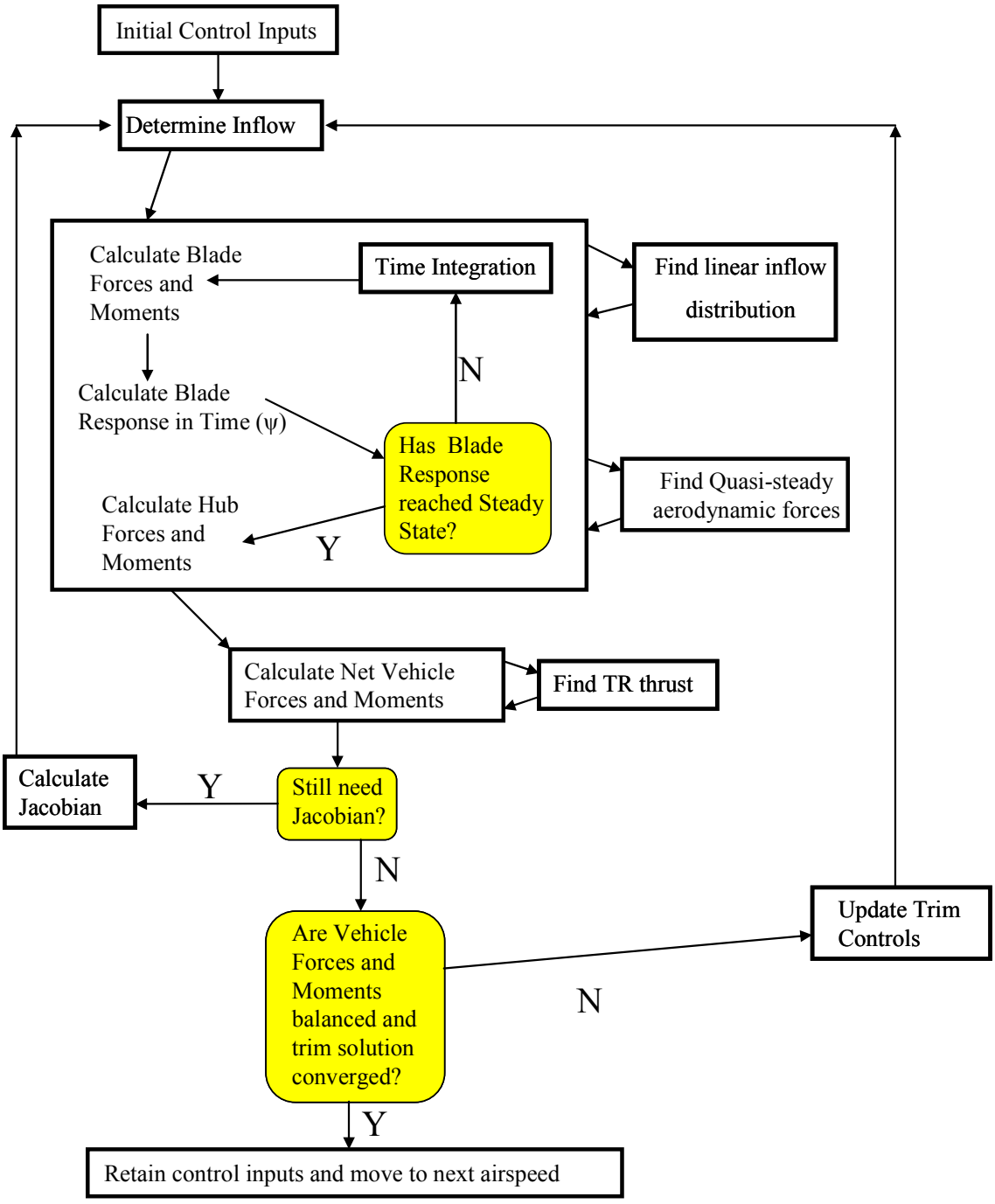

Figure 2-13: Computer Model Flow Chart

Chapter 3

Results and Discussion

This chapter presents the results obtained by applying the analytical model detailed in Chapter 2. Analysis of significant results and physical features worth highlighting are presented. The chapter begins with the simulation results from the conventionally controlled UH-60A. These results are compared to results produced by CAMRAD II and flight test data, which are taken from the NASA-Army UH-60 Airloads Program as summarized by Yeo, Bousman and Johnson in [45]. All subsequent references to CAMRAD II or flight test data in the text or on plots refer to this report. This comparison serves as a validation of the rigid blade model in use for the present study (Section 3.2). Once conventional results are validated, the swashplateless results are presented for a "baseline" swashplateless, TEF-controlled helicopter with a horizontal tail positioned in accordance with the standard schedule. These results are compared to Shen and Falls' work in Section 3.2 as a measure of validation and to identify differences in the analyses. A discussion of these baseline swashplateless results follows in Section 3.4. A parametric study that analyzes pitch index and torsional stiffness will then be covered in Section 3.5 and Section 3.6. After choosing optimal values for pitch index and torsional stiffness, Section 3.7 details the consequences of considering inputs by the moveable horizontal tail. Control inputs are significantly reduced by means of a collectively and differentially actuated horizontal tail. Power implications, and the reasons for these power changes, will also be presented and analyzed. The process will

be repeated for a rotor with higher pre-pitch and for a stiffened rotor in Sections 3.7.2 and 3.7.3 respectively.

3.1 Preliminary Concepts and Discussion

As stated in Chapter 1, there are many technical barriers that stand between the current state of the art and the successful implementation of a swashplateless rotor. One of the more significant of these is the large required TEF deflections currently predicted by other studies. The goal of this study is to demonstrate the effectiveness of *horizontal tail* inputs as a means of reducing the TEF deflection requirements. Although other techniques exist, they will not be considered because their effects have already been established. Some of these different techniques include chord-wise and span-wise sizing of the flap and aerodynamic balance of the flap through the use of flap overhang.

3.1.1 Sizing and Placement of the Trailing Edge Flaps

It is established that larger span-wise flaps can reduce flap deflection magnitude. However this method has several drawbacks. Larger flaps will increase blade weight, present structural integrity challenges, and increase attachment and actuation complexity. Furthermore, a larger flap will operate with more of its control surface in regions of lower dynamic pressure, which lessens its effectiveness. Larger flaps also must deal with the elastic deformation and structural twist of the blade. Therefore, this study focuses on

smaller flaps and study seeks to reduce the elevon deflection requirements via other means.

Although early work [8] pointed to the ability of aerodynamic balance to reduce hinge moments, this study will not explore this technique for two reasons. Flap overhang makes the entire system more complex, harder to actuate, less sturdy, and it is also harder to accurately model its aero-loads. Recent CFD analysis has indicated that introducing flap overhang results in an unexpectedly large loss in lift and moment coefficient increment [22]. The only reason aerodynamic balance was initially considered by designers was to reduce the hinge moment. However, reducing elevon deflections will also yield smaller hinge moments, eliminating the need for aerodynamic balance. Accordingly, hinge moment and actuation power are not presented in this study.

Because flap size and span-wise location will not be the subject of a parametric study in this thesis, these values must be selected based on previous work. For span-sizing, this study will consider only TEF's that are 20% of the rotor radius. This follows recommendations by Shen and is comparable to designs by Kaman. Chord-wise sizing is also an important parameter. Chapter 1 discussed that the maximum pitching moment derivative is achieved with a flap length of 25% chord, but that from 20-30% chord, the pitch moment derivative varies less than 5%. Following the recommendations of Shen once again, a TEF chord of 20% of the base blade is used. Finally, span-wise location of the flap is an important consideration. Shen recommended moving the flap into as high pressure a location as possible. Ultimately, he identified .83R as the best place to locate the mid-point of the TEF. To allow for clearance near the swept tip of UH-60 blade at .93R, a TEF midpoint value of .80R is used (i.e. flap extends from 0.7R to 0.9R).

3.1.2 TEF Deflection Envelope

Earlier researchers have focused on reducing first harmonic cyclic flap deflections at specific airspeeds through pre-pitch, flap sizing, and torsional softening [8, 20]. However, the range of angular deflections that the TEF must meet *across the range of flight speeds* is the most important consideration when comparing the actual TEF deflection requirements among different configurations. Focusing only on high speed flight and its large cyclic flap requirements can cause one to overlook the large positive δ_0 requirement in flight at moderate airspeeds requiring low power. It is critical, therefore, to consider the entire flap deflection envelope required for an entire range of airspeeds, which is defined in Eq. 3.1.

$$\Delta\delta_{TOT} = \max(\delta_{\max}) - \min(\delta_{\min}) \tag{3.1}$$

In addition to the flap deflection envelope, which allows comparisons between different designs, another metric is required to determine a design's suitability with respect to current actuator technology. This value is termed $\delta_{MAX,}$ and it describes the maximum deflection that a TEF must reach considering all airspeeds. If δ_{MAX} is greater than the capability of the piezo-electric actuator under consideration, then the design is not feasible. Based on the results reported by Dieterich [27], a nominal value of ±5° will be used as the current actuator capability for this study. Thus, not only is the entire range of deflections an important consideration, but where this band lies relative to the actuator's ability to deflect a flap to 0±5° is equally important. For example, a rotor with a TEF deflection envelope of 9°, ranging from -4.5° to 4.5° would be preferable to a

design whose TEF deflection envelope was only 6° but ranged from 0-6°. The actuator can meet the demand in the first case, but it cannot in the second. It is essential, therefore, to know the maximum excursion that the TEF is required to make with respect to δ=0. δ_{MAX} is defined in Eq. 3.2, where δ_{high} and δ_{low} represent the lowest and highest value that the TEF takes on at each airspeed.

$$\delta_{MAX} = \max\left(\max(\delta_{high}), \left|\min(\delta_{low})\right|\right) \tag{3.2}$$

3.1.3 Blade Response and Vehicle Attitude

The goal of any control input is to achieve the blade response required to trim the helicopter. One would expect that this blade pitching and flapping response would be similar to the case of a swashplate-controlled helicopter, because the same helicopter is being trimmed in the end. Although the blade pitch values may differ slightly due to the lift increment provided by the TEF, the flapping response should be almost identical and should be relatively independent of factors such as pitch index, torsional stiffness, and flap size. This is demonstrated in the pitch index parametric study and is thereafter not highlighted in later analyses. Furthermore, vehicle attitude should be independent of these main rotor parameters as well, since it is one more step removed from the influence of the TEFs in terms of system response.

3.2 Conventional UH-60 Validation Study

This section will present the comparisons between the rigid blade model developed for this study and the published UH-60 results. The properties of the UH-60 pertinent to this analysis are presented in summary form in Table 3-1 and more comprehensive data on the UH-60 that was used in this work is detailed in Appendix A.

Table 3-1: UH-60 Helicopter and Rotor Properties

Weight	W	18,300	lbs	***Nondimensional Rotating Frequencies***		
hover blade loading	c_t/σ	0.079		1st Flap	υ_β	1.04
Rotor Radius	R	26.8	ft	1st Lag	υ_ζ	2.71
Blade Chord	c	1.73*	ft	1st Torsion	υ_θ	4.27
Blade twist	$\theta_{\tau w}$	varies nonlinearly		***Moments of Inertia (slug-ft^2)***		
angular velocity	Ω	258	RPM	Flapping	I_β	1861
Shaft tilt	α_{Sx}	3°	forward	Lag	I_ζ	1861
Solidity	σ	0.0822		Torsion	I_f	0.978
Induced Power Correction Factor	κ	1.15		Inertial Flap-Torsion coupling	I_x	1.5147
airfoil section		SC1095*	* varies span-wise			

The current trim procedure trimmed the UH-60A configuration up to a forward speed of 170 knots (μ = .40). The following trim plots for this analysis demonstrate reasonable correlation with flight test data and CAMRAD II simulation results. As detailed in Chapter 2, a three degree-of-freedom model was employed in the rotor to model rigid blade in flapping (β), lag motion (ζ), and rigid pitching (θ). Figure 3-1 details the pitch inputs and response for the conventional helicopter. There are significant differences between the pitch input (θ_{in}) and response (θ_{FF}) of the blade. All of the elastic twist and bending that occurs naturally in the blade has been lumped at the

root along with the compliant swashplate, yielding a baseline ν_θ=4.27/rev, which is the reason the static blade response appears to be larger than expected (Figure 3-1**)**. Although lumping the elastic torsional deformation at the root is unrealistic for conventional rotors, it becomes more realistic in the case of torsionally soft rotors whose first elastic torsional mode is 2-3 times stiffer than the pitch spring that has replaced the pitch change link. One can see that the trend in θ_0 matched well with both flight test and CAMRAD II, and that both the values and the trends for θ_{1s} follow CAMRAD II quite well until μ = .32, and this is beyond the speed where swashplateless analysis is conducted.

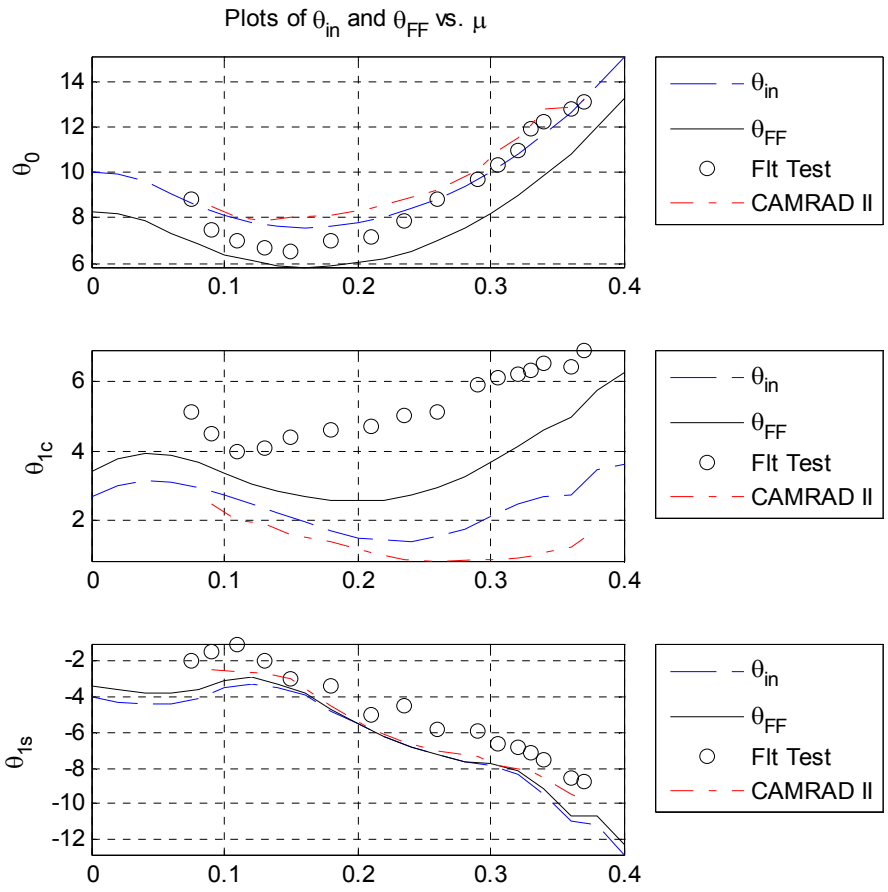

Figure 3-1: Pitch Control and Response, Conventional UH-60

The following two plots (Figure 3-2) demonstrate the blade response to the aerodynamic environment. One can see that there is good agreement in β_0 and ζ_0. Coning follows the trends of the flight test and CAMRAD II, and the mean lagging angle matches the CAMRAD II results. Longitudinal flapping follows the trends closely enough to yield overall results that are satisfactory. The second harmonic response in flapping is also depicted. This response mode remains very small across the flight envelope such that by $\mu = .4$, it has reached a magnitude of 0.72°. Although this baseline result contains negligible β_2, this feature will become more pronounced in the swashplateless case and will begin to affect aggregate vehicle response. The lagging rate is very small (no greater than 1 degree per radian). As such, the tangential velocity component of the blade as a result of lagging motion will be quite small, and its effect on blade flapping and pitching through the Coriolis effect is small enough to be neglected. For this reason, the lag degree of freedom was not used in the swashplateless analysis.

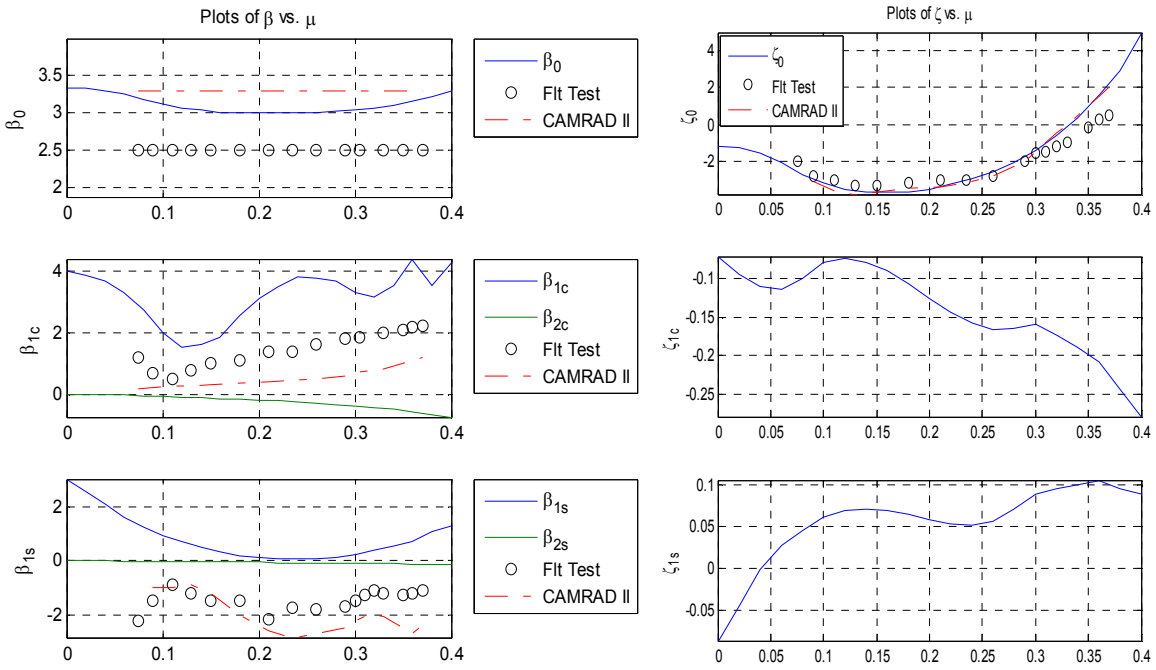

Figure 3-2: Blade Response, Conventional UH-60

The following plots of vehicle attitude in Figure 3-3 demonstrate close correlation with CAMRAD II and flight test data. The pitch attitude of the vehicle at airspeeds above μ=.10 is dominated by the horizontal tail incidence angle and the main rotor downwash effect on the horizontal tail. As discussed in Chapter 2, and expanded upon in Appendix B, the main rotor effects were modeled using a main rotor wake incidence angle, χ_{ht}, that is akin to the commonly used wake skew angle, χ_{MR}. The values of χ_{ht} were chosen to achieve a trimmed pitch attitude equal to CAMRAD II. When the moveable horizontal tail is applied, this same factor is included to model the main rotor wake interference effects. Roll angle appears to correlate adequately with the flight test data. Additionally, Figure 3-4 shows the comparison of power coefficient for each of the three methods. Again, close correlation with both CAMRAD II and flight test is

achieved, due to the use of the induced power correction factor, $\kappa = 1.15$. This result is a basis for making aggregate observations on the effect of various trailing edge flap parameters on power.

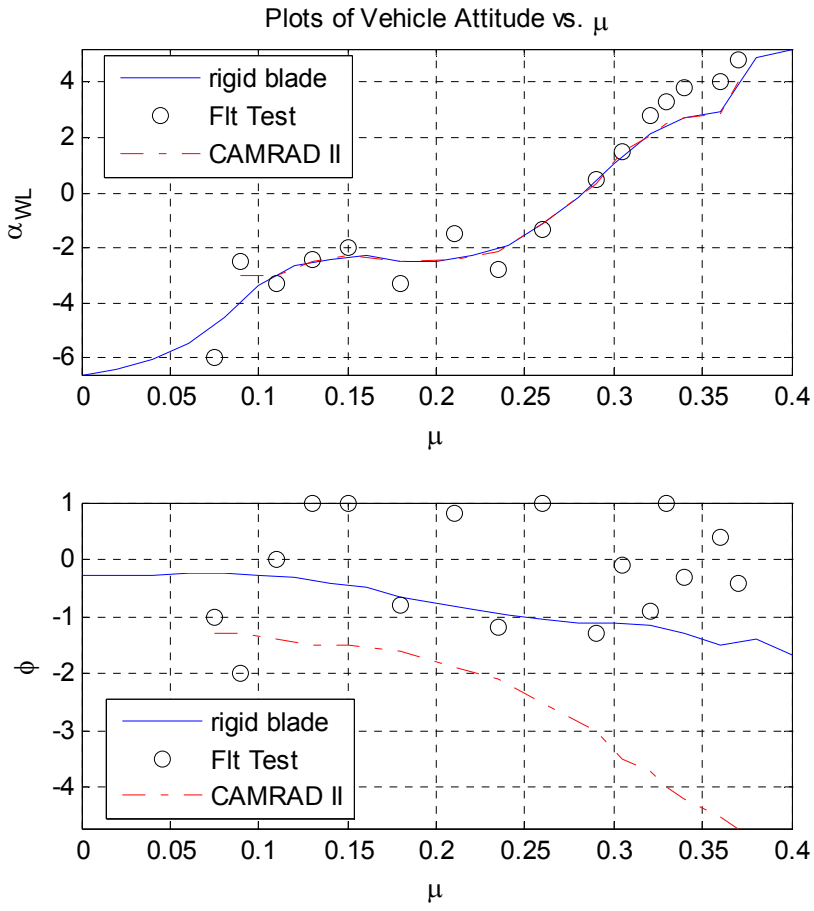

Figure 3-3: Vehicle Attitude, Conventional UH-60

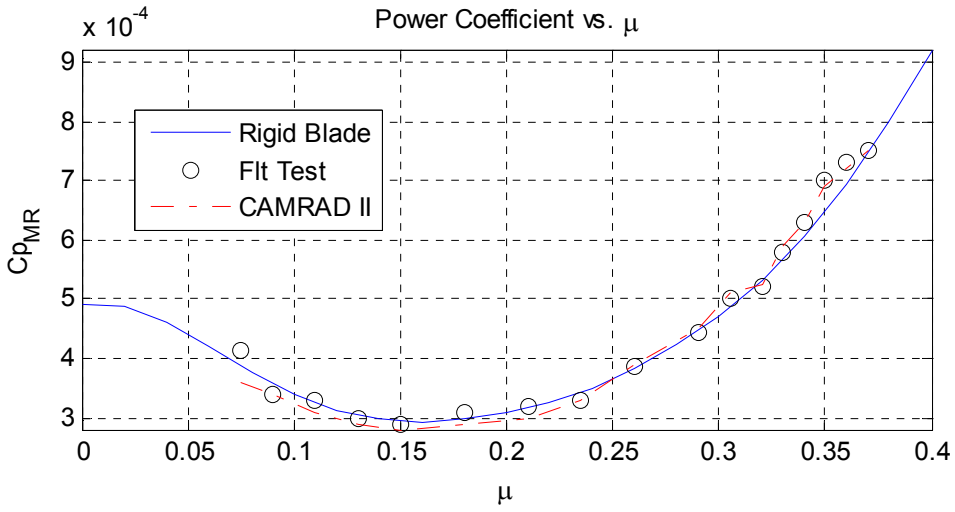

Figure 3-4: Main Rotor Power, Conventional UH-60

In summary, this rigid blade model accurately represents the blade response and vehicle attitude for the UH-60 throughout its flight envelope. This was achieved by incorporating many of the unique features of the UH-60. Since blade response and vehicle attitude are the factors that will most directly effect the analysis with the horizontal tail, the model is satisfactory for the present study. Additionally, the baseline model will serve as a basis of comparison for the performance of the swashplateless configuration.

3.3 Swashplateless Validation and Comparison

The purpose of this section is to present baseline results for a UH-60 with the swashplate removed, torsional stiffness reduced, and trailing edge elevons placed on the

blades to serve as the only method for primary control. All other UH-60 parameters remain the same including CG location, tail rotor cant angle, and built-in shaft tilt. These results will serve as a basis for comparison of the various parameters of the helicopter once parametric studies are undertaken and the horizontal tail is added. Two important parameters that need to be selected as nominal values for this baseline swashplateless configuration are pitch index and torsional stiffness. Based on the work of Falls [20] and Shen [8], the recommended values of $\nu_\theta = 2.1$ and a pitch index of 16° will be used, which also allows for comparison with their work. After these comparisons are made, further analysis of the physics of the swashplateless rotor will be reviewed.

Falls' analysis of a UH-60 [21] provides the most direct basis for comparison of the TEF models. Falls' configuration utilized a flap that was 40% of the blade span and 15% of the blade chord. She published results including both a free wake and a uniform inflow model. Her analysis utilized airfoil-flap look up tables for c_L, c_D, and c_M that were compiled using CFD analysis [22]. Figure 3-5 displays the results for these three cases and illustrates the differences between the three studies. Of note, only collective TEF deflections are published for Falls' uniform inflow case. The trends between Falls' uniform inflow case and the current linear inflow model are very parallel. The difference between the two most likely arises from the smaller (15%) chord-wise flap that Falls used as well as the fact that the CFD tends to under-predict pitching moment [43]. However, Falls' results including free wake inflow are quite different from the current analysis, highlighting the significant effect that aerodynamic modeling differences can have on the system performance and response. However, since the goal of this study is to reduce the flap deflections through fixed frame inputs, the results produced by Theodorsen reported

herein still offer a reasonable basis of comparison for the TEF deflection improvements that may be possible. In fact, since Falls' comprehensive analysis predicts unacceptably large average 1/rev TEF inputs, her work provides an even stronger rationale for adding fixed frame control redundancy in order to reduce TEF deflections, thereby making a swashplateless rotor more feasible. Finally, despite the differences, there are significant similarities between Falls' work and the current analysis. The first is the recognition of a significant second harmonic response in both pitch and blade flapping, and the second is a difficulty in achieving vehicle trim above μ=0.3. Both of these features will be discussed in detail in the next section.

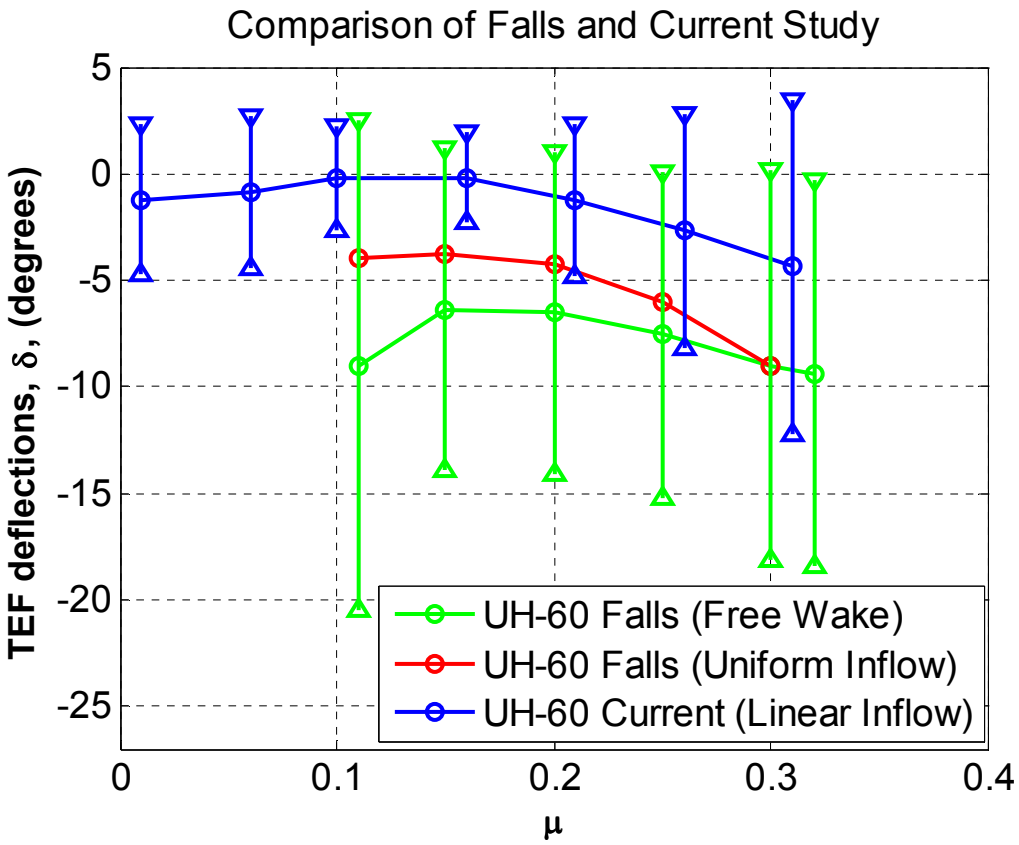

Figure 3-5: TEF Deflection Envelope Comparison

Before proceeding, in light of the discrepancies between Falls' analysis and this work, it would be negligent not to compare current results again Shen's work as well. In Figure 3-6 the current study is compared to Shen's analysis of the MDART rotor [18]. Although the rotors are significantly different, the flap size and location is very similar, and both the trends and the magnitudes of the deflections align acceptably. The difference in δ_0 can be accounted for by the large tip sweep on the UH-60 which does not exist on the MDART. This tip sweep imparts an additional large pitch down moment on the blade. Otherwise, the δ_0 trends are in agreement. Much of the difference in δ_{1c} and δ_{1s} can be accounted for by the unusual hover attitude of the UH-60 and the 3° of longitudinal blade flapping that are required in hover. Aside from the hover values, the δ_{1c} and δ_{1s} values are congruent, as are the corresponding θ_{1c} and θ_{1s}.

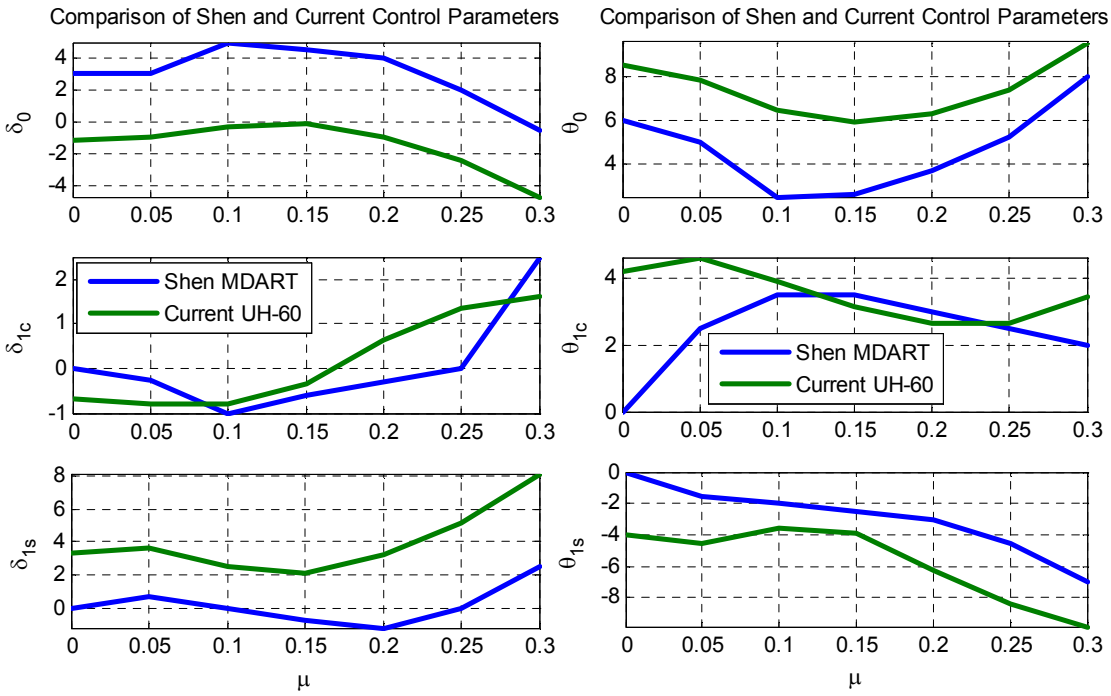

Figure 3-6: Elevon Inputs and Pitch Response Comparison

Since the differences between Shen and Falls' analysis and the current study can be accounted for, the current model is sufficient to judge the effectiveness of the horizontal tail. Additionally, despite some shortcomings in the Theodorsen elevon model used in this work, many of the trends and physical effects that are observed offer insight into all of the physical interactions that need to be understood and accounted for in designing a TEF-controlled rotor.

3.4 Swashplateless Baseline Analysis

The baseline analysis serves as a point of departure for both parametric studies and for the horizontal tail analysis. It also provides an opportunity for the unique physics of the swashplateless rotor to be reviewed so that further study is well-grounded. Figure 3-7 displays the control inputs that are required to trim the helicopter over various airspeeds. One can see that δ_0 starts slightly below zero, increases slightly at moderate speeds and then trends sharply negative with increasing power demands as the aircraft reaches high speeds (μ>0.25). This negative flap deflection imparts a nose up collective motion on the blade, causing it to fly at higher values of pitch. The collective pitch for the swashplateless aircraft is a little bit higher than on the conventional helicopter because the negative flap input results in a reduction of lift from the blade and the pitch must increase to compensate. Lateral flap input (δ_{1c}) generally increases with speed, although its range is small. This control imparts the required lateral flapping to counter the tail rotor thrust and otherwise laterally balance the forces and moments on the helicopter. As in the conventional case, this effect is small. Longitudinal flap inputs (δ_{1s})

start at a moderate level, and generally increase throughout the speed range, with the rate of change increasing as well at higher speeds. These positive values of δ_{1s} yield a positive flap deflection on the advancing side and a negative value on the retreating side. This corresponds directly to the negative θ_{1s} that is required of conventional helicopters, and one can see the correlation in Figure 3-7.

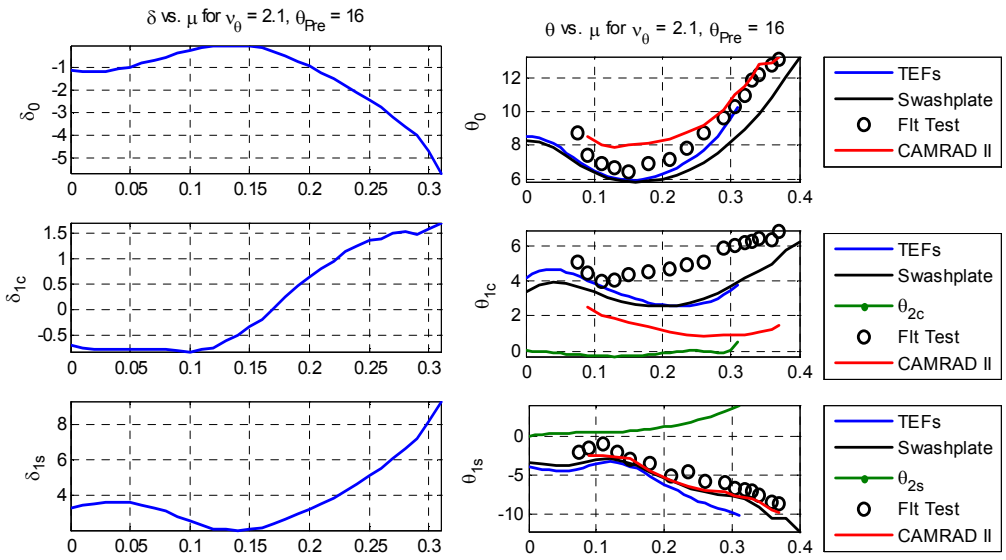

Figure 3-7: TEF Deflections and Blade Response, Baseline Swashplateless UH-60

Additionally, the swashplateless helicopter only achieves trimmed flight up to μ=.31. This is largely due to two phenomena. The first is that the increasingly negative δ_0 required at high speed requires an increasingly large δ_{1s}. Lift dissymmetry that prevents trim is reached much faster than in the conventional configuration since the negative collective TEF input is removing lift from the rotor at all points around the disk.

Although higher pre-pitch or lower stiffness can delay this effect to a higher airspeed, it is an inevitable feature of TEF-controlled helicopters that limits their forward speed.

The second reason that difficulty in trim is encountered is the emergence of the second harmonic response in pitch. Falls also noted this response [22] and likewise had difficultly in achieving a converged blade response coincident with the rise of this second harmonic pitch response. As airspeed increases, the components of the aerodynamic forcing that contain second harmonics increase in magnitude. Since the natural frequency of the pitch degree-of-freedom is very close to this value, these modes are excited and their influence affects the overall response. Although the phasing of the second harmonic response is important and must be treated in each case individually, most of the second harmonic response can be described by θ_{2s}. Since this causes the blades to fly to a non-optimal value at certain points around the disk, an increase in required power is realized, which also impedes the ability to trim. No attempt in this study has been made to reduce or mitigate the effects of the second harmonic. It represents a barrier under which the trim must be accomplished. However, mitigating this second harmonic response may prove to be an important area for continued research.

In addition to elevon and blade pitch response, the plots of vehicle attitude and blade flapping demonstrate that the blade and vehicle response one and two steps removed from the control mechanism are almost identical to the baseline case. One difference that appears is again tied to the emergence of a second harmonic response in blade flapping (Figure 3-8). Since higher second harmonic response is excited in the swashplateless case, the first harmonic results must change slightly from the conventional results to compensate. Vehicle attitude is almost identical in both cases, as expected.

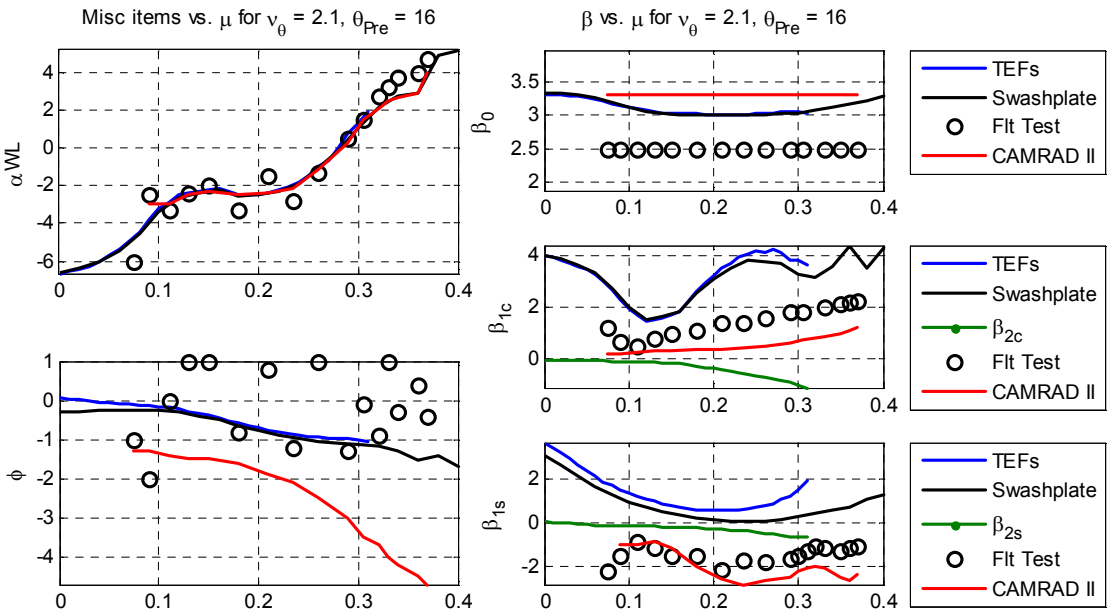

Figure 3-8: Vehicle Attitude and Blade Response, Baseline Swashplateless UH-60

Although the switch to the TEFs had only a small effect on blade flapping and vehicle attitude, it has a larger effect on power, as can be seen in Figure 3-9**.** Using the drag model developed in Section 2.2.3, the power is greater than the baseline across the flight envelope, and the power penalty associated with the TEF deflections grows with airspeed, primarily due to the ever-larger $-\delta_0$ that is required and the higher-than-normal θ_0 that results. As represented here, this power penalty ranges from 175 horsepower (or 10%) at hover to 562 horsepower (or 32%) at μ=0.3. As it currently stands, this is an unacceptable power penalty, although it should be noted that no attempt to reduce the fuselage equivalent flat plate drag has been made as a result of removing the swashplate and pitch links. Additionally, one may note that, as described in Section 2.2.3, the conservative drag model for the TEFs was chosen because it is never less than the best CFD data available. It shows close correlation at some Mach Numbers and α's, but it

often over-predicts the TEF drag. As such, it is also worthwhile to examine the power predictions of the rotor with the drag increment removed from the analysis. Interestingly, power is still worse than the conventional helicopter. This is due to the fact that at the chosen θ_{Pre} and ν_θ, δ_0 is always negative. The negative flap deflection removes lift, requiring a higher than necessary blade pitch, which increments the drag above the conventional helicopter accordingly. As will be more fully demonstrated in Section 3.5, pitch index has a dramatic effect on power.

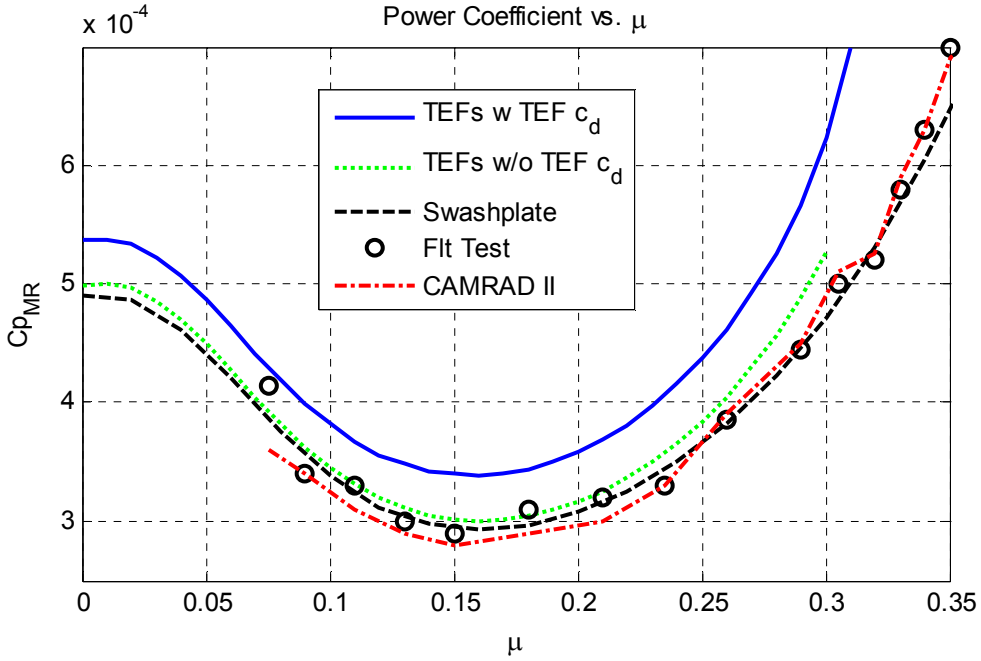

Figure 3-9: Main Rotor Power, Baseline Swashplateless UH-60

In order to better assimilate the results to come, it is useful to see where the power can be influenced by the introduction of the trailing edge flaps. Power is typically classified in terms of induced power, profile power, and parasitic power. All three of these components will be affected by the introduction of both trailing edge flaps and a moveable horizontal tail. Parasitic power is the most straightforward to analyze. Since

this study cannot account for the reduction in drag due to removing the swashplate assembly and streamlining the hub, the only parasitic power consequences come from changing the overall fuselage attitude and from a small increment that may arise from flying the horizontal tail at a higher angle of attack. In general, this will place the current design at a disadvantage. The profile power of the rotor with TEFs added is a complex matter to analyze since it involves many different drag coefficients, multiplied by different dynamic pressures, acting at different moment arms just in one rotor revolution. Needless to say, anything beyond the most modest TEF deflections will result in increased profile power. Generally, negative δ_0 will also require higher power since it causes the entire blade to fly at a higher collective pitch than necessary, and the amount of drag reduced at the flap location is small in comparison. Induced power is likely to be the hardest to grasp and calculate, especially in the absence of a sophisticated wake model. Although the lift and induced flow may be beneficially re-distributed in a span-wise direction due to flap deflections, the average inflow, λ_0, may increase based on the vehicle and rotor attitude with respect to the relative wind. In general, greater disk tilt will yield higher inflow and more induced power. However, this effect is mitigated by the fact that the overall disk tilt shouldn't change significantly from the baseline configuration to the TEF and horizontal tail design—only the means of achieving a particular disk angle will change.

Because power implications are always on the mind of the designers, it is important to choose a drag model that predicts an appropriate increment in drag based on the combination of α, δ, and Mach number rather than neglecting this important aspect of the analysis. As such, all the subsequent results presented in this thesis utilize the TEF

drag model introduced in Section 2.2.3. Recognizing that this model over-predicts drag in many cases (and never under-predicts drag), no further comparisons between the conventional helicopter performance and the TEF-controlled rotor will be discussed. However, the consistent use of this study's drag model will allow for power comparisons once the horizontal tail is added.

To summarize this section, the helicopter is trimmed in the same way—blade pitch creates the steady hub forces and moments required to trim. Only a small change in thinking is required in order to understand the effect of the flap deflections on the blade pitch. The typical $-\theta_{1s}$ that is required of most helicopters in forward flight is produced by a $+\delta_{1s}$. Additionally, power increases with the use of trailing edge flaps. Whether this power increase can be reduced to a level that is offset by the benefits of removing the swashplate remains to be seen. Additionally, one must also be aware of secondary effects such as the second harmonic pitch response.

3.5 Parametric Study of Pitch Index

As mentioned earlier, this parametric study has very little effect on blade response and no effect on vehicle attitude, except at the highest airspeeds, as can be seen in Figure 3-17 (flapping response), Figure 3-18 (vehicle response), and Figure 3-19 (blade pitch response) at the end of this section. Most of this analysis, therefore, will focus on the effect of pre-pitch on the control inputs required of the trailing edge flaps. The study will use a rotating non-dimensional torsional stiffness of $\nu_\theta = 2.1$/rev because both earlier studies utilize a value very near 2.0 for their studies as well. As mentioned earlier,

Kaman helicopters use a variety of pre-pitch values on their different airframes, from 5° to 27° [10]. Previously, Shen and Falls conducted research in this area on rotors with 15°, 16°, and 18° of pre-pitch [15, 21]. Since this study focuses on the UH-60, it must consider higher values of pitch index for two reasons. First, the SC1095 airfoil produces a negative pitching moment at almost all Mach number and angle of attack combinations commonly experienced by the blade. Secondly, the swept rotor tips add a significant nose-down pitching moment at all flight speeds and positive blade angles of attack.

The most basic analysis demonstrates that higher pre-pitch has a direct impact on the δ_0 requirements (Figure 3-10). For reasons that shall be explained in the forthcoming discussion, a positive δ_0 has favorable effects on the ability to achieve trim at high airspeed, the 1/rev TEF range at a given airspeed, and power. Typically, the higher the pre-pitch the more flap deflection is required to generate the nose-down moment required to achieve the desired blade response and trim the helicopter. As more and more thrust is required, especially at higher airspeed, eventually the TEFs reach their δ_0 crossover point and they take on negative values in order to pitch the blade to a higher value than the free flight value with no TEF input. This point is delayed to a higher airspeed for high values of pre-pitch. Finally, the difference in the amount of flap deflection required by different pitch index values is rather insensitive to airspeed.

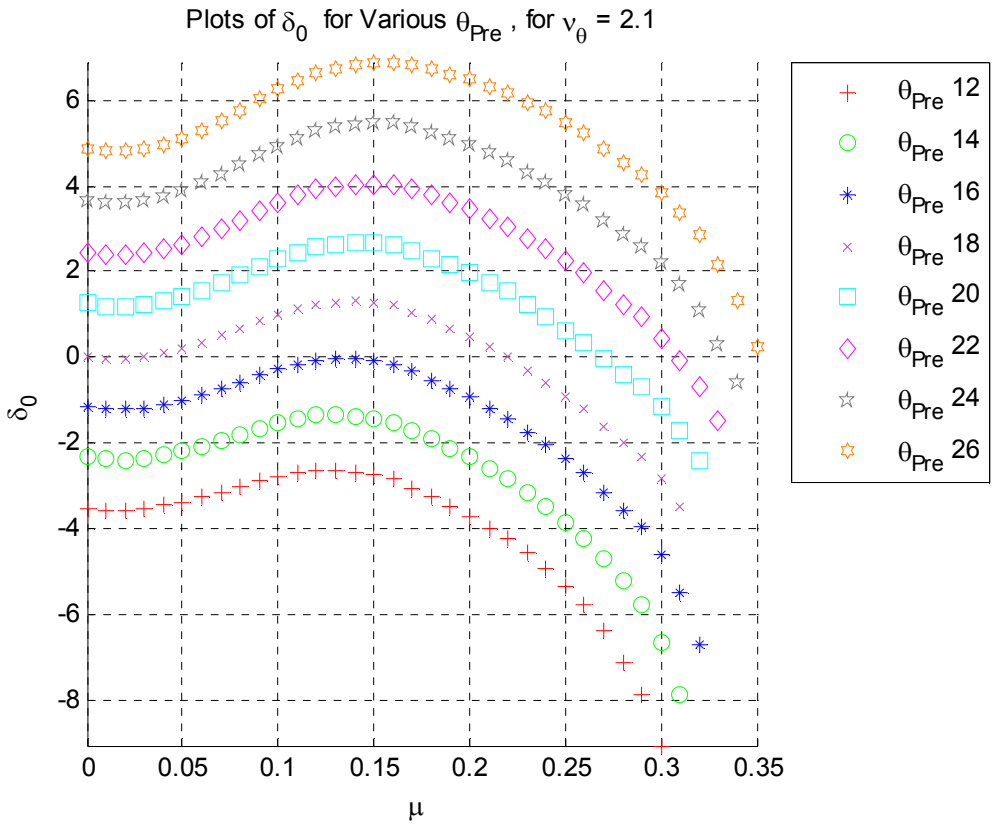

Figure 3-10: Collective TEF input vs. μ, Various values of θ_{Pre}

In addition to the effect of pitch index on δ_0, one can see a significant effect on 1/rev TEF inputs (δ_1) in Figure 3-11. This effect is dependent on airspeed with no difference among pre-pitch values at hover and significant differences at higher speeds. This feature is directly related to the δ_0 values that were discussed above. In high speed flight, as lower and lower blade pitch is required on the advancing side, positive flap inputs are required on the advancing side to achieve this low blade pitch as depicted in Figure 3-12 . However, if the low pre-pitch value has already caused a negative δ_0 to be required, even higher values of δ_{1s} are required to present an overall positive TEF deflection on the advancing side.

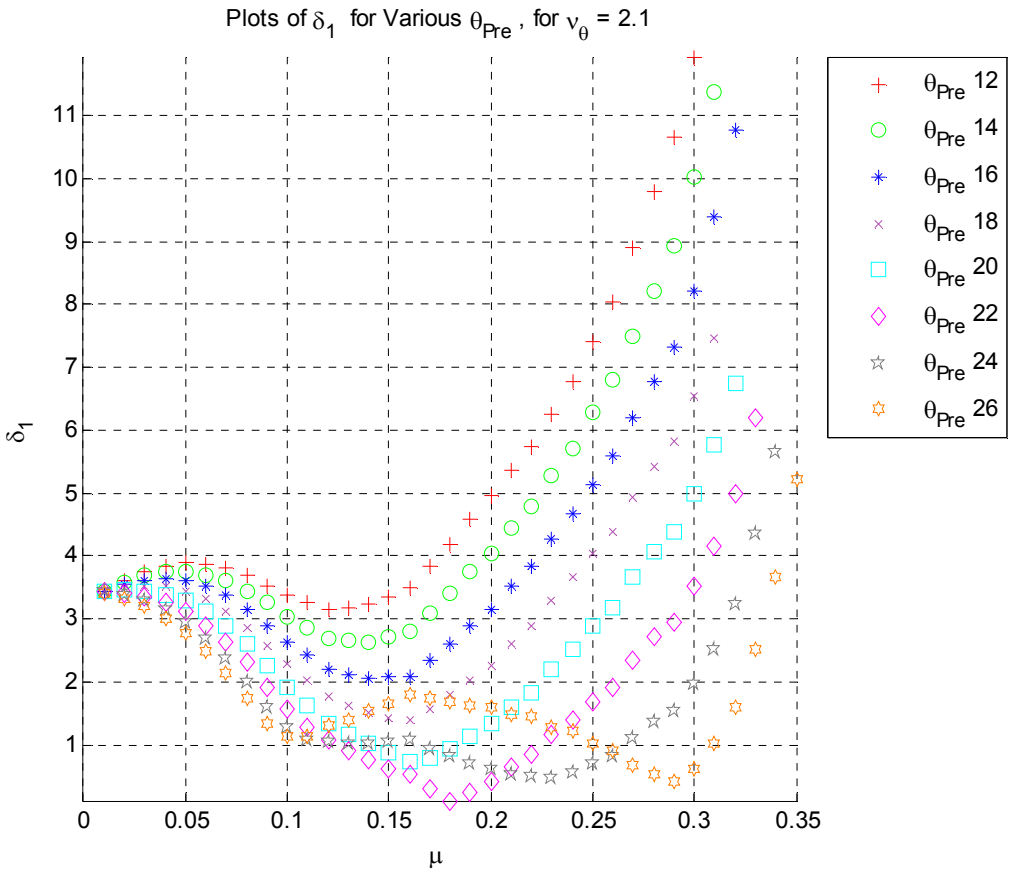

Figure 3-11: Differential TEF input vs. μ, Various Values of θ_{Pre}

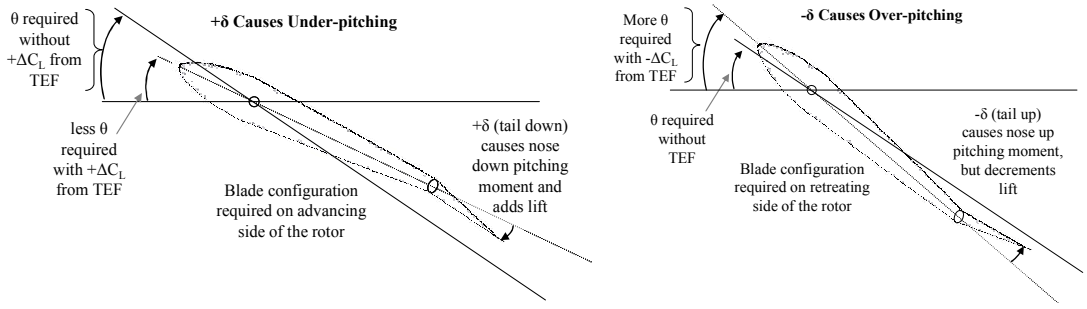

Figure 3-12: Pitch-Flap Combination Required on Each Side of the Rotor

Another interesting feature of pitch index is the ability to trim to higher airspeed with higher pre-pitch. This phenomenon is a result of two features of TEF-controlled rotors that are soft in torsion. At high speed flight, in order to achieve a desired blade flapping response for propulsive trim at a given vehicle attitude, torsion stiffness and pre-pitch, an azimuthal variation of lift must be achieved on the advancing and retreating side of the rotors. This azimuthal variation in lift will derive primarily from the difference in blade pitch on each side as in a standard helicopter. Table 3-2 outlines the pitch requirements on the advancing and retreating side for two cases of pre-pitch. Based on the pre-pitch and required flapping, the helicopter needs to achieve just under 0° pitch on the advancing side and approximately 18-19° pitch on the retreating side, regardless of configuration. However, in order to get this blade pitch response, significantly different TEF inputs are required. For higher pre-pitch, slightly more $+\delta$ is required on the advancing side and much less $-\delta$ is required on the retreating side. The average between them will dictate δ_0. Since $-\delta_0$ removes lift from the rotor, the size and sign of δ_0 will determine whether enough thrust can be produced by the rotor to balance the weight and drag. The more negative δ becomes, the less likely it will be able to achieve an average blade pitch high enough to offset all of the lift removed from the rotor via the negative flap deflection. Once again, this demonstrates the advantage of higher pre-pitch.

Table 3-2: Pitch and TEF Requirements at ψ=90° and ψ=270°

In order to achieve these values of pitch, the rotor requires…			...these values of TEF inputs		Average the two to get	
	θ		δ		δ_0	
	ψ=90°	ψ=270°	ψ=90°	ψ=270°		
θ_{Pre}=16°	-0.24°	19.42°	3.6°	-13°	-4.7°	Large negative
θ_{Pre}=20°	-0.48°	17.82°	3.88°	-6.32°	-1.22°	Minor negative

Secondly, the high pre-pitch values also delay the emergence of the second harmonic response in pitch (Figure 3-13). This feature was explained in the preceding section, but it is important to note that this delay exists, and is most likely tied to the negative δ_0 deflections as well.

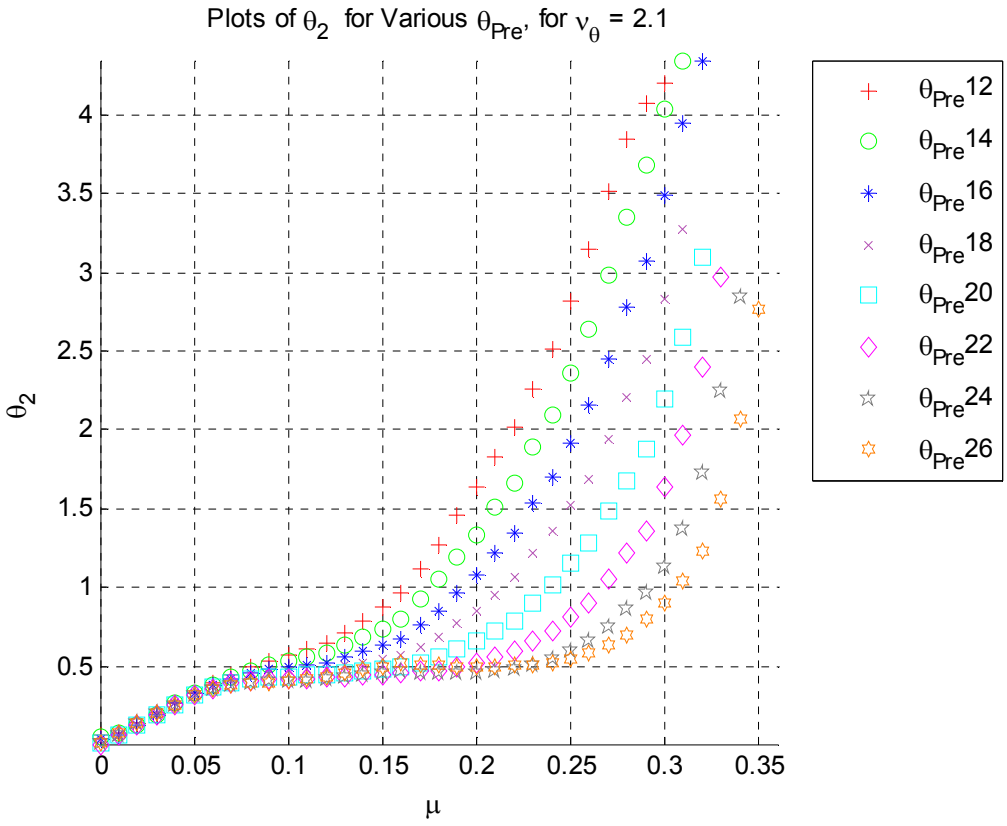

Figure 3-13: Growth of Second Harmonic Pitch vs. μ, Various Values of θ_{Pre}

Figure 3-14 depicts the power consequences of pre-pitch, a feature that is dominated by the profile power of the rotor. Generally, profile power is minimized when TEF deflections are kept as low as possible, at all azimuths. Focusing on high speeds, where the power differences are more apparent, higher θ_{Pre} translates directly to power savings. This is because higher pre-pitch delays the δ_0 cross-over point. With increasing

airspeed and $\delta_0<0$, the system is in a losing battle in terms of producing thrust. It may be able to generate a required level of thrust with negative δ_0, but it must do so in a condition that requires much more power than should be required because the blade must over-pitch in order to compensate for the loss in lift due to the negative flap deflections. Also, once δ_0 is negative, the nose-up pitching moment produced by the TEF is now working against the significant nose-down pitching moment of the base blade. Rather than working in concert with the nose-down tendencies already resident in the rotor system, it must overcome them. This yields ever-larger 1/rev TEF deflections, which also translates into higher profile power. This situation very quickly becomes a case of diminishing returns. On the other hand, with high enough pre-pitch, δ_0 takes on small positive values at high speeds since the blades do not need much collective pitch down moment. Additionally, the 1/rev deflections also decrease hand-in-hand per the discussion related to Table 3-2. Thus, small collective and 1/rev TEF deflections keep profile power low and the $+\delta_0$ allows the blade to fly at a slightly smaller collective value than otherwise, further decreasing power. Lastly, higher pre-pitch enables the tendency of a torsionally soft rotor to self-trim into an oncoming flow. The detailed discussion of this phenomenon is delayed until the torsional frequency study in Section 3.6.

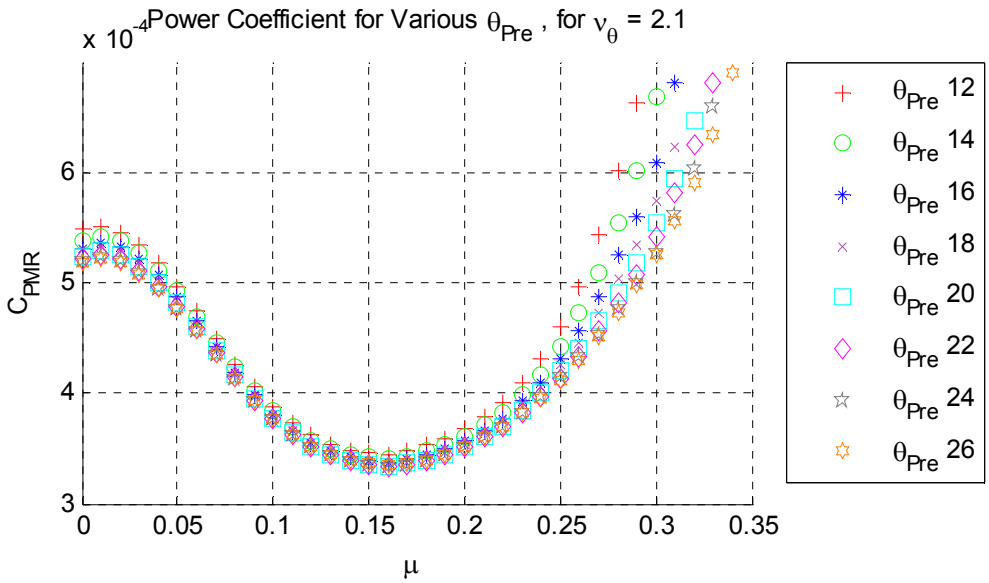

Figure 3-14: Power Coefficient vs. μ, Various θ_{Pre}

While high speed power savings with high pitch-index may be straightforward, one expects to pay a power penalty at speeds that require much lower collective pitch. Figure 3-15 presents a closer look at this flight regime. In this case, the lower pre-pitched rotors are still at a disadvantage. Rotors whose values of θ_{Pre} are so low that they always require a $-\delta_0$ will always demand more power. Looking back at Figure 3-7, one can see that θ_{Pre}=16° always requires $-\delta_0$. Beyond 20° of pre-pitch, the highest pre-pitched rotor technically consumes more power, but the increase is almost unchanged (less than 5 horsepower) and is not significant enough to offset the large advantages of large pre-pitch at higher speeds.

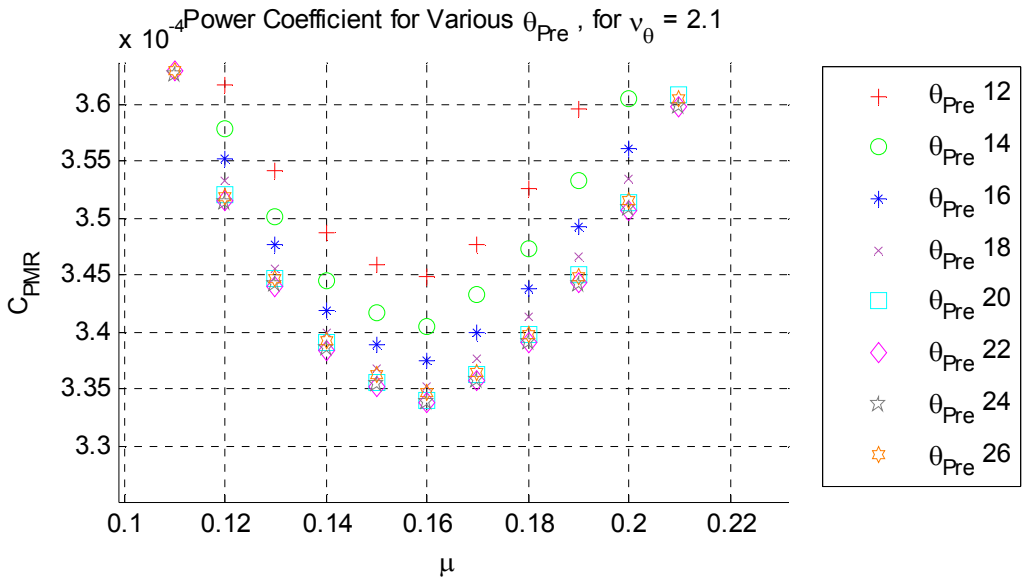

Figure 3-15: Power Differences at Moderate Speeds, Various θ_{Pre}

As mentioned earlier, pre-pitch values that require large $-\delta_0$ at high speeds have a detrimental effect on the TEF deflection envelope. Indeed, the flap deflection envelope, $\Delta\delta_{TOT}$, and the maximum flap deflection, δ_{MAX}, are the most limiting metrics to be considered in this parametric study. As defined in Section 3.1.2, the flap deflection envelope comprises the total absolute deflections required of the TEF from positive to negative across a range of flight speeds. As pre-pitch increases, the flap deflection envelope both moves across all airspeeds, and it also shrinks at high speeds. The movement of the entire flap deflection envelope is easy to grasp. When the blade is pitched to a higher starting value, more δ_0 is required to bring it to a desired level of pitch. However, as was explained in detail in the discussion pertaining to Table 3-2, higher values of pre-pitch also require a less negative δ_0. This results in a shrinking of the TEF deflection envelope at the high speed end. Thus, if $\Delta\delta_{TOT}$ is sufficiently small,

but lies above or below the actuator capability band, it can be brought within the band by adjusting θ_{Pre}.

Even more important than the flap deflection envelope, the maximum flap deflection is highly dependent on pitch index. δ_{MAX} is defined in Section 3.1.2 as the single largest deflection magnitude that the flap must reach within the flight envelope. This parameter relates directly to the external constraints that exist on the flap deflection requirements, most notably actuator stroke limit. The assumption throughout this thesis is that the band of actuator capability is ±5°, represented by the black dashed lines in Figure 3-16. As θ_{Pre} increases, the δ_{MAX} decreases dramatically. However, where δ_{MAX} occurs in the flight envelope also begins to change. With low values of pre-pitch, the δ_{MAX} always occurs at the highest speed and it is always negative. With the highest values of pre-pitch, the δ_{MAX} occurs in hover, and the combination of large δ_0 (from with large θ_{Pre}) and the δ_1 required in hover for a UH-60.

In terms of selecting a recommended value of θ_{Pre} to utilize in the studies to come, one must consider both $\Delta\delta_{TOT}$ and δ_{MAX}. The flap deflection envelopes for pre-pitch values of 16° is almost $\Delta\delta_{TOT}$ =17°. For θ_{Pre} = 22° the deflection envelope is only $\Delta\delta_{TOT}$=7°, but all of the low speed values (which cannot be assisted by horizontal tail), lie outside the 5° limit. Indeed, both the θ_{Pre}=20° and the θ_{Pre}=22° rotors have the same δ_{MAX}=6°, but the θ_{Pre}=20° case exceeds the 5° limit above μ=.30. Knowing that the goal of this study is to reduce elevon deflections at high speed through tail inputs, one can select a pre-pitch value whose TEF deflection requirement lie inside the physical limits of the actuator for low speeds, and exceed it only at high speeds where the horizontal tail would become effective. In this case a pre-pitch value of 20° is the most acceptable.

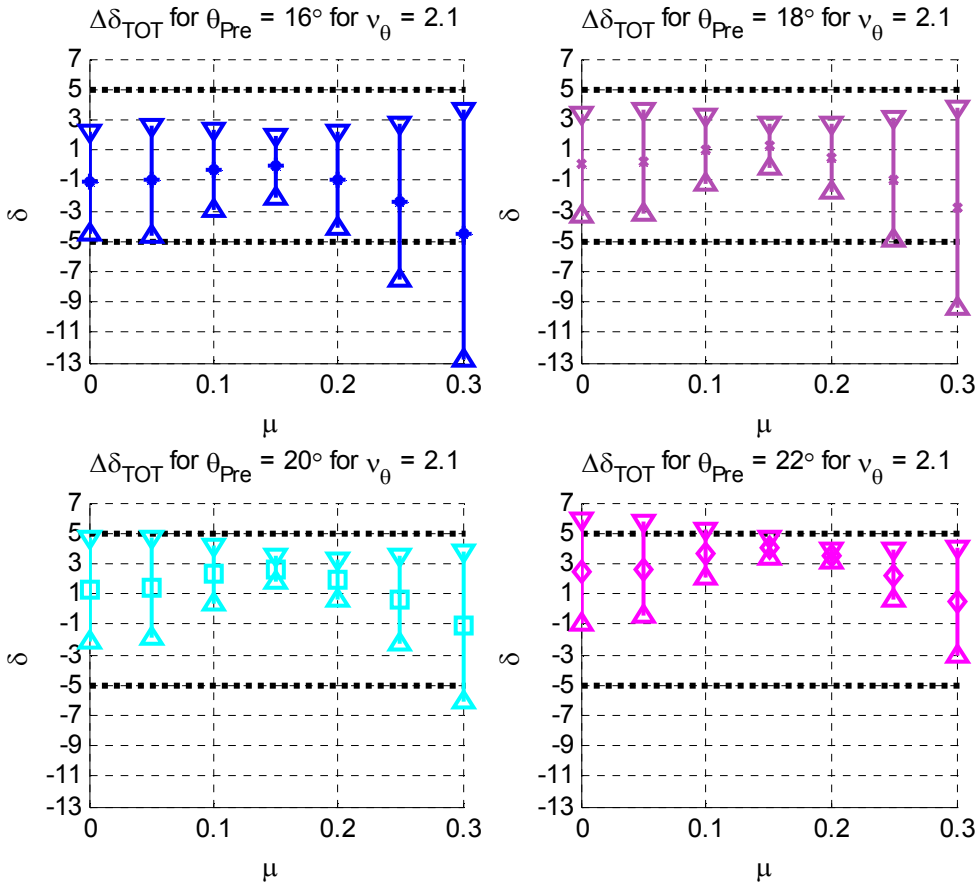

Figure 3-16: TEF Deflection Envelope, Various Values of θ_{Pre}

Although the discussion so far has pointed to the many advantages of higher pre-pitch, especially in the absence of external constraints, higher pre-pitch does come with several tradeoffs. The first can be seen back in Figure 3-10**.** A higher pre-pitch angle requires larger positive TEF deflections in flight at moderate airspeed. Too high a pre-pitch can result in an unacceptably high (positive) flap deflection at moderate speeds. Additionally, with a large pre-pitch, one is presented with the practical problem of managing rotor thrust and vehicle control during the start and run-up of the aircraft as well as concerns over the ability to successfully autorotate the helicopter. Although these

concerns are not directly addressed in this study, their importance will reinforce the selection of a pre-pitch value that may appear to be sub-optimal from the standpoint of the TEF deflection magnitudes alone. For these reasons, pre-pitch value of 16° and 20° will be investigated throughout the thesis.

The last aspect of pre-pitch that needs to be demonstrated is the effect of pre-pitch on blade pitch, rotor flapping and vehicle attitude. As described in Section 3.1.3, rotor blade and vehicle response will be insensitive to the intra-rotor parameters such as pre-pitch, torsional stiffness, flap sizing, etc. This is demonstrated for the pre-pitch case as it relates to blade flapping (Figure 3-17) and aircraft pitch (Figure 3-18) and roll attitude. However, blade pitch will be affected by the change in lift produced by the local flap deflection with respect to azimuth. As described earlier, the goal of any control system is to achieve the required azimuthally distributed lift to trim the helicopter. Thus, the same helicopter at a given airspeed will have the same azimuthal distribution in lift regardless of the control method employed. However, the pitch required to achieve this lift distribution will vary based on the increment or decrement in lift that the TEF is contributing to the blade at each azimuth. This stands out most clearly in Figure 3-19 where θ_0 is plotted for various values of θ_{Pre}. For lower pre-pitch, the TEF must fly at a negative deflection, removing lift and requiring higher pitch at all flight speeds.

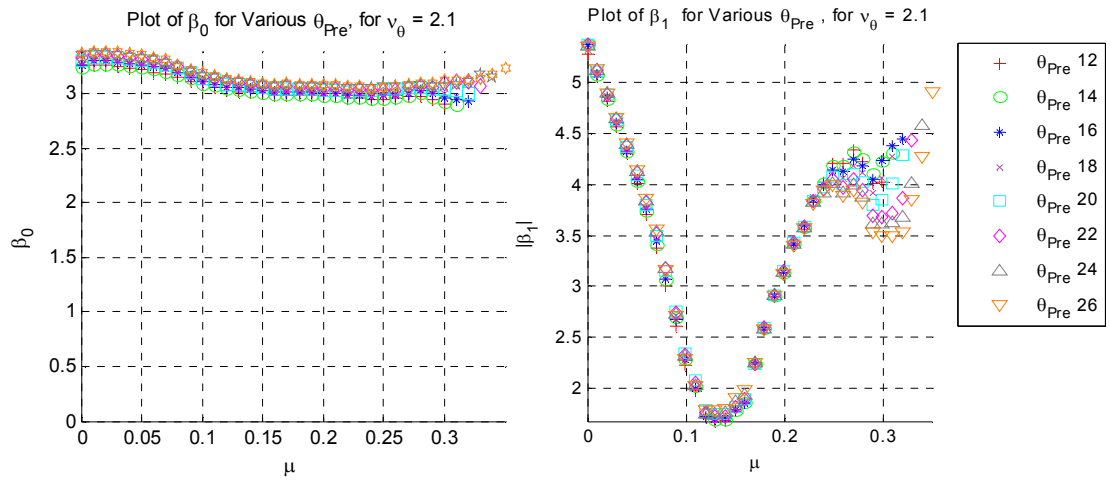

Figure 3-17: Blade Coning and Flapping Response for Various θ_{Pre}

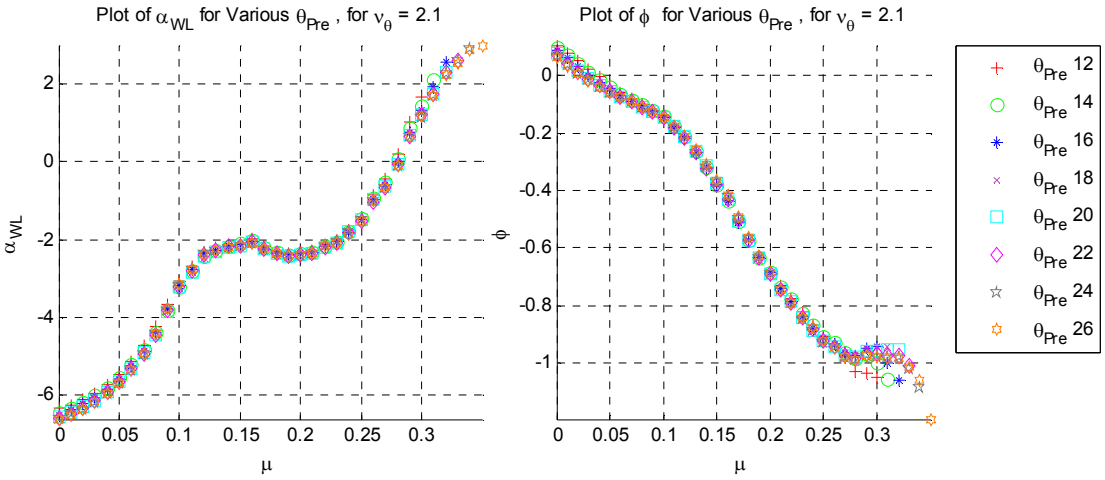

Figure 3-18: Vehicle Attitude for Various θ_{Pre}

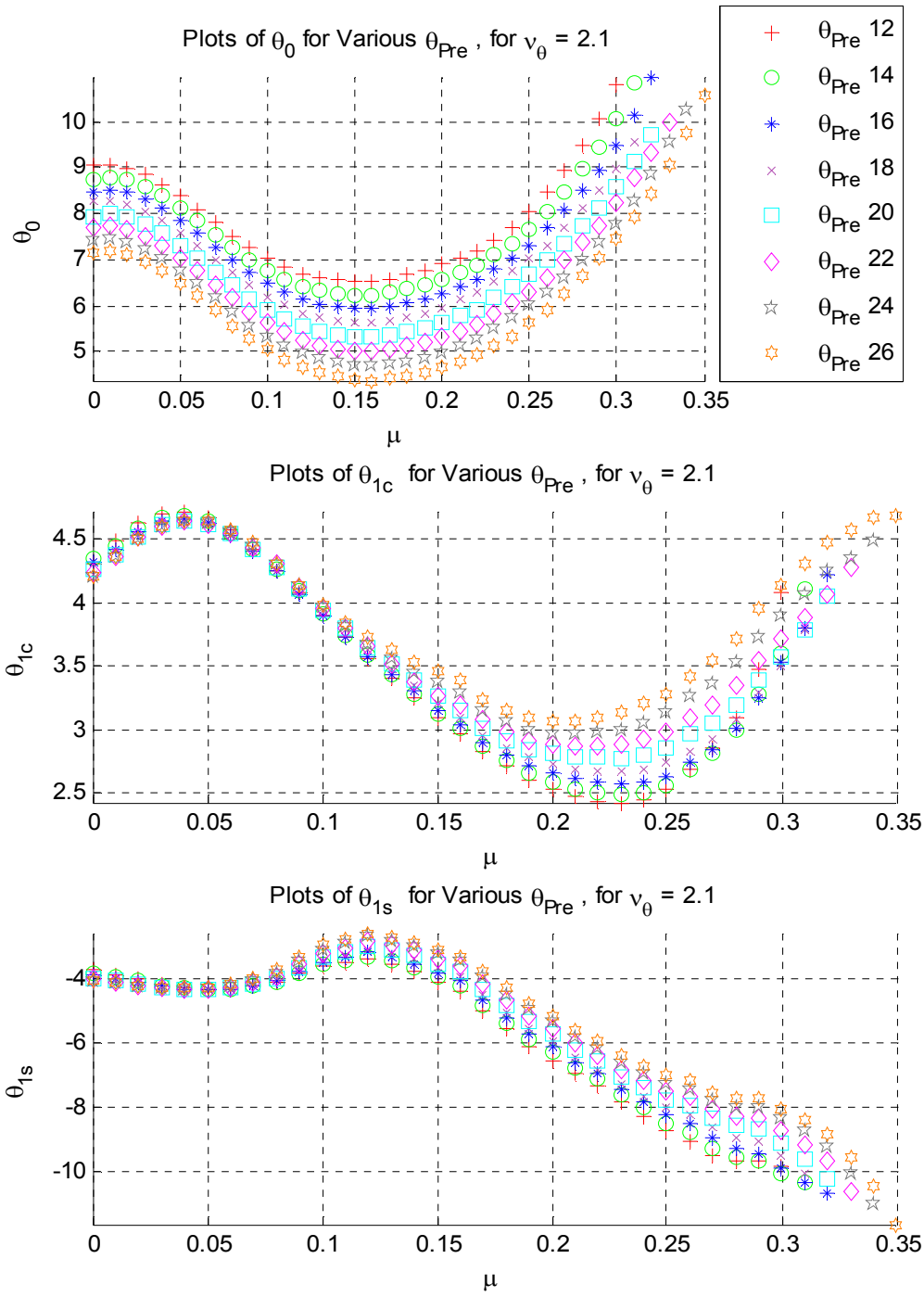

Figure 3-19: Blade Pitch Response for Various θ_{Pre}

3.6 Parametric Study of Torsional Stiffness

Once again, since blade response and vehicle attitude are only marginally affected by changing the blade root torsional stiffness, the focus of this portion of the study is on the effect of torsional stiffness on TEF deflection requirements. One expects the trailing edge flap requirements to decrease with decreasing torsional stiffness, because the root spring produces a smaller restoring moment for the aerodynamic forces to overcome. However, the rate of this change and its impact on other parameters is also important.

As stated in Chapter 2, torsional stiffness is represented by the non-dimensional rotating natural frequency of the blade in the pitching mode (ν_θ). This value is derived primarily from the root spring torsional stiffness (expressed in ft-lb/radian or ft-lb/deg). For reference, Table 3-3 displays representative stiffnesses of a blade root torsional spring and its equivalent value in non-dimensional form.

Table 3-3: Pitch Link Stiffness and Torsional Natural Frequency

ν_θ	5.55	4.38	4.2	3.6	3.0	2.4	2.1	1.5
K_θ ft-lbs/rad	20830*	12726	11645	8370	5599	3331	2386	875
K_θ ft-lbs/deg	364	222	203	146	98	58	42	15

**value for UH-60 pitch change link stiffness as reported in [42]*

The first place to look at the effect of torsional stiffness is in hover where the axi-symmetric flow regime allows for more straightforward analysis (Figure 3-20). Considering the case of no flap deflection, once the rotor is rotating, both the inherent nose-down pitching moment of the base blade and the propeller moment drive the blade to a value less than the pre-pitch (in this case, θ_{Pre}=16°). The stiffer the blade is, the less the deviation from the pre-pitch. Considering flap deflections with negative values

(producing a nose up pitching moment), one can see that the blade increases its angle of attack relative to the 0-deflection case. At δ=-10°, the blade has basically reached its pre-pitch value for all cases of stiffness. On the right hand side of the plot, the blade continues to pitch down with increasingly positive TEF deflections. As blade stiffness decreases, the blade pitch response increases. As can be seen, for the case of ν_θ=2.1, δ=0 yields θ=6.8°, and it can yield θ_0=0 with only 5° of TEF input, thanks in part to the negative pitching moment of the SC1095 airfoil and the UH-60 tip sweep. This kind of control authority would be critical for operations such as autorotation and ground operations.

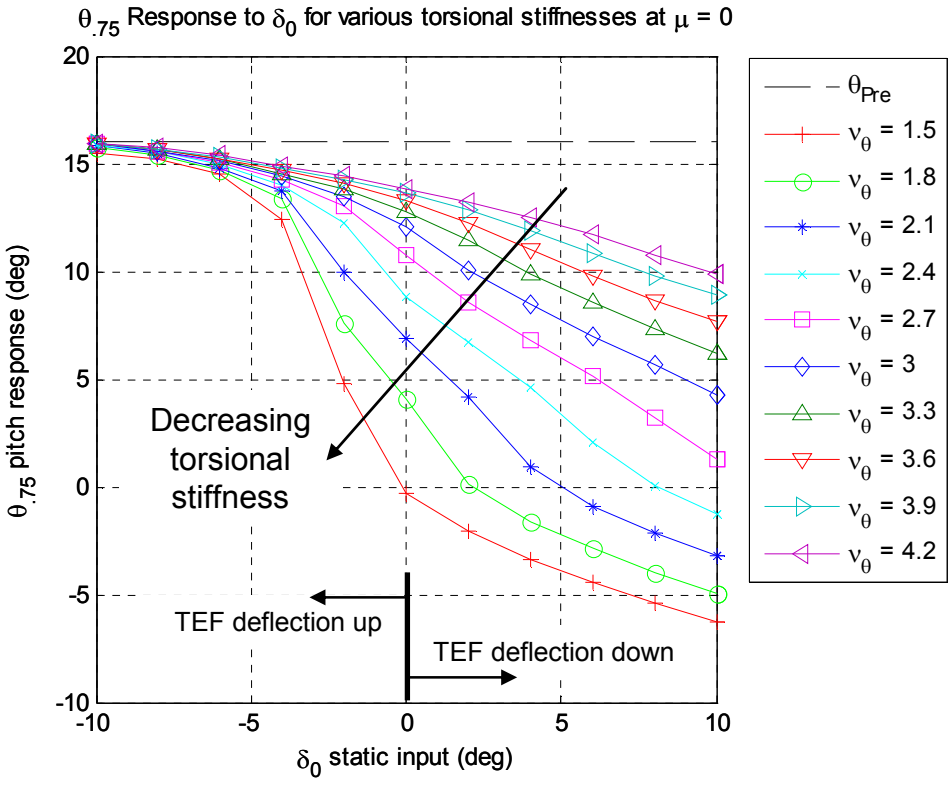

Figure 3-20: Collective Pitch Response for Flap Input, Various ν_θ

When considering high speed operation (μ=.3), another interesting result is observed. Figure 3-21 depicts a rotor with only δ_0 applied. And yet, significant cyclic blade pitch results from the asymmetric aerodynamic environment in a very beneficial way. When the blade with a δ>0 encounters the high dynamic pressure on the advancing side, a greater pitching moment is produced than when it flies through the lower dynamic pressure on the retreating side. This imparts an effective $-\theta_{1s}$ for the softer rotors. This self-trimming effect is another way in which the trailing edge flap configuration capitalizes on some of the operational features of the helicopter that designers have typically viewed as challenges to overcome (such as asymmetric dynamic pressure).

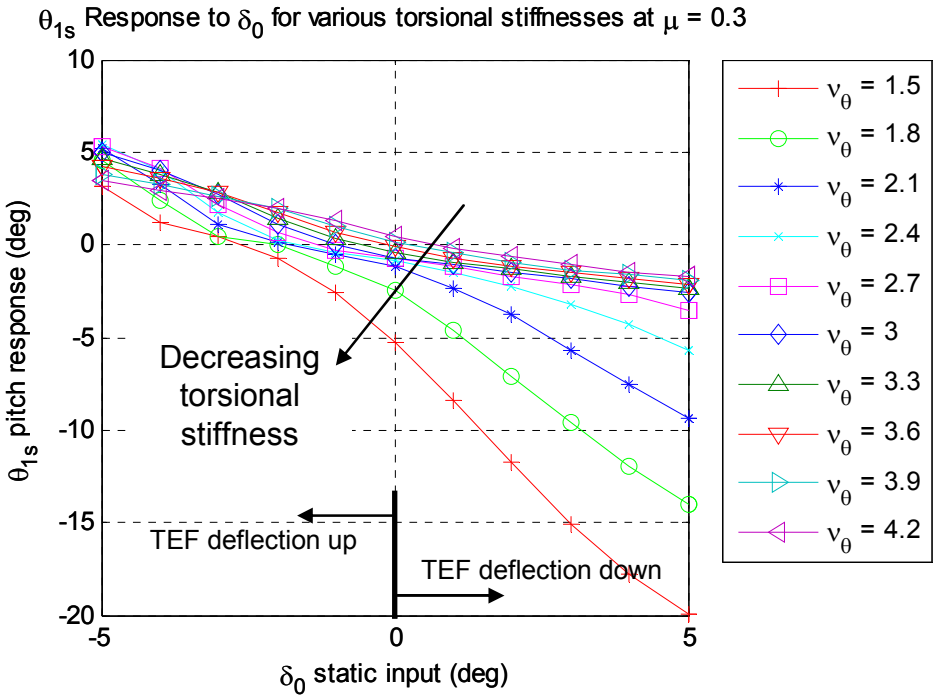

Figure 3-21: Lateral Cyclic Pitch Response for Flap Input, Various ν_θ

Once a full airspeed sweep has been completed, two important principles become immediately apparent. The first, which is most clearly seen in the plot of δ_0 against μ for

various ν_θ (Figure 3-22), is that rotors that are stiffer in torsion demand TEF deflections that lie outside current actuator capability, and almost certainly outside the stall boundary of an airfoil-flap combination (a phenomenon which is not captured by the Theodorsen model in use). The required change in δ_0 is due to the change in thrust required across numerous airspeeds that is an inescapable phenomenon of rotorcraft operation. This demonstrates what was first discussed by Ormiston [9] that suitably low torsional stiffness is a requirement for a swashplateless rotor unless some other means of controlling thrust is also considered. This thesis will later undertake the case of a rotor stiffened to ν_θ =3.0 to determine the effectiveness of the horizontal tail.

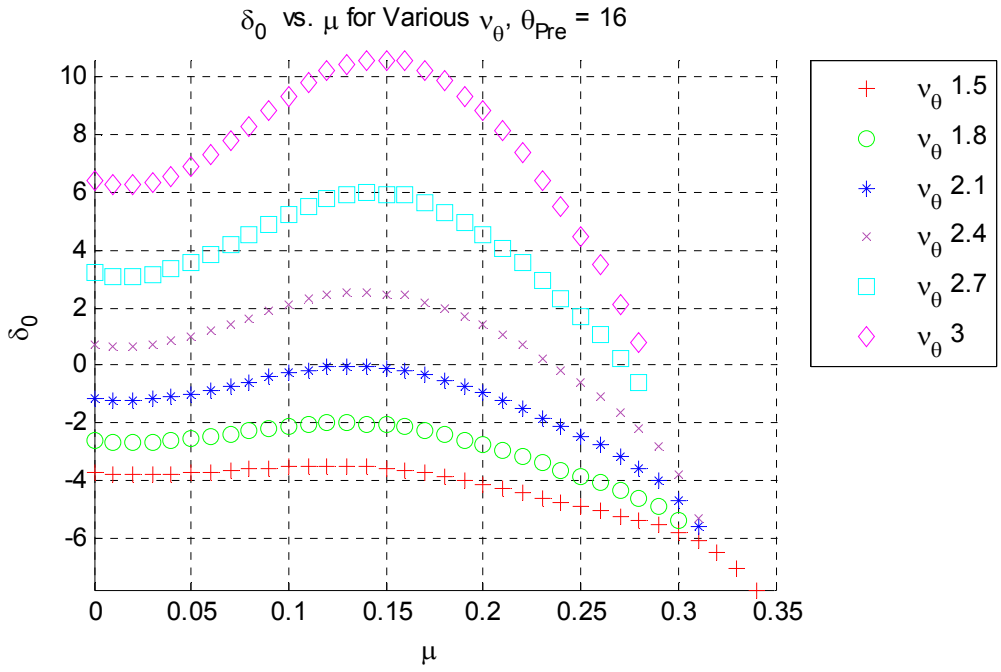

Figure 3-22: Collective Flap Requirements vs. μ, Various ν_θ

Figure 3-23 demonstrates the effect of torsional stiffness on 1/rev TEF inputs. The change in δ_1 is due primarily to the longitudinal cyclic flapping that is required. For rotors with $\nu_\theta > 2.4$, the flap deflections are excessive, even for moderate airspeeds.

Additionally, the large δ_1 requirement in hover due to the UH-60's unusual hover attitude presents problems in stiffening the rotor. A helicopter with a more level hover attitude may find a stiff rotor to be more feasible.

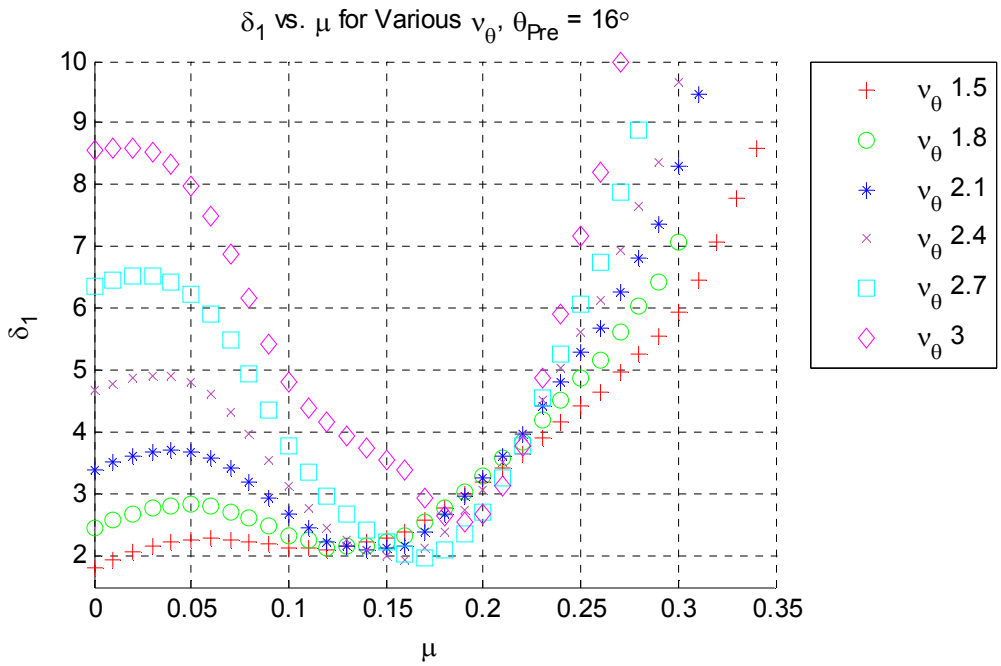

Figure 3-23: Cyclic Flap Requirements vs. μ, Various ν_θ

Once again, it is worthwhile to examine the impact of ν_θ on the TEF deflection envelope and δ_{MAX}. The trend with $\Delta\delta_{TOT}$ is that more stiffness requires a large envelope. Indeed Table 3-4 demonstrates that feature. Interestingly, however, the cause of the size of $\Delta\delta_{TOT}$ and the location of δ_{MAX} vary with stiffness. Soft rotors' deflection envelopes are driven primarily at higher speed deflection requirements, where the stabilator inputs are expected to reduce the deflections. Accordingly, the softer rotors' δ_{MAX} occurs at high speed, and this value should therefore be subject to improvement through tail inputs. In the soft rotors, the growth of the TEF deflection envelope depends primarily on the increase in δ_1 with speed, while the δ_0 requirements remain fairly unchanged.

Table 3-4: TEF Deflection Envelope and Maximum Flap Deflection, Various ν_θ

	ν_θ=1.5	ν_θ=2.1	ν_θ=2.7	ν_θ=3.0
$\Delta\delta_{TOT}$	13°	16°	17°	19°
δ_{MAX}	12°	13°	11°	15°

In the case of the stiff rotors, the deflection envelope and δ_{MAX} depend on the requirements in hover and low speed. Indeed, the δ_{MAX} for both ν_θ=2.7 and ν_θ=3.0 occurs at μ=.05. Again, the additional of horizontal tail controls will not relieve the TEF deflections in hover. As stated before, this problem may be solved by changing the hover attitude of the UH-60 by moving the CG and by lowering the pre-pitch. Aside from the hover requirements, the stiffer rotors also face the challenge of large variation in both δ_1 and δ_0 with airspeed. These matters will be taken up in Section 3.7.3.

In terms of selecting a value of torsional stiffness for the purposes of this study, Figure 3-24 demonstrates that ν_θ=2.1 appears to have the best potential for taking advantage of tail inputs. The deflection envelope for ν_θ=2.1 does not exceed the constraints until μ>.2, which is fast enough for a horizontal tail input to have authority. Furthermore, the deflection requirements grow substantially with airspeed. In the softer rotors, however, this growth is only due to the increase in δ_1. In the stiffer rotors, both δ_0, and δ_1 have large ranges, again demonstrating the importance of utilizing an adequately softened rotor.

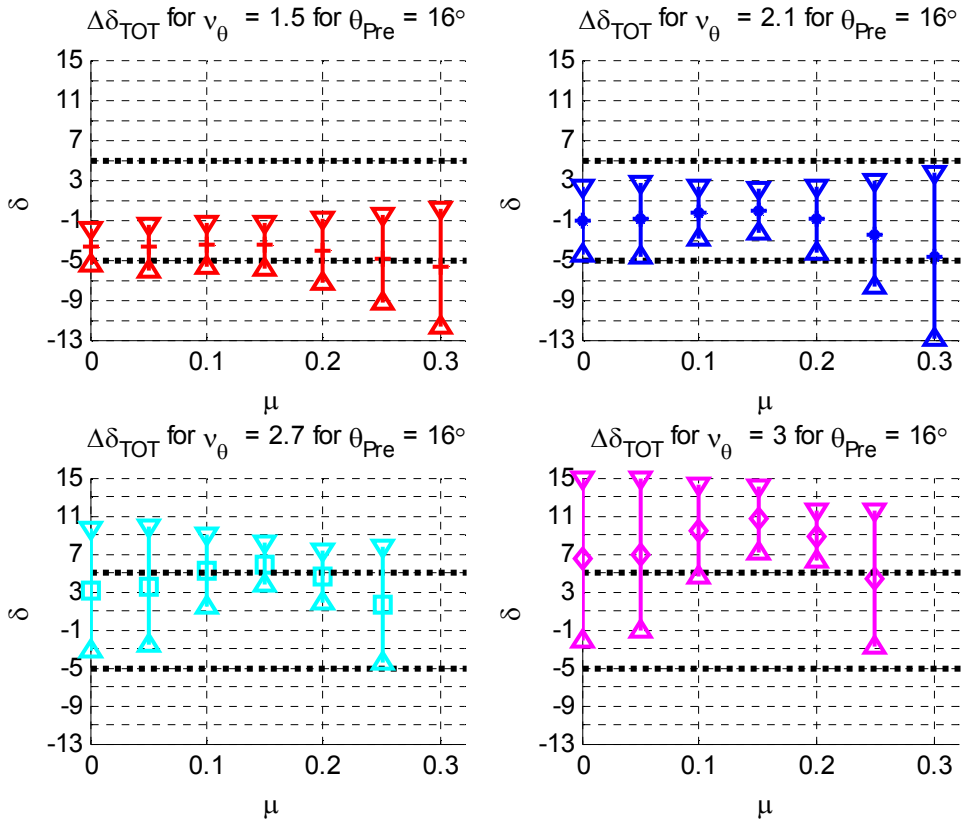

Figure 3-24: TEF Deflection Envelope, Various ν_θ

Finally, the power implications of each stiffness are also important. Although torsional stiffness seems to have little impact on power except for extreme cases of speed or stiffness (Figure 3-25), the rotor with ν_θ=2.1 has the lowest power over most of the flight envelope. This is because its aggregate TEF deflections are closer to zero than any other configuration until higher airspeed, where once again, one expects the horizontal tail inputs will be effective.

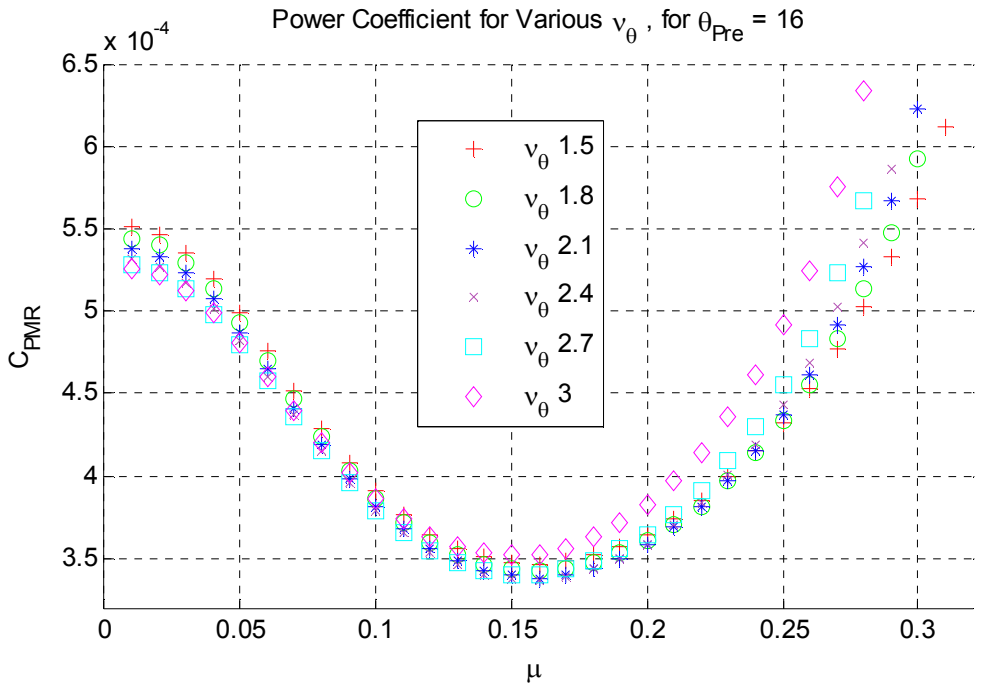

Figure 3-25: Power vs. μ at Moderate Airspeed, Various ν_θ

Due to all of the above considerations, the nominal value for ν_θ is chosen to be 2.1. This agrees well with prior work in this area—both Shen and Falls selected torsional frequencies near 2.0/rev. Additionally, when one considers the physical meaning of the torsional stiffness by reviewing Table 3-3, one can understand a designer's hesitance to pick a blade root spring with stiffness lower than 40 ft-lbs per degree. Such a system would have stability concerns that are not addressed in this thesis, and would require careful design of the rotor or active controls.

It is appropriate to highlight one final feature that has been documented by previous research [13] prior to undertaking further analysis. As the rotor is stiffened in pitch, the mechanism that the TEFs must utilize to effect control of the rotor begins to change. With blades that are free to rotate about a root restraint, the flaps act primarily as

"pitch flaps" to utilize the terminology introduced by Ormiston [9]. This refers to the fact that their primary means of control is by causing the entire blade to change pitch. Thus, cyclic variation in lift is achieved *primarily* by the pitch of the entire blade. As the rotor stiffens, the ability of the TEFs to pitch the entire blade diminishes rapidly. Thus, with a stiffer rotor, the blade is pre-pitched less, and more of the cyclic lift variation comes from the actual increment in lift coefficient as a result of deflecting the flap.

3.7 Horizontal Tail Study

The application of fixed frame forces and moments through the horizontal tail is now considered. Although the mechanism by which the horizontal tail relieves cyclic flapping and TEF deflections is straightforward, the amount of application necessary and its effect on other helicopter trim parameters and power are important considerations that have yet to be established. Since the horizontal tail on the UH-60 is commonly termed the stabilator, both terms are used in this thesis. Additionally, the terms slew, tail incidence angle, and collective/differential deflections all refer to the stabilator's angle with respect to the aircraft waterline (x-axis). The tail's aerodynamic angle of attack refers to the angle of the tail incident to the freestream as modified by the main rotor wake. The angle that the tail makes with the horizon is not of interest.

Before the results are identified and discussed, some preliminary issues must be addressed. As detailed in Chapter 2 and described in Figure 3-26 , the aerodynamic angle of attack that the horizontal tail describes with respect to the free stream is a function of the horizontal tail slew angle with respect to the body axis, ε, the pitch attitude of the

helicopter, $\alpha_{wl,}$ and the downwash angle produced by main rotor wake redirecting the free-steam velocity, χ_{ht}. The wake skew angle is a function of airspeed. This function is shown in Appendix B, however, its effect on the tail's angle of attack is reproduced in Figure 3-27 below in order to highlight the fact that a high horizontal tail incidence angle at low speed is almost wholly compensated for by the main rotor skew angle. Thus, at μ=.1, the standard stabilator slew angle is 39°, however the stabilator's aerodynamic angle of attack is only 9° more than the aircraft's flight attitude. Additionally, once a horizontal tail is added that is free to move both collectively and differentially, each side of the stabilator must be evaluated independently. Therefore, based on the aircraft attitude, the main rotor wake skew angle, and the horizontal tail inputs, one side of the tail may be in a stall while the other may not. These effects are all modeled aerodynamically, and their effects on the aircraft drag, yaw moment, and roll moment are accounted for as well.

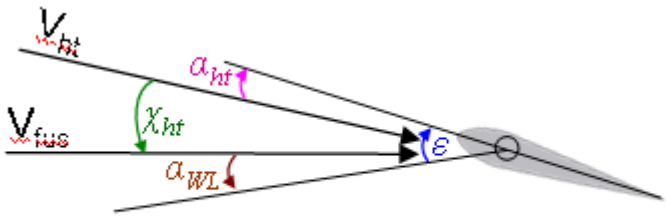

$$\alpha_{ht} = \varepsilon - \alpha_{WL} - \chi_{ht}$$

Figure 3-26: Description of α_{ht}

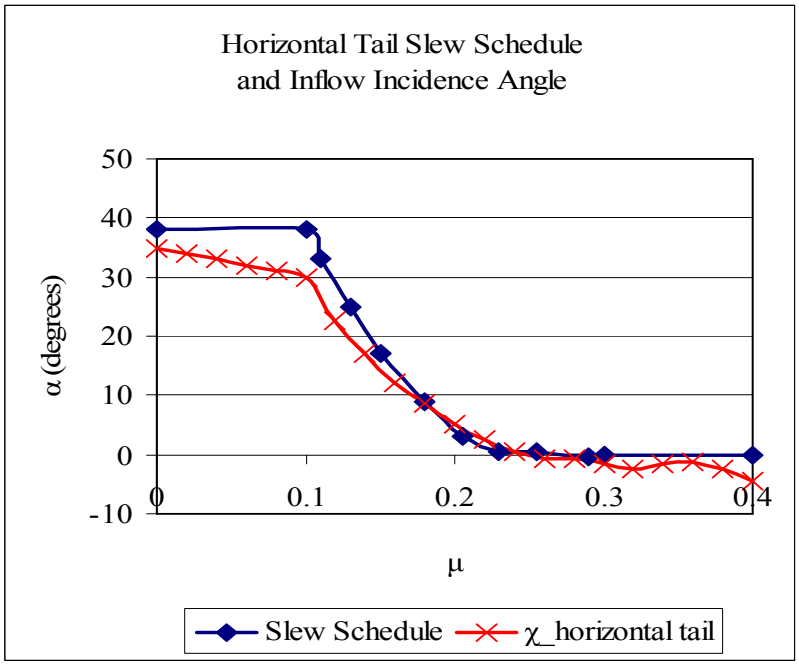

Figure 3-27: Stabilator Slew Schedule [47] and Wake Skew Angle

At this point, trends relating to the stabilator's pitching and rolling moments can be discussed. Generally, in order to affect translational flight, the rotor thrust must tilt forward. This is usually accomplished with longitudinal rotor flapping. This technique will still be used in low speeds by the moveable horizontal tail configuration. However, as airspeed increases, the horizontal tail's ability to impart a pitching moment on the airframe increases. The horizontal tail on most helicopters is used to produce a downward force, and thereby a nose up pitching moment in order to provide a more level flying attitude at high speed and to present less fuselage frontal area to the oncoming flow. However, this arrangement requires ever increasing rotor flapping. The opposite principle will be used in this study. Once the horizontal tail has control authority due to forward airspeed, it can be used to pitch the airframe forward, thereby relieving the

requirement for rotor flapping. The higher the collective slew angle (ε_{coll}), the more pitching moment is generated.

The roll authority of the stabilator is much the same. A differential deflection (with leading edge up on the right side for positive values of ε_{diff} to yield a positive roll moment on the fuselage), causes the two sides of the horizontal tail to deflect in opposite directions. For positive values of ε_{diff}, the right half of the stabilator increases slew angle and the left side decreases its slew angle. Thus, increasing values of ε_{diff} will result in increasingly positive roll moments on the helicopter. Because the rotor must flap laterally to trim lateral forces arising from tail rotor thrust and the rotor's own side force, this roll moment allows the helicopter to roll in such a way that gravity imparts a side force in the body axis system so that the requirement for lateral flapping is also reduced. As standard rotors' lateral flapping requirements are not typically large, one does not expect the roll moments required by use of ε_{diff} to be large either.

The foregoing discussion highlights the impact of any given helicopter's geometric configuration on the magnitude of the stabilator control inputs. This is important for two reasons. The first is the amount of force required to actuate each side of the stabilator. Although this is a significant design consideration, no attempt is made to calculate these values in this thesis. The second is the amount of control inputs required. The UH-60's unusual configuration makes it an ideal platform on which to apply this technique. The UH-60's stabilator has a very large surface area (45 square feet) and it is already placed as far aft on the vehicle as possible (28 feet behind the CG). Both of these translate directly into a high level of control authority for the pitching moment, which should yield relatively mild control deflection magnitudes. Additionally,

the UH-60's stabilator has a large span (more than 14 feet). This large span places the overall center of pressure of each half of the stabilator at a considerable moment arm from the aircraft x-axis, resulting in lower inputs to achieve the desired roll moment. In contrast, many other helicopters feature much smaller horizontal tails that are fixed part-way down the tailboom. These configurations can expect to require much larger tail control inputs.

The plots that are presented in the subsequent sections represent the effect of a range of horizontal collective and differential tail inputs at different airspeeds. The black line represents the standard slew schedule stabilator position. The intersection of the blue lines indicates the horizontal tail control inputs resulting in the smallest cyclic TEF deflections (δ_1). If a red marker appears on the plot, this denotes the compromise solution necessary to ameliorate vehicle attitude, yet remain within the band of capability of current actuators. The values that are displayed on the plots in the appropriate color denote the value of the plot at either the standard stabilator position or the new horizontal tail solution.

3.7.1 Horizontal Tail Analysis for Pre-pitch of 16°

The tail will first be applied to a rotor pre-pitched to 16° and analyzed at $\mu = 0.10$, 0.20, and 0.30. This will facilitate comparisons to this study's baseline swashplateless results as well as those of Shen and Falls.

Figure 3-28 details the effect of horizontal tail at low speed flight of $\mu = 0.10$, the slowest airspeed at which the tail is expected to have any real authority to change TEF

deflections or vehicle attitude, albeit with large tail deflections (ε_{coll} ranges from 0-60°). Collective TEF inputs can range from less than -0.9° to -0.21°, and δ_1 can vary from 2.49° to more than 5°. Likewise, a significant range in vehicle attitude is also possible (Figure 3-29), ranging from -2.92° to -9° in pitch attitude. However, the ε_{coll} and ε_{diff} inputs for minimal δ_1 are very close to the standard UH-60 slew schedule. Very little improvement is possible at this airspeed, but the plots show the general effect on the helicopter response.

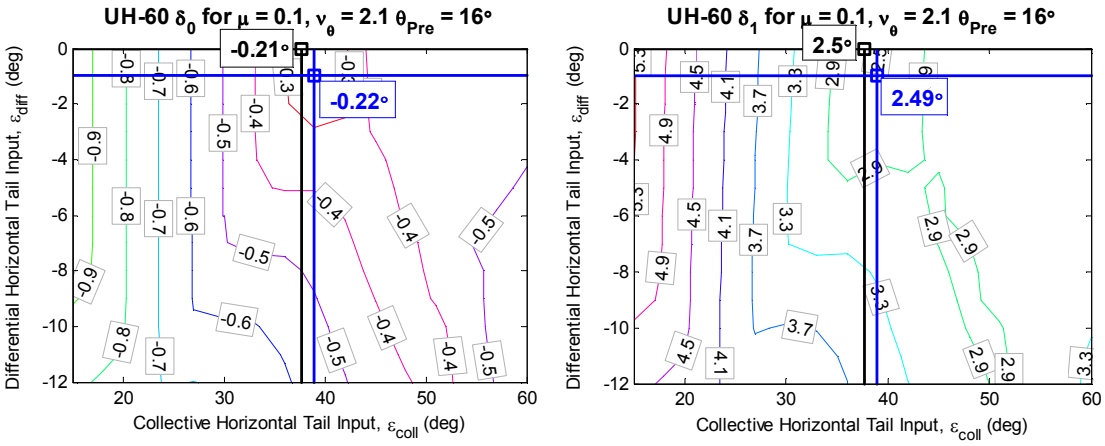

Figure 3-28: TEF Deflections and Horizontal Tail Inputs, μ=0.10

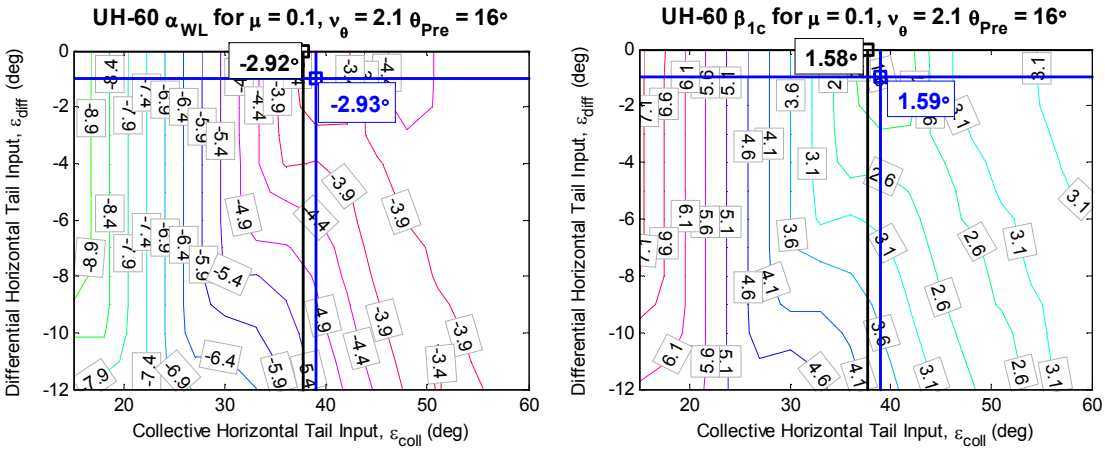

Figure 3-29: Pitch Attitude, Longitudinal Flapping and Horizontal Tail Inputs, μ=0.10

Moving to a higher airspeed, the required ε_{coll} and ε_{diff} are smaller since the tail has higher dynamic pressure and since the wake skew angle is reduced considerably (<5°). There is also now a significant difference between the standard slew schedule and the solution for minimal δ_1 (Figure 3-30). As expected the tail is set to a higher collective incidence angle to yield a more nose-down vehicle attitude (Figure 3-31). There is also a significant differential tail deflection, which produces a negative rolling moment on the helicopter. The cyclic TEF deflection requirements are reduced from δ_1=3.11° to δ_1=0.5°. The collective TEF deflections also decrease from -0.92° to 0.31°. This represents an all-around improvement in configuration that is reflected in the vehicle attitude and power as well. Figure 3-31 shows that, rather than flying with a 2.29° nose high attitude, the new pitch attitude is 1.94° nose down. The longitudinal blade flapping has been reduced from β_{1c}=3.01° to -1.13°. Thus, a slight rotor blow back is permitted. The power improvement resulting from achieving such large absolute reductions in TEF deflections is almost 50 horsepower better than the TEF rotor without a moveable horizontal tail.

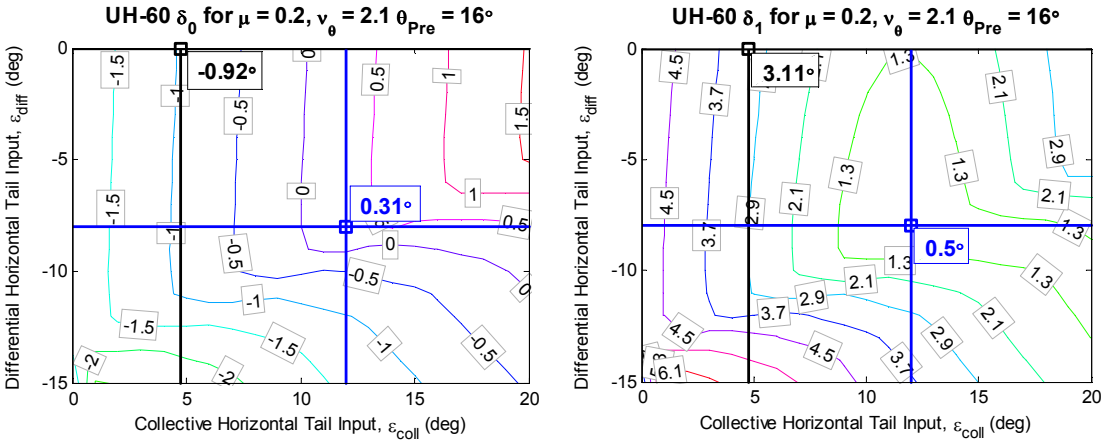

Figure 3-30: TEF Deflections and Horizontal Tail Inputs, μ=0.20

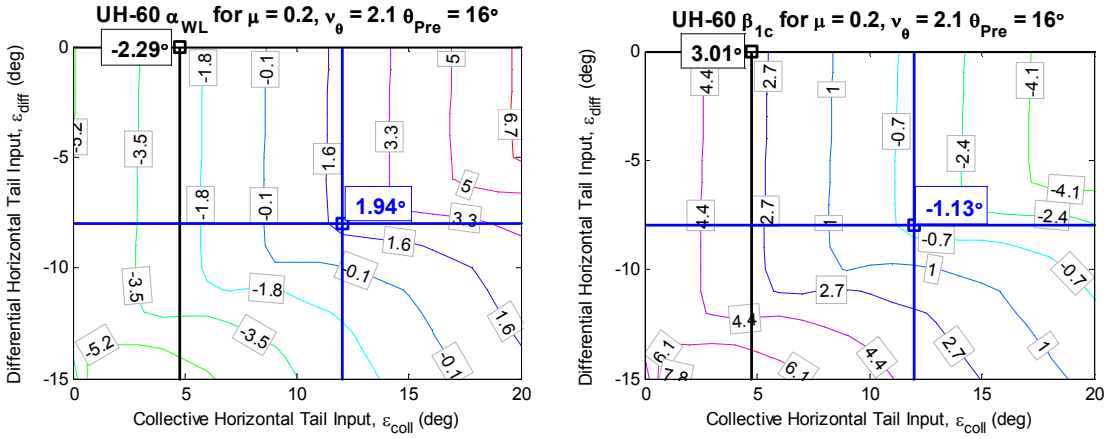

Figure 3-31: Pitch Attitude, Longitudinal Flapping and Horizontal Tail Inputs, μ=0.20

Finally, the horizontal tail's effectiveness at high speed is examined. Although the required forces and moments to fly at this airspeed are much higher, the needed tail deflections are small since higher dynamic pressure is available to the stabilator. Figure 3-32 shows that there is a significant difference between the standard slew positions and the tail inputs required to minimize δ_1, which is reduced from 8.29° to 0.24°. The collective TEF deflection magnitude is also reduced considerably, from -4.7° to -1.05°. However Figure 3-33 demonstrates that, in this position, a significant price must be paid in other areas, namely blade flapping and vehicle attitude. Blade longitudinal flapping goes from β_{1c}=3.74° to -5.50°. This represents an unacceptably high level of blowback for the rotor. Additionally, α_{WL} goes from 1.34° to 10.29° nose-down. This flight attitude is too nose-low, providing an awkward ride for crew and passengers and presenting a high flat plate drag area to the oncoming flow. Although power savings between the baseline swashplateless (2312 hp) and the min-TEF solution (2017 hp) are substantial (12%), the unusual flight attitude increases power slightly.

Despite these negative side-effects, there is a significant range of parameters between the two solutions to find various compromise solutions. One such solution is presented in Table 3-5 where the vehicle attitude and blade flapping is much more acceptable and the TEF deflections have been constrained to ±5°, the assumed limit of actuator capability.

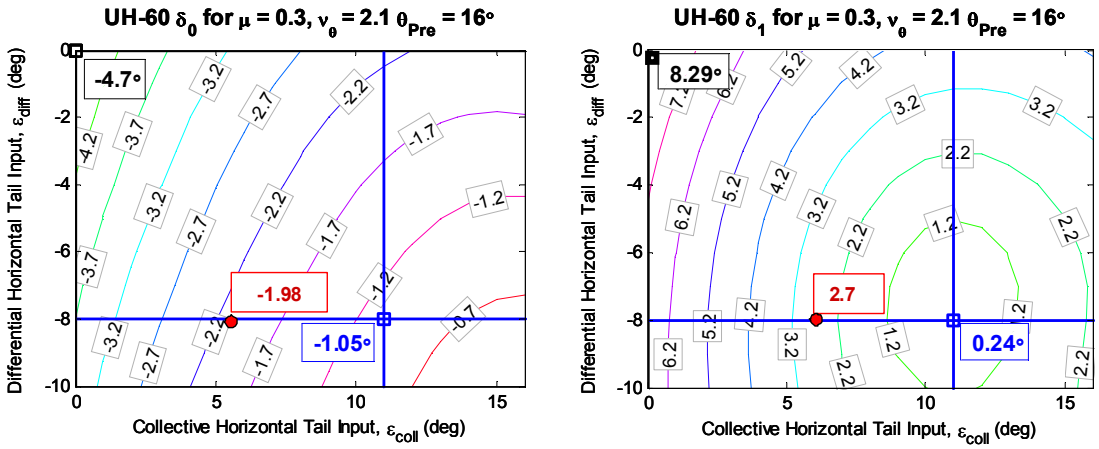

Figure 3-32: TEF Deflections and Horizontal Tail Inputs, μ=0.30

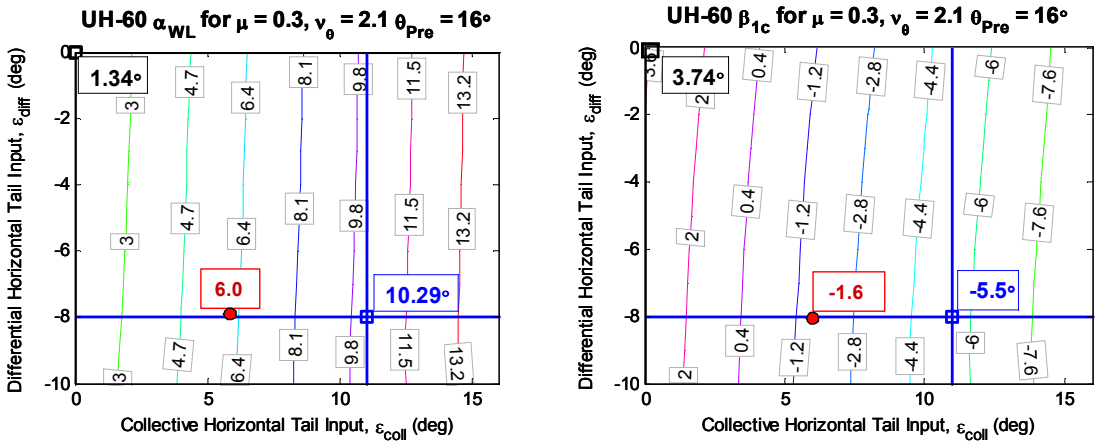

Figure 3-33: Pitch Attitude, Longitudinal Flapping and Horizontal Tail Inputs, μ=0.30

Table 3-5: Summary of Horizontal Tail Solutions, θ_{Pre}=16°

ν_θ = 2.1 θ_{Pre}=16°	μ = 0.20		μ = 0.30		
	Baseline swash-plateless	**Hor Tail swash-plateless** *min δ_1*	**Baseline swash-plateless**	**Hor Tail swash-plateless** *min δ_1*	**Hor Tail swash-plateless** *compromise*
ε_{coll}	4.75°	12°	0°	11°	6°
ε_{diff}	-	-8°	-	-8°	-8°
δ_0	-0.92°	0.31°	-4.7°	-1.0°	-1.98°
δ_1	3.11°	0.5°	8.3°	.25°	2.7°
α_{WL}	-2.3°	1.94°	1.3°	10.3°	6.0°
β_{1c}	3.0°	-1.13°	3.7°	-5.5°	-1.6°
Power (hp)	1318	1276	2311	2017	2055
δ_{MAX}	12.18°	4.71°	12.18°	4.71°	4.71°
$\Delta\delta_{TOT}$	15.6°	6.9°	15.6°	6.9°	6.9

One will also notice the large variation in δ_0 with application of horizontal tail even though tail control is designed to reduce cyclic TEF requirements. It is important to understand the reason for this because it highlights some of the peculiarities of the softened, pre-pitched rotor once a horizontal tail is added for control. Section 3.5 detailed the mechanism for feathering the blades to achieve a desired flapping response. The standard means of developing propulsive thrust is to require low pitch on the advancing side and high pitch on the retreating side. The average between the TEF deflections required between the two sides dictates the value for δ_0. If this value was a negative number, the edge of the control margin was very near. However, once the horizontal tail is added, this rule does not directly apply. Two additional features taken in conjunction drive this phenomenon: relaxed blade flapping requirements and the self-

trimming tendency of soft, pre-pitched rotors. First, blade flapping is no longer the only means of achieving force and moment balance. Therefore, the difference in required blade pitch and TEF deflection requirements between advancing and retreating sides is not as stringent, because forces and moments can be developed elsewhere to supplement the rotor. Taken to its logical extreme, if no TEF inputs are made and all of the vehicle roll and pitch moments are developed by the horizontal tail, then the rotor is free to flap in whatever way it wants as long as the horizontal tail has enough authority to overcome the moments that such action would develop. On a standard rotor, this arrangement would result in onerous flight attitudes and counterproductive rotor blow back and side-tilt. However, these effects are somewhat mitigated by the self-trimming feature of a soft rotor with pre-pitch as described in Section 3.6. As depicted in Figure 3-21, a rotor with pre-pitch that is free to respond in pitch to an incident freestream will respond with $-\theta_{1s}$, strongly mitigating rotor blowback. Therefore, in the case of the horizontal tail inputs, since less emphasis is on getting a certain value of rotor flapping, the blade pitch and TEF deflections do not need to be driven to such left-to-right extremes at high speed. Since the rotor no longer requires such high $-\delta$ on the retreating side of the rotor, the δ_0 requirements improve dramatically as well by becoming less negative.

Although mentioned briefly, it is worth reexamining the power predictions for the μ=.2 and .3 cases (Figure 3-34). In both cases, the required power is decreased with the decrease in TEF deflections. This is due primarily to the minimization of the deflections themselves causing reduced profile drag on the rotor blades. Since the moveable tail application in the μ=.2 case caused an improvement in aircraft pitch attitude, this also contributes slightly to a lower required power. However, for the higher speed case, we

see that the unusual vehicle attitude limits the amount of power savings that can be expected. Thus, a compromise solution that does not necessarily minimize TEF deflections does not yield substantially higher power.

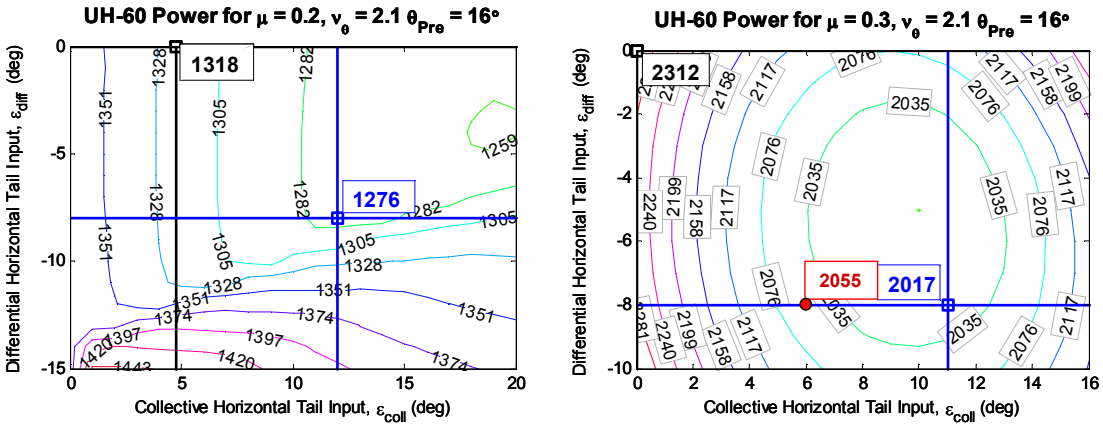

Figure 3-34: Power and Horizontal Tail Deflections, μ = 0.20, 0.30

At this point it is useful to compare the TEF deflections that were made possible with the moveable tail in light of the baseline TEF requirements. Although this is done numerically in Table 3-5 above, the results displayed over the entire flight envelope are a good demonstration of the horizontal tail's ability to reduce the TEF deflection envelope and δ_{MAX} discussed previously. Figure 3-35 displays a dramatic reduction in TEF deflection envelope and δ_{MAX}, demonstrating the authority of the tail at higher speeds to control the vehicle. In fact, δ is reduced so much at high speed that δ_{MAX} is defined at low speed rather than high speed, as is usually the case. As stated earlier, the hover TEF deflection requirements can be minimized by selecting a helicopter configuration that provides for a more level hover attitude. The plot on the right demonstrates that flying at a more level attitude with greatly reduced rotor blowback can be achieved and still remain in the TEF deflection envelope dictated by current actuator capability with

$\delta_{MAX}<\pm5°$. Indeed, δ_{MAX} and $\Delta\delta_{TOT}$ remain unchanged for both the minimum δ_1 solution and the compromise solution.

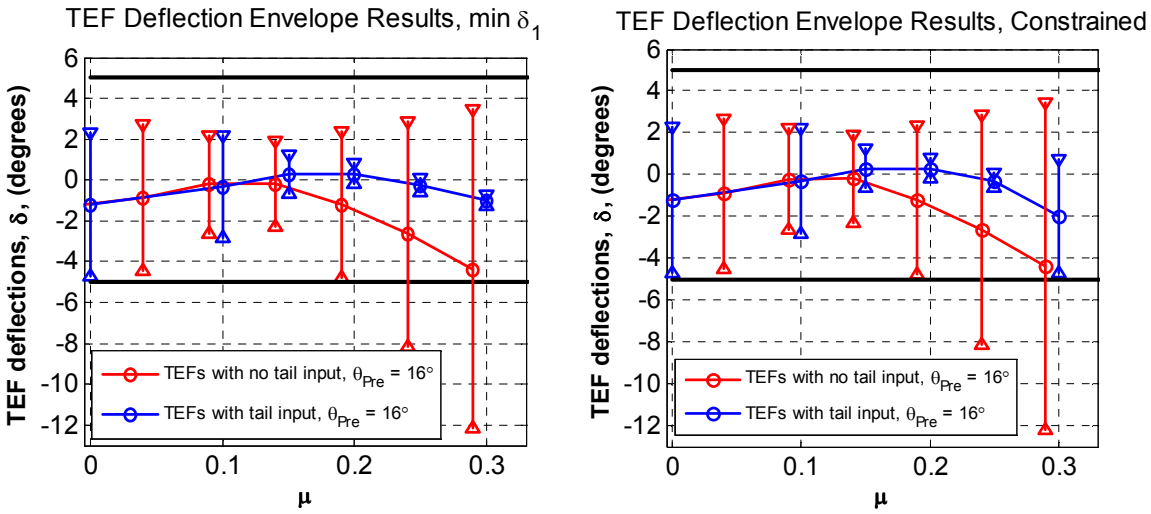

Figure 3-35: TEF Deflection Envelope Improvements

One may note that the largest component of the 1/rev TEF deflection corresponds with δ_{1s}, which is ultimately responsible for longitudinal blade flapping. This reduction is achieved through collective tail control. Since the UH-60 already includes the capability to deploy the stabilator as a unit, it is useful to examine the amount of TEF deflections that could be achieved without considering the differential tail inputs. Figure 3-36 illustrates that under baseline tail scheduling, the TEF deflection envelope is almost 16° and δ_{MAX}=12.2°. With only collective stabilator input, $\Delta\delta_{TOT}$ can be reduced to less than 9° (2.79° to -6.08°) and δ_{MAX} can be reduced to 6.8°. Although this is almost a 100% improvement, δ_{MAX} still exceeds -5°. However, one can see that there is ample "unused" actuator between +3° and +5° that could most likely be used if a higher pre-pitch were employed. This will be examined in the next section. While these results seem to suggest the possibility of neglecting the differential tail input, it is important to

understand the attendant limitations with this concept. All of the δ_1 required in Figure 3-35 at speeds above μ=.10 is phased with δ_{1c} since the application of ε_{coll} eliminates the need for δ_{1s}. Recall from Figure 3-1 that for μ=.30, 4° of cyclic pitch variation is required to laterally trim the rotor. This leaves little deflection range left for maneuvers. Additionally, since all of the δ_{1s} was eliminated with tail input, the aircraft is left at the 10° nose low attitude that was discussed above. A compromise solution with only ε_{coll} input is not feasible, which highlights the necessity of both ε_{coll} and ε_{diff} at this θ_{Pre}.

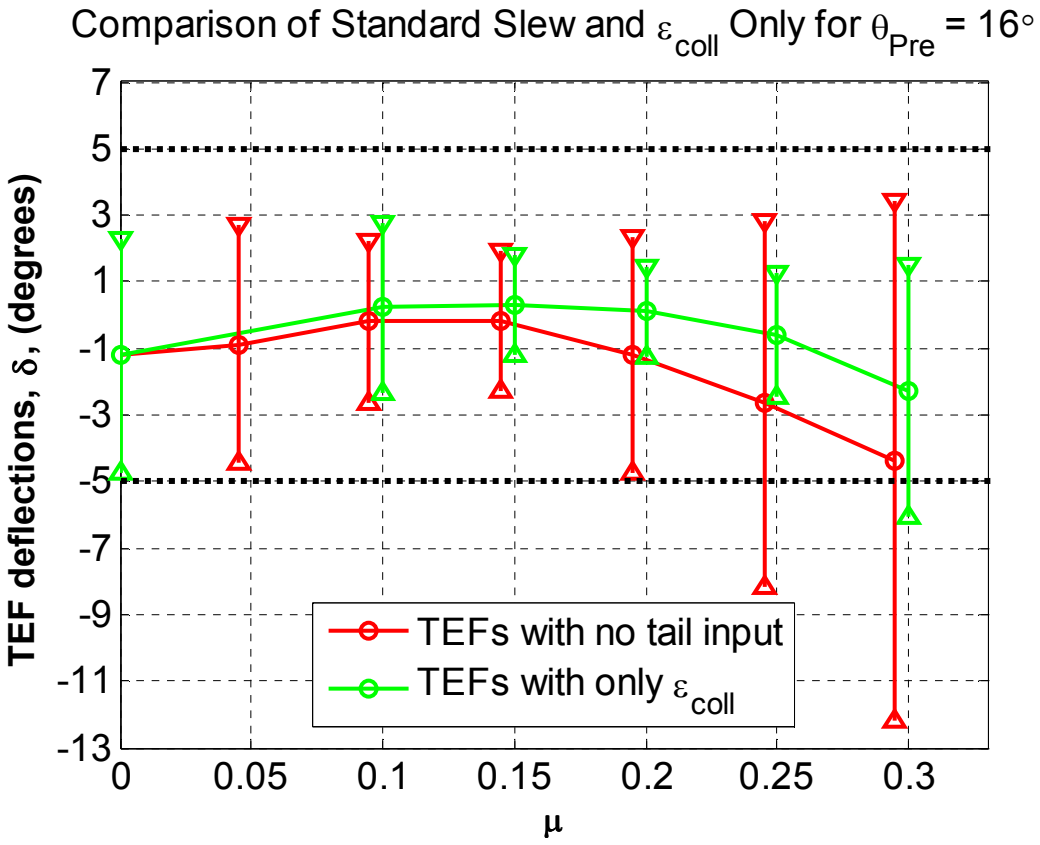

Figure 3-36: TEF Deflection Range Due to ε_{coll} only, θ_{Pre}=16°

Clearly, the addition of the horizontal tail significantly reduces the δ_0 and δ_1 required to trim. At most airspeeds, this is accomplished without a penalty in terms of

vehicle attitude or performance. At high speed, a solution can be found that allows for a reasonable aircraft attitude and still keeps 1/rev flap deflections under 3.5° and $\delta_{MAX}<5°$.

3.7.2 Horizontal Tail Study for Pre-pitch of 20°

All of the preceding analysis of the UH-60 with a moveable horizontal tail was conducted with a pre-pitch value of 16° in order to be able to compare the effects of the horizontal tail with the baseline swashplateless results. However, during the parametric study, a torsional stiffness of $\nu_\theta=2.1$ and $\theta_{pre}=20°$ was deemed to render the most satisfactory results in terms of trim variables across the range of flight speeds. Thus, it is necessary to apply a moveable horizontal tail to this configuration to determine if there are any noteworthy changes in the vehicle response. The values are presented in Table 3-6, and the associated contour plots are presented in Appendix C because their presence in this chapter is not necessary for the current discussion. However, Figure 3-37 displays the reduction in the TEF envelope possible with the selection of the higher pre-pitch which is discussed below.

Table 3-6: Summary of Horizontal Tail Solutions, θ_{Pre}=20°

	μ=0.20		μ=0.30		
θ_{pre}=20°	**Baseline swash-plateless**	**Hor Tail swash-plateless**	**Baseline swash-plateless**	**Hor Tail swash-plateless**	**Hor Tail swash-plateless**
		min δ_1		***min δ_1***	***example compromise***
ε_{coll}	4.75°	8°	0°	7°	4°
ε_{diff}	-	-4°	-	-4°	-4°
δ_0	2.0°	2.56°	-1.22°	1.05°	.35°
δ_1	1.25°	.12°	5.1°	.2°	1.65°
α_{WL}	-2.31°	-0.47°	1.2°	6.8°	4.45°
β_{1c}	2.99°	1.15°	3.7°	-2.3°	0°
Power (hp)	1298	1280	2072	1920	1957
$\Delta\delta_{TOT}$	10.9°	7°	10.9°	7°	7°
δ_{MAX}	6.2°	4.7°	6.2°	4.7°	4.7°

In general, these values have lower deflection magnitudes, fewer negative deflections, and lower power—all of which reinforce the selection of the higher pre-pitch as a better configuration for this gross weight. First, the required horizontal tail inputs are lower, reflecting lower rotor moments required with the higher pre-pitch. The moments are lower because there is less blade flapping (blow-back and side tilt) to generate pitching and rolling moments that the horizontal tail must overcome.

The situation is not clearly improved at μ=0.20 for a higher pre-pitch. The solution for minimum TEF defections yields a better vehicle attitude than the standard slew schedule solution, so a compromise solution is not needed. The horizontal tail input is also lower since the minimum δ_1 solution yields positive longitudinal flapping. This is due to the self-trimming feature of the TEF configuration in high speed once the δ_1 inputs

have been taken out of the system as long as δ_0 is greater than 0°. This feature will re-occur at μ=.30, which is another benefit of the higher pre-pitch angle.

At μ=0.30, more significant gains over the standard tail schedule case are possible, especially as pertains to δ_1. But once again, there is a vehicle attitude and blade flapping penalty associated with the minimum δ_1 solution, although it is not as bad as the case for θ_{Pre} = 16°. The compromise solution selected in this case minimizes blade flapping with respect to the shaft and provides a more moderate vehicle attitude. This solution requires very small overall inputs at this airspeed. Comparing this case to θ_{Pre}=16°, every single parameter is improved for the higher pre-pitch. This design uses much less power (100+ hp), and results in a better vehicle attitude with less control cost. Once again we see the self-trimming feature of the TEF system at the minimum δ_1 solution. In this instance, with a $+\delta_0$, the blow back is only 2.3° (much less than 5.5° for θ_{Pre}=16°) because the positive flap deflection causes more of a nose-down pitch response on the advancing side than the retreating side of the rotor disk. The main source of the power gains are also from the positive δ_0 (vice the $-\delta_0$ in the θ_{Pre}=16° case). This analysis has again revealed several beneficial features of higher pre-pitch and the positive δ_0's that result at a higher speed.

As can be seen in Figure 3-37, the TEF deflection envelope and δ_{MAX} change dramatically as well based simply on pitch index. Both δ_0 and δ_1 appear to have improved values for the case with no tail inputs. Although the δ_0 lines are more or less parallel, the 1/rev deflections are much smaller for μ>.10. This results in a reduced $\Delta\delta_{TOT}$ even before stabilator inputs are added. Once tail inputs are added, the deflection envelope shrinks from 10.9° to 7.0°. Additionally, the δ_{MAX}, which lies just beyond 5° at

6.2° for the case with no tail inputs, it δ_{MAX} reduces to 4.7° for both the minimum δ_1 solution, and the compromise solution (since it occurs at the hover condition). The compromise solution is plotted below in green; the minimum δ_1 solution is omitted since it is not a realistic solution.

All of the trim controls are well within the capabilities of current actuators, even with the unusual hover attitude. This fact significantly increases the amount of actuator stroke available for maneuver. Although not addressed in this study, the amount of TEF deflection left over for maneuver at any single airspeed is the least of the differences between half-peak-to-peak values and actuator limitations. For example, at μ=.2, the θ_{Pre} with no tail input (in blue) line goes from 0 to 3.5°. This means that at this airspeed, the actuators have 1.5° of actuator capability remaining for a maneuver. Two observations can be made at this point. First, this rotor will not have the same amount of maneuver authority at all airspeeds. Referring this time to the green line in Figure 3-37, the rotor actually has more maneuver authority at μ=.30 than at μ=.15. This is because the greatest maneuver authority occurs where *both* δ_0 is close to 0° *and* δ_1 does not saturate the actuators in trim. As has been discussed at length, the horizontal tail can assist with reducing the δ_1, but some other means of increasing and decreasing rotor thrust across various flight speeds is likely a necessity in order to leave enough TEF actuation stroke to allow for maneuvers.

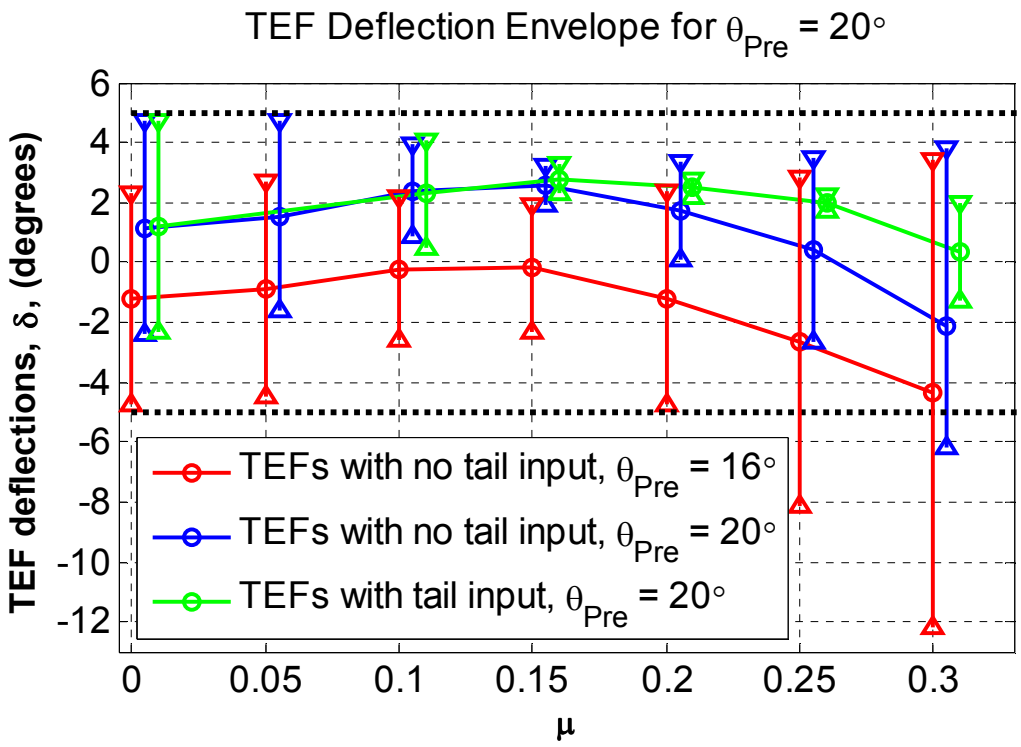

Figure 3-37: TEF Deflection Envelope with Horizontal Tail, θ_{Pre}=20°

Once again, it is instructive to analyze the case of lone ε_{coll} inputs. In the case of higher pre-pitch, lone ε_{coll} inputs provide a feasible solution. The entire flight range resides within a feasible TEF deflection envelope as depicted in Figure 3-38. As before, the ε_{coll} solution that minimizes TEF deflection at high speeds causes the aircraft to fly with an unusual attitude. However, there is much greater room for a compromise solution to be found that provides a better aircraft pitch attitude because there are smaller rotor roll moments to balance, and therefore, smaller lateral TEF deflection requirements. These smaller rotor roll moments stem from the fact that the higher pre-pitched rotor produces experiences less dissymmetry of lift at this airspeed. Thus, the tendency of an adequately pre-pitched rotor to pitch down on the advancing side benefits both longitudinal equilibrium (through longitudinal flapping) and lateral equilibrium (through

less dissymmetry of lift). One such compromise solution is listed in Table 3-7 and is plotted on Figure 3-38. The compromise solution yields a $\Delta\delta_{TOT}$=7.6° and a δ_{MAX}=4.7°, both of which are within the capability of current actuators. The increased potential to rely on simply collective tail inputs to reduce elevon deflections to a desirable level is yet another benefit of higher pre-pitch rotors

Table 3-7: Values for Collective Only Solution with θ_{Pre}=20°

	ε_0	δ_0	δ_1	α_{WL}	β_{1c}
μ=0.20	8°	2.5°	.43°	-.50°	1.2°
μ=0.30	4°	-.10°	2.8°	4.3°	.40°

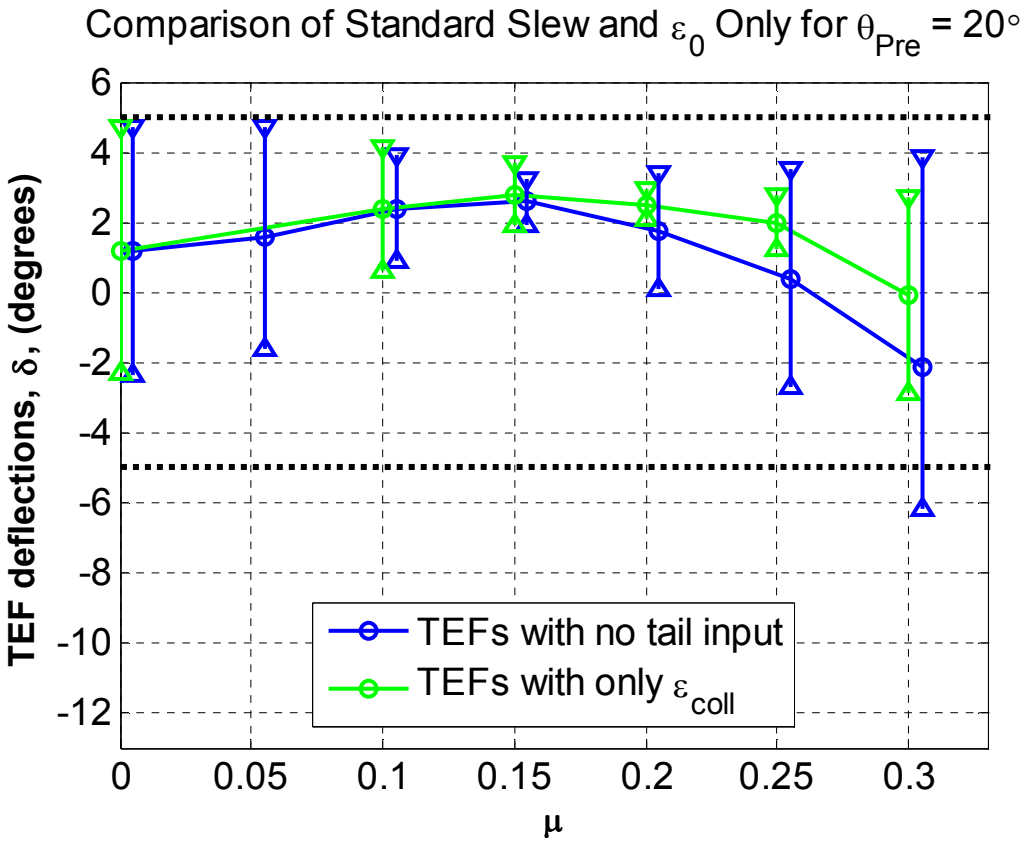

Figure 3-38: TEF Deflection Envelope Due to ε_{coll} only, θ_{Pre}=20°

This section has demonstrated the many advantages of utilizing the horizontal tail technology with a rotor that has been pre-pitched to a higher value. The high pre-pitch is beneficial for power, control requirements, and vehicle attitude. Additionally, it makes trim with only collective inputs more feasible. However, this section also introduced the considerations that will likely be required should maneuvering flight need to be considered. Although this higher pitch index has many benefits, it may have limited maneuver authority, unless other means of controlling thrust and vehicle attitude are employed.

3.7.3 Horizontal Tail Study for Stiffened Rotor, v_θ=3.0, θ_{Pre}=16°

In addition to the benefits outlined above, the inclusion of a moveable horizontal tail may also permit designers to utilize a rotor with higher pitch stiffness. There are several reasons why designers may find a low pitch stiffness to be undesirable. Chief among these are flutter instability concerns and the requirement for higher pre-pitch values with softer rotors. Additionally, the failure of a TEF in flight could be less catastrophic on a stiffer rotor that was less free to respond to local wind velocities. In light of these potential benefits and the many required trade-offs inherent in stiffening the rotor, it should be established here that the stiffened rotor does not prove to be a viable solution. Although the horizontal tail is effective in reducing TEF deflections, solutions that are within actuator capability produce unacceptable vehicle attitudes, and solutions that have acceptable vehicle attitudes have δ_{MAX} values that lie outside of current actuator capability.

With these concepts in mind, the rotor was stiffened to a torsional frequency of ν_θ=3.0, and the baseline value of pre-pitch was selected to be θ_{Pre}=16°, which allows a trim solution to be found without tail inputs, albeit with large TEF deflections. Additionally, in order to reduce the extreme TEF deflections required in hover, the CG location was moved forward from 1.525 feet behind the mast to 1.1 feet behind the mast. This reduces the need for β_{1c} (from 3° to 0°), but it makes β_{1s} worse by 0.4° (from 3.02° to 3.47°). This trade-off is due to the UH-60 forward shaft tilt, tail rotor height, and tail rotor cant angle that couple moments in all three directions. Blade flapping in hover cannot be reduced further unless a lateral CG variation is considered—a step not take in this study. Despite a small trade-off in terms of flapping, the required δ_1 inputs dropped from 8.3° to 6.5° after the CG was moved. From this starting point, simulations were performed in order to determine the level of flap deflections necessary to trim the rotor and the amount that could be reduced with moveable tail inputs.

In order to demonstrate the high levels of TEF inputs required to trim the aircraft without stabilator inputs, the TEF-deflection envelope plots for ν_θ=3.0 is reproduced in Figure 3-39. The stiffer the rotor becomes, the less the TEFs behave as pitch flaps and the more they behave like lift flaps. Thus, in order to achieve the cyclic lift required, the TEF deflection envelope for this stiffer rotor is $\Delta\delta_{TOT}$=26.6°, its δ_{MAX}=17.9°, and its forward speed is capped at less than μ=0.30. All three of these results are unsatisfactory, and four problems become immediately apparent. The first is that the large TEF envelope is driven primarily by the large change in δ_0 required across the various airspeeds. The second is the large δ_{MAX} in moderate airspeed that is also strongly tied to the large δ_0 required at this airspeed. The third is the large δ_1 in hover, and the fourth is

the large δ_1 required at high speed. The first problem might be mitigated by a second means of thrust control such as a variable RPM rotor. The second issue can be partially remedied through a lower value of pre-pitch. The third objection can be addressed through a better CG location. Finally, the large δ_{MAX}, the limited forward speed, and the large δ_1 at high speed can be demonstrably improved by addition of horizontal tail inputs. Clearly, a new design incorporating these features has taken a serious departure from the standard UH-60 that was in view earlier in the study. However, should a stiff rotor be needed, these are some of the issues that arise and ways of accommodating them. On the other hand, the number of unusual solutions to the problems posed by a stiff rotor does highlight its difficulty in implementation.

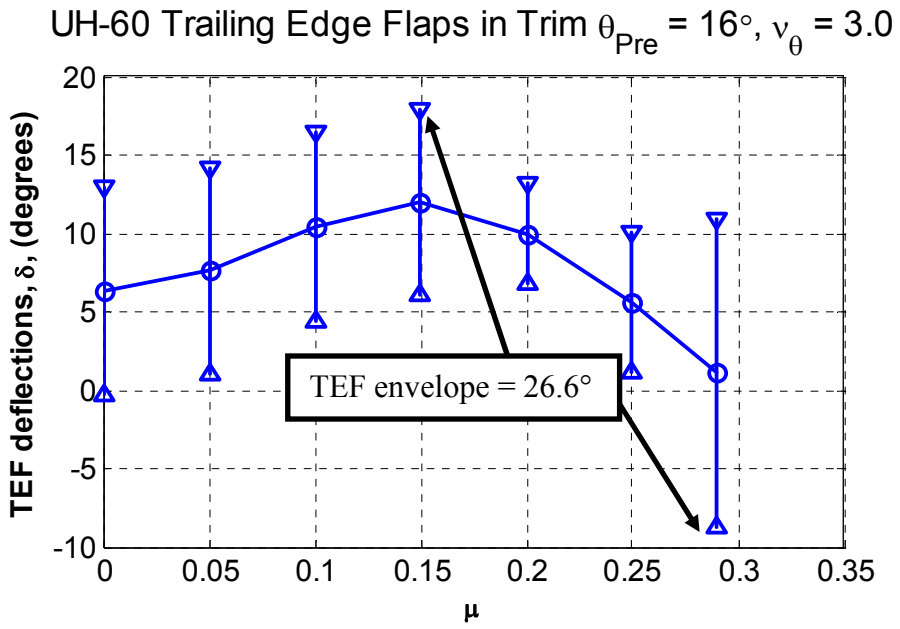

Figure 3-39: TEF Deflection Envelope for Stiff Rotor, ν_θ=3.0

Figure 3-40 demonstrates the dramatic improvements in δ_{MAX} and $\Delta\delta_{TOT}$ that result once horizontal tail inputs are added to the stiffened rotor. Once again, the results

for μ=0.20 and 0.30 are summarized in Table 3-8, and the contour plots are published in Appendix D. Several interesting results are worth noting. First, the horizontal tail is quite effective in reducing cyclic flap requirements. At both airspeeds presented, the 1/rev flap deflections are reduced to less than 1°. Of interest is the μ=0.30 case, where the reduction in δ_1 is accompanied by a significant beneficial increase in δ_0, which is preferable for several reasons. First, it constitutes a much smaller TEF range for that airspeed. Rather than traversing a 20° sweep during one revolution, the TEF only needs to vary by 1° each rotation. It also reduces the large range of values that δ_0 takes on, and since both δ_0 and δ_1 are both important in driving the size of the deflection envelope, minimizing the size of both is equally important.

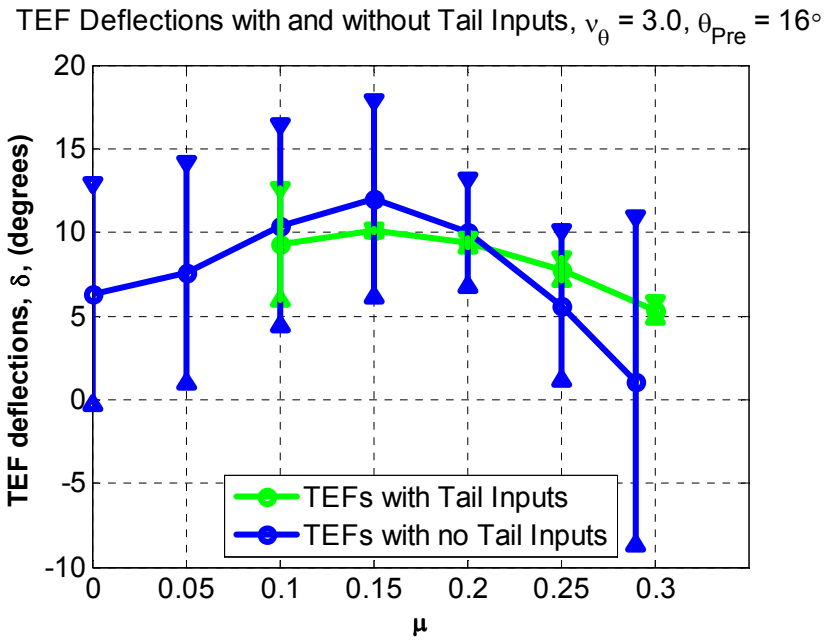

Figure 3-40: Improvement in TEF Deflection Envelope, Stiffened Rotor, θ_{Pre}=16°

The mechanism by which the δ_0 requirements change with relaxed flapping requirements is explained in detail in Section 3.7.1, but it is interesting to note that this

principle still operates on the stiffer rotor. One question associated with such a large change in δ_0 is that δ_0 and θ_0 typically indicate a change in required thrust, which shouldn't be needed. At the same flight speed, with almost the same vehicle attitude (producing a fairly constant amount of drag), one would expect almost the same main rotor thrust. Indeed, despite the large change in δ_0, and a corresponding change in θ_0, the main rotor thrust differs by only 30 lbs. This is because the reduction in θ_0 is offset by the positive lift increment arising from the positive flap deflection. The power savings, then, arise from reducing the very large cyclic flap deflections.

Table 3-8: Summary of Stiffened Rotor, Horizontal Tail Solutions, θ_{Pre}=16°

	μ = 0.20		μ = 0.30	
θ_{pre}=16° ν_θ=3.0	**Baseline swash-plateless**	**Hor Tail swash-plateless**	**Baseline swash-plateless**	**Hor Tail swash-plateless**
		min δ_1		***min δ_1***
ε_{coll}	4.75°	3°	0°	3°
ε_{diff}	-	-5°	-	-5°
δ_0	10.1°	9.4°	1.07°	5.34°
δ_1	3.36°	.26°	9.8°	.5°
α_{WL}	-0.83°	-1.94°	2.1°	4.2°
β_{1c}	1.5°	2.6°	2.7°	-.25°
Power (hp)	1365	1379	2343	1910
$\Delta\delta_{TOT}$	26.6°	13.2°	26.6°	13.2°
δ_{MAX}	17.9°	12.9°	17.9°	12.9°

In order to appreciate the gains made by the horizontal tail, Table 3-8 shows the values of $\Delta\delta_{TOT}$, δ_{MAX}, and the vehicle attitude for multiple airspeeds with and without stabilator inputs. $\Delta\delta_{TOT}$ is improved by 100% and δ_{MAX} improves by 38%. Additionally,

one can see that this configuration does not present an objectionable attitude at any airspeed, nor does it entail unacceptably high blade flapping. Thus a compromise solution is not required. The problem with the above results, however, is that, although many gains are made with the horizontal tail, the hover solution is still a limiting factor. More importantly, the entire TEF deflection envelope for the case with horizontal tail inputs lies well above the band of actuator capability. The natural method of fixing this problem is to reduce the pre-pitch. This is considered next.

3.7.4 Horizontal Tail Study for Stiffened Rotor, v_θ=3.0, θ_{Pre}=12°

Figure 3-41 demonstrates the improvement in both δ_{MAX} and $\Delta\delta_{TOT}$ with a decrease in pitch index. The solutions with horizontal tail inputs for θ_{Pre}=12° appears almost parallel to the solution for θ_{Pre}=16°, with the exception of larger 1/rev requirements at μ=0.30. This is due to a loss in self-trim with the lower pre-pitch. One can additionally see how much improvement the moveable stabilator brings with respect to the θ_{Pre} results without tail inputs. Without tail inputs, a solution for θ_{Pre}=12° is not possible for μ>0.25. With tail inputs, the solution exists, but it still strays beyond the capability of current actuators in hover and at low speed. This is due to the lateral flapping required in hover and due to the change in δ_0 required in moderate speed flight. This feature can be improved if an additional means of controlling thrust such as a variable RPM rotor is to be considered, although that lies outside the scope of this thesis.

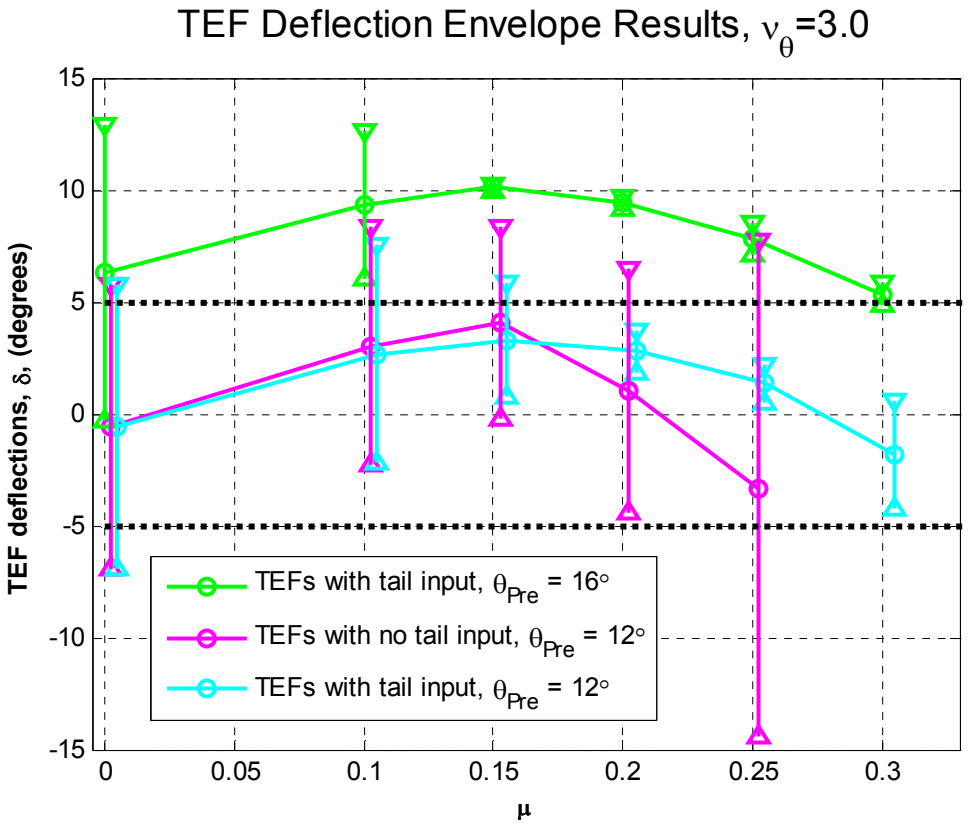

Figure 3-41: Improvement in TEF Deflection Envelope, Stiffened Rotor, θ_{Pre}=12°

However, before continuing, one must examine the impact of the lower pre-pitch on vehicle attitude. Table 3-9 details the impact of the horizontal tail inputs on attitude and power, and the detailed contour plots are included in Appendix 4. As usual, at μ=0.20, the tail inputs actually cause a slight improvement in vehicle attitude and power. However, at μ=0.30, the now-familiar large nose down attitude with excessive blow-back results. In this case, however, there is very little room to find a compromise solution. The best that this configuration can do while staying within the actuator limits at this airspeed does not constitute an improvement whatsoever in attitude or flapping for three reasons. First, since the rotor is stiff in torsion, it takes more TEF inputs to yield a

resulting pitch and blade flapping response. Therefore, the TEFs reach their actuator limits before they have had much effect on the rotor response. Secondly, because the rotor is pre-pitched so low, there is a reduced opportunity for self-trim in pitch. Thus, all of the lift variation derives from control inputs, and not from any inherent elegance in the design of the system as in the case of soft, highly pre-pitched rotors. Finally, the lateral flapping demands as a result of moving the CG have not gone away, and their presence only decreases the amount of control authority that can be applied toward improving pitch attitude before reaching actuator saturation.

Table 3-9: Summary of Stiffened Rotor, Horizontal Tail Solutions, θ_{Pre}=12°

	μ=0.20			**μ=0.30**	
θ_{pre}=12° ν_θ=3.0	**Baseline swash-plateless**	**Hor Tail swash-plateless *min δ_1***	**Baseline swash-plateless**	**Hor Tail swash-plateless *min δ_1***	**Hor Tail swash-plateless *compromise***
ε_{coll}	4.75°	9°	*Trim*	11°	9°
ε_{diff}	-	-11°	*not*	-11°	-11°
δ_0	1.01°	2.78°	*possible*	1.81°	-2.31°
δ_1	5.42°	.97°		2.44°	3.1°
α_{WL}	-.85°	1.3°		10.52°	8.97°
β_{1c}	1.48°	.63°		-5.54°	-4.24°
Power (hp)	1355	1284		1998	2011
$\Delta\delta_{TOT}$	22.8°	12.7°		12.7°	12.7°
δ_{MAX}	14.4°	6.92°		6.92°	6.92°

To summarize the results for the stiff rotor, the horizontal tail is quite effective in reducing 1/rev inputs and even δ_0 requirements, but it does not yield a feasible solution for the torsionally stiffened rotor. This design has problems in hover, in low to moderate

speeds and at high speeds. First, the design is always bound by the hover condition, and even after moving the CG forward to improve hover attitude and flapping, the hover solution still remains outside current actuator limits for both values of pre-pitch considered. Across the flight speed range, both torsionally stiff rotors require large variation in δ_0 due to the lower power that is required in moderate speed flight. This fact will always inflate both the $\Delta\delta_{TOT}$ and the δ_{MAX}, usually causing a δ_{MAX} at a low airspeed where the horizontal tail is not able to improve the solution. At high speed, one is met with a no-win trade off situation. High pre-pitch values provide high speed solutions well within actuator capability and without vehicle attitude problems. And yet, higher pre-pitch only exacerbates all of the low-speed and hover problems just listed. A lower pre-pitch mitigates the low-speed problems and even offers a solution that appears to lie within actuator limits at high speed, but the resulting vehicle attitude and lack of compromise solutions disqualify this as a feasible solution. The only way this might work is with the inclusion of an additional means of controlling thrust, such as a variable RPM rotor. A variable RPM rotor also would have the interesting feature of being variable stiffness (in torsion), since the propeller moment changes with the square of the RPM.

3.8 Results Summary

This section of the thesis provided several distinct analyses of the swashplateless rotor. First, the model was validated against known simulations (CAMRAD II) and flight test. Then a baseline swashplateless case was analyzed with parameters based on

recommendations published in previous research. Then, pitch-index and torsional stiffness studies were accomplished to examine the physical workings of the system and to recommend values for the horizontal tail case. In short, higher pre-pitch values and low root stiffnesses allowed for flight at higher speed, better power savings, and smaller TEF deflections. A combination of ν_θ=2.1 and θ_{Pre}=20° was selected as optimal for this configuration. Finally, horizontal tail studies were done for the baseline case (ν_θ=2.1, θ_{Pre}=16°), the case recommended by the current parametric studies (ν_θ=2.1, θ_{Pre}=20°), and a stiffened rotor (ν_θ=3.0, θ_{Pre}=16°). In each case, the cyclic TEF deflections were dramatically reduced with appropriate tail inputs. With the proper selection of pre-pitch and horizontal tail, the aircraft could be trimmed up to μ=.30 while keeping the entire TEF deflection envelope within the limit of current actuators (±5°) and without unrealistic flight attitudes.

Chapter 4

Summary and Conclusions

Many technical hurdles stand between the current state of technology and a fully-realized swashplateless rotor with trailing edge elevons. One of these hurdles is the large deflections that are required of a TEF-controlled rotor. The purpose of this study was to determine the effectiveness of horizontal tail inputs in reducing TEF deflections and to determine what other system responses would be realized. To that end, the thesis detailed a review of the state of technology for swashplateless control of a helicopter through trailing edge flaps and other means. A simulation model was developed to analyze the response and performance of such a vehicle to various parameters in trim. Parametric studies of the more significant parameters were performed, the results were discussed, and important physical phenomena were highlighted. Finally, a new moveable horizontal tail technology was applied to the helicopter, and elevon deflections and main rotor power were significantly reduced from the baseline swashplateless configuration with only a meager cost in terms of vehicle attitude and blade flapping. This technique has also been applied to a torsionally stiffened rotor, and its effect has been examined.

4.1 Modeling Summary

This study utilized a model designed to accurately predict blade, hub, and vehicle behavior in propulsive trim. It incorporated rigid blade analysis that was free to deflect in

flap, lag, and pitch for the conventional helicopter, and free to deflect in flap and pitch for the swashplateless rotor. It modeled inflow with Drees' linear distribution, captured quasi-steady airloads arising from the blade and TEF's static angles, pitching rates and accelerations, and plunging rates and accelerations through Theodorsen's classic theory. It modeled aerodynamic forces and moments resulting from the fuselage, the horizontal tail, the tail rotor, and the main rotor wake. This model incorporated many refinements specifics to a UH-60 in order to yield a high degree of fidelity in aircraft response to various inputs, especially the new horizontal tail inputs.

4.2 Results Summary

First, this study presented numerical analysis results for a standard swashplated helicopter in order to demonstrate the accuracy of the vehicle trim code in control inputs. Then, the research examined the case of a swashplateless model including a single 20% chord, 20% span trailing edge flap located between 70% and 90% rotor radius. The root restraint was softened to a nominal non-dimensional natural frequency of ν_θ=2.1/rev, and the blade was pre-pitched to various angles. Comparisons were made between Shen's MDART analysis and Falls' UH-60 TEF analysis. Additionally, two new parameters were defined in order to assist in analyzing the various configurations. $\Delta\delta_{TOT}$ comprises the difference between the very highest and the very lowest predicted flap deflections. δ_{MAX} represents the single largest deflection magnitude that the flap must attain when all airspeeds are considered.

After confirming that matching trends existed between the current study and prior work and that other differences arose primarily from modeling differences, parametric studies were performed of pre-pitch and torsional stiffness. Of note, pre-pitch has a direct effect on the size of collective TEF application required at low to moderate speed (more pitch index required more δ_0 at low speeds), but it also enables the aircraft to fly faster since it delays TEF reversal to a higher airspeed. An increase in pitch index was also found to be a key parameter in finding amenable trim control values. Once the pre-pitch study was complete, a study of the effect of torsional stiffness was conducted. As expected, an increase in torsional stiffness requires more collective TEF (or less pre-pitch) and more cyclic TEF application. A combination ν_θ=2.1 and θ_{pre}=20° was found to offer the best solution in terms of mild control inputs, reduced TEF deflection envelope, and ability to trim at high speed.

Once the parametric studies were complete, a moveable horizontal tail free to make collective (ε_{coll}) and differential (ε_{diff}) angular inputs was applied to the helicopter. The aircraft was then re-trimmed at airspeed increments of 20 knots from 43 knots (μ=0.1) to 120+ knots (μ=0.3) with a sweep of horizontal tail inputs. These results provided the opportunity to observe the effect of the horizontal tail inputs on all of the other pertinent trim controls as well as rotor and vehicle response. The horizontal tail inputs were capable of practically eliminating cyclic TEF input requirements at airspeeds greater than μ=0.2 for both values of pitch index tested. These results are summarized in Figure 4-1 . At low to moderate airspeeds, the horizontal tail inputs reduced δ_1 while simultaneously improving vehicle attitude and power required as depicted in Table 4.1. Between the two values of pre-pitch, the higher pre-pitch value yielded better results.

Table 4.1: Results of the Various Rotor Models at $\mu = 0.20$, $\nu_\theta = 2.1$

μ = .2	**ε_{coll}**	**ε_{diff}**	**δ_0**	**δ_1**	**α_{WL}**	**β_{1c}**	**Power** (hp)
Conventional (swashplate)	4.75°	-	n/a	n/a	-2.5°	3.09°	1139
$\theta_{Pre} = 16°$							
Baseline swashplateless	4.75°	-	-0.92°	3.11°	-2.3°	3.0°	1318
Horizontal Tail Swashplateless*	12°	-8°	0.31°	0.5°	1.94°	-1.13°	1276
$\theta_{Pre} = 20°$							
Baseline swashplateless	4.75°	-	2°	1.25°	-2.31°	2.99°	1298
Horizontal Tail Swashplateless*	8°	-4°	2.56°	0.12°	-0.47°	1.15°	1280

* solution for minimum cyclic TEF inputs (min-δ_1)

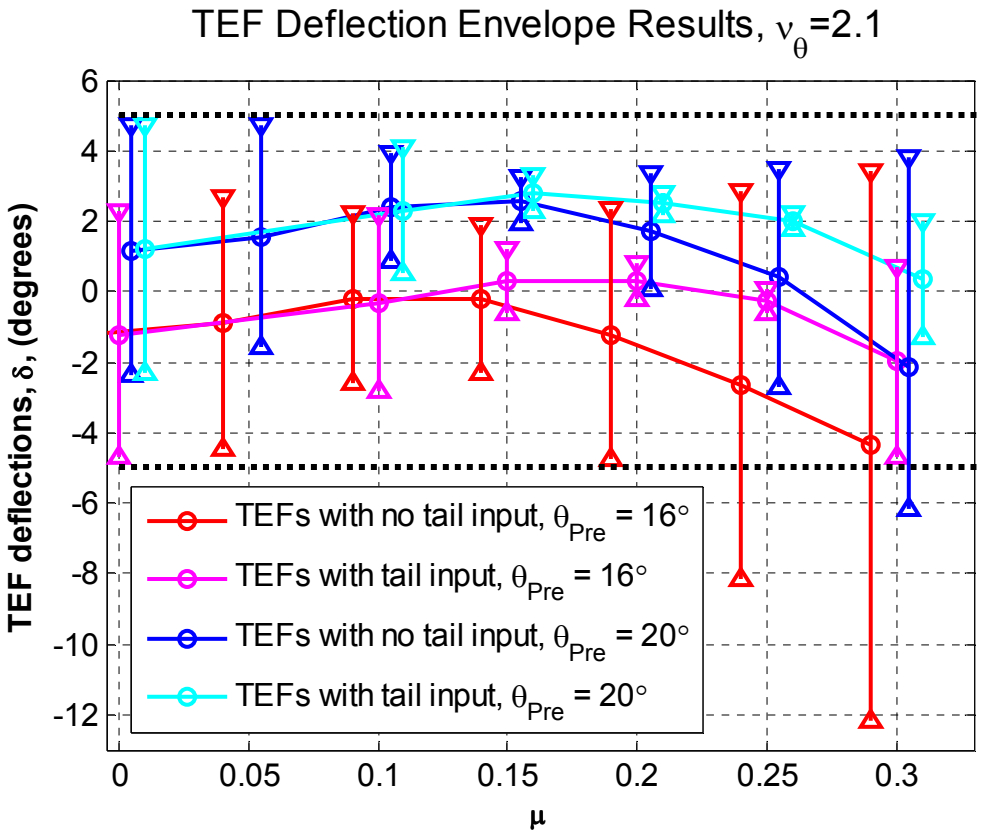

Figure 4-1: TEF Deflection Envelope for Various θ_{Pre}, ν_θ=2.1

Table 4.2 lists the results for both values of pre-pitch at μ=0.30. At higher airspeeds, the elimination of δ_1 inputs caused unfavorable blade flapping and vehicle attitudes. As such, a compromise solution was found that restricted the flap deflections at this airspeed to ±5° while sustaining a more natural flight attitude.

Table 4.2: Results of the Various Rotor Models at $\mu = 0.30$, $\nu_\theta = 2.1$

μ = .3	ε_{coll}	ε_{diff}	δ_0	δ_1	α_{WL}	β_{1c}	**Power** (hp)
Conventional (swashplate)	0°	-	n/a	n/a	1.08°	3.28°	1745
$\theta_{Pre} = 16°$							
Baseline swashplateless	0°	-	-4.7°	8.3°	1.3°	3.7°	2311
Horizontal Tail Swashplateless minimum-δ1	11°	-8°	-1°	.25°	10.3°	-5.5°	2017
Horizontal Tail Swashplateless compromise	6°	-8°	-1.98°	2.7°	6.0°	-1.6°	2055
$\theta_{Pre} = 20°$							
Baseline swashplateless	0°	-	-1.22°	5.1°	1.2°	3.7°	2072
Horizontal Tail Swashplateless minimum-δ1	7°	-4°	1.05°	.2°	6.8°	-2.3°	1920
Horizontal Tail Swashplateless compromise	4°	-4°	.35°	1.65°	4.45°	0°	1957

Additionally, as summarized in Table 4-3, the TEF deflection envelope $\Delta\delta_{TOT}$ <10° for both values of pre-pitch tested on the soft rotor once horizontal tail inputs were added. Additionally, δ_{MAX} remained less than 5° for both values of pre-pitch. These two criteria, along with the resultant vehicle attitude and power, define the feasibility of the system. As can be seen in Table 4-3, both soft rotors represent feasible solutions, although the higher pre-pitch rotor is a better design. Interestingly the $\Delta\delta_{TOT}$ and δ_{MAX}

for both of these systems is defined by the hover condition, which is why they are virtually identical. One must remember, however, that the UH-60 hover attitude is quite unusual and requires significant blade flapping. A helicopter with a more level hover attitude may not predict the largest control inputs to be at the hover condition. However, for this study, one result of adding horizontal tail inputs is moving the driving considerations for the TEF deflection envelope and δ_{MAX} from high-speed to low speed, where the tail has less control authority.

Table 4-3: Deflection Envelope and δ_{MAX} summary

	θ_{Pre}=16° ν_θ=2.1	θ_{Pre}=20° ν_θ=2.1	θ_{Pre}=16° ν_θ=3.0	θ_{Pre}=12° ν_θ=3.0
$\Delta\delta_{TOT}$	6.9°	7.0°	13.2°	12.9°
δ_{MAX}	4.71°	4.71°	12.9°	6.92°
Feasible	Yes	Yes	No	No

In addition to manipulating the horizontal tail both collectively and differentially, the system was restricted to only collective adjustment and the cases were re-examined. Only the higher pre-pitch of 20° could find trim solutions that fell within current actuator capability of ±5°. This is because the self-trimming feature of soft rotors with high pre-pitch caused less lateral dissymmetry of lift at the same airspeed. This translates into lower lateral TEF deflections required to trim the rotor. In spite of the improved performance of the rotor with θ_{Pre}=20°, the 1.5° of 1/rev actuator capability that remained after achieving trim with only ε_{coll} input leaves the capability to maneuver in doubt. Thus, in order to leave the maximum actuator stroke available to maneuver, the size of the TEF deflection envelope is not the only important consideration. Figure 4-2 demonstrates that the placement of the TEF deflection envelope within the band of

actuation capability at each airspeed is also important. For example, at μ=.16, the 1/rev TEF deflections are very modest. However, they are off-center within the bands of actuator capability (±5° depicted in black) such that only 1.7° of actuator stroke is left to perform maneuvers. By contrast, although the δ_1 is three times higher at μ=.31, there is more actuator left for maneuver because it is more centered within the capability bands. In general, the TEF deflection envelope should be centered as much as possible on δ_0=0°, thereby yielding the smallest δ_{MAX} for a given $\Delta\delta_{TOT}$. Such an arrangement would only be possible by augmenting thrust with some other parameter, such as variable RPM. A lower pre-pitch will not solve this problem, because while improving the TEF range at moderate speeds, it will worsen performance at the high speed end of the flight envelope.

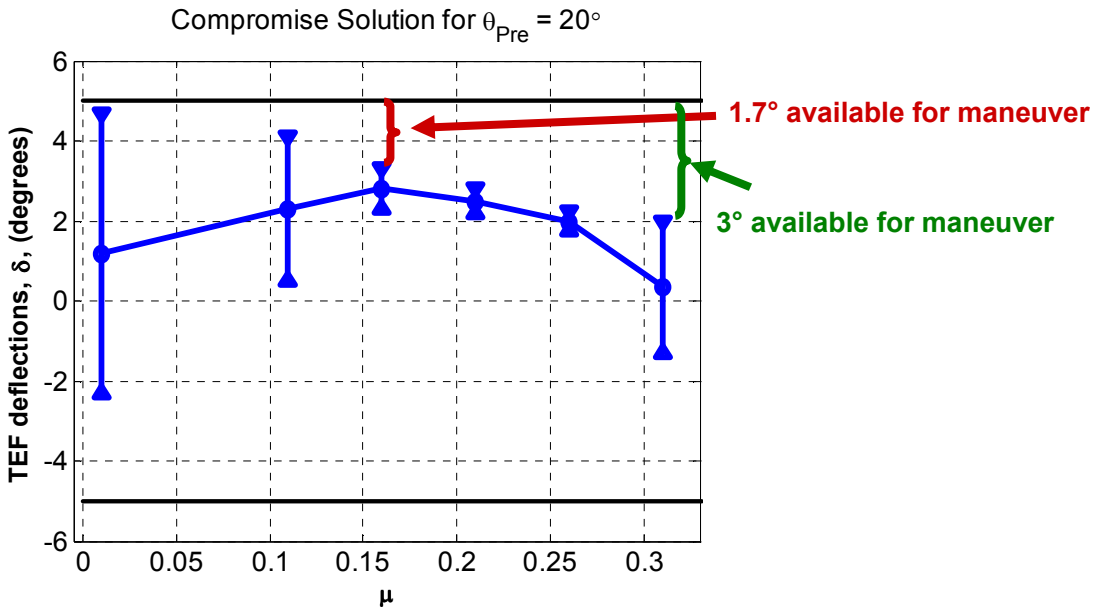

Figure 4-2: TEF Deflection Envelope Impact on Maneuver Capability

Finally, the rotor was then stiffened in the torsional degree of freedom to ν_θ=3.0 in order to determine if the cyclic deflections could be minimized in a similar fashion. Two

values of pre-pitch were considered (θ_{Pre}=16° and 12°). Figure 4-3 displays the results of the two values of pre-pitch with horizontal tail inputs included. Although favorable δ_1 and blade response resulted from this application, the TEF deflection envelope and δ_{MAX} remained unacceptably high due to the inescapably large δ_0 deflections that were required across the flight envelope and due to the unusual hover attitude of the UH-60, even after the CG had been moved forward to eliminate β_{1c}. However, the horizontal tail did have an effect on the system response by generally saving power and reducing cyclic deflections. Once again, the horizontal tail moves the $\Delta\delta_{TOT}$ and δ_{MAX} limiting condition from high speed to low speed. Numerical results are not reproduced in this chapter since the stiff rotor does not constitute a feasible solution with respect to current actuator capability, but these results are detailed in Sections 3.7.3 and 3.7.4.

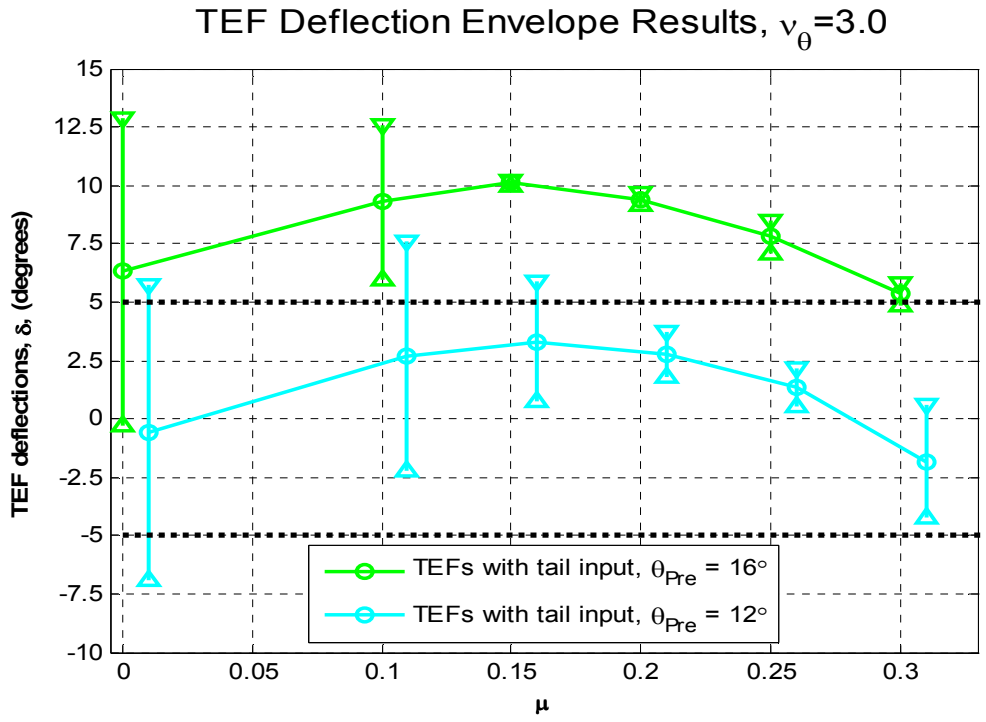

Figure 4-3: TEF Deflection Envelopes for the Stiffened Rotor, ν_θ=3.0

In addition to these direct results of the various simulations, several physical features were made manifest throughout the analysis. The first was the importance of δ_{MAX} as the ultimate criterion for suitability of a TEF-controlled rotor. This parameter is always a consideration because anytime one parameter is changed to improve performance at one end of the flight envelope, its effect elsewhere on the TEF deflection envelope, and therefore δ_{MAX}, must also be accounted for. Additionally, the many advantages of appropriately high pitch index (θ_{Pre}) were detailed. In short, rotors with higher pre-pitch could fly to faster airspeeds, consumed less power, realized smaller TEF deflection envelopes due to an improvement of 1/rev inputs at high speed, were better able to self-trim in high speed flight, and suppressed the emergence of the second harmonic pitch response. Additionally, the horizontal tail inputs, while improving the 1/rev TEF inputs at high speed simultaneously reduced the negative δ_0 inputs at high speed as well, yielding a very beneficial side-effect.

In short, thesis confirmed several previously established principles and also determined the significant effect that horizontal tail control inputs on making the swashplateless rotor concept more feasible.

4.3 Recommendations for Future Work

Because this research topic is still in its infancy, there are many areas of research that need to establish how a TEF controlled rotor supplemented with a horizontal tail would perform under various conditions. Trim in forward flight is a base requirement that needs to be demonstrated, and it allows for the physical underpinnings of the system

to be explored. Parametric studies such as are included in this thesis help to accomplish exactly that. However, there are several directions in which research of this technology could proceed: modeling improvements, improving the system response as it stands, and exploring the maneuver and flight safety ramifications of this technology.

The first area that should receive attention is to refine the modeling techniques available to designers attempting to explore the feasibility of TEF controlled rotors. Much work has been done in this area already. Of vital importance is establishing the actual increment in lift, drag, and moment generated by a flap deflection as a function of Mach number, blade angle of attack, and flap angle of attack with compressibility effects and flow separation fully captured. Theories based on thin airfoil theory have played a crucial role in the analysis of TEF rotors to date, especially for TEFs designed to reduce vibrations. However, the deflections required to trim an aircraft are much higher and require greater fidelity than thin airfoil theory can provide. Although attempts are underway to establish these relationships via CFD analysis, experimental tests that allow for a wide range of both positive and negative δ's are also necessary to confirm the CFD results. Additionally, it has already been demonstrated that the performance of the blade-flap is highly dependent on the shape of the base airfoil. CFD and wind tunnel tests need to be done on the blade that will be utilized on a TEF-controlled rotor.

In a similar vein, modeling improvements in the calculation of the wake induced effects are required, especially before any in-depth analysis of power is attempted. The wake model that is needed must be able to handle the differences in local circulation produced by TEF deflections, as well as the stronger trailed vorticity that will be shed from the edges of the flap. Additionally, wake effects on the horizontal tail need

refinement, especially as the rotor attitude changes the wake skew angle. If maneuvering flight studies are to be undertaken, it will also have a very large effect on the simulation.

Another important direction to pursue would be to maximize the performance of the TEF controlled rotor. In short, for a TEF controlled rotor to be successful, it must be able to produce the maximum blade flapping for a certain elevon input in a configuration that is stable. There are multiple means of achieving this. The first is to attempt to maximize the blade pitch due to an elevon input. The most direct way of doing this is reducing the torsional stiffness even further. Once that is done, careful study must be made to determine if the blade-flap system is stable, and what must be done to make it more stable. Aside from attempting to improve the pitch response of the blade, one can vary other parameters in order to affect the blade flapping response. In particular, use of a $-\delta_3$ angle would mechanically couple blade flapping to blade pitch, and increase the blade flapping as a result. Once again, the stability of such a system would be an important area of research. A somewhat less effective way of maximizing the blade flapping is to lower the blade flapping frequency (which could be done by $-\delta_3$ as well).

A second way of maximizing the performance of the TEF controlled rotor is to reduce the higher harmonic response of blade pitching. Several means could be used to achieve this. Mechanical coupling between blade pitch and blade flapping tends to reduce the second harmonic response in pitch due to the significant aerodynamic damping of blade flapping that exists. Either positive or negative δ_3 could be used to achieve the desired effect. Additionally, a torsional damper could be used to reduce the second harmonic response. This must be investigated thoroughly since a torsional damper may have beneficial side effects in terms of stability, but it will also reduce the

desired 1/rev pitch response as well. Aside from structural means of improving response, properly phased 2/rev TEF inputs may also reduce unwanted 2/rev pitch response. This sort of input would not be difficult to superimpose on top of a 1/rev primary control input if the design is using smart material actuators. Cheng and Celi have reported that a second harmonic input may have additional power benefits as well that are worth exploring [48].

Beyond simply improving the rotor response, issues pertaining to the vehicle's stability, control, and maneuverability must be examined. Maneuvering flight capability is a significant concern as TEF-controlled rotors may saturate their actuators in achieving trimmed flight, leaving little margin for control of dynamic flight. These limitations should benefit from horizontal tail application for two reasons. Smaller absolute TEF deflections in trim leave a margin for maneuver via the TEFs themselves, and horizontal tail inputs may also be used to apply maneuvering forces and moments directly, a feature that may be required in the case where the TEF deflections are offset by δ_0 far enough that they leave very little actuator stroke on one side of the deflection range for maneuver. In addition to forward flight maneuverability, hover and low speed maneuverability as well as autorotation are also significant concerns for this kind of design. Each of these must be explored in detail.

In addition to the maneuver implications of horizontal tail inputs, this system potentially offers a heretofore non-existent means of redundant control, significantly improving the safety and viability of the TEF-controlled rotor concept. Much in the same way that hydraulic failures are currently handled on light helicopters, horizontal tail inputs could allow a helicopter that experienced a TEF failure to be safely controlled and

flown to an appropriate landing zone where a roll-on landing could be accomplished. In addition to this possibility, the effect of one or more TEF failures to different states must be addressed. One must establish the ramifications of one or more TEFs failing to a free flight condition. Furthermore, a TEF failure to a fixed input value would induce an entirely different system response, and this must also be documented.

Once a higher fidelity model is available to researchers, an extensive study of the power ramifications of different configurations would be possible. In particular, CFD or wind-tunnel based data that properly models the drag of the blade-flap is key to power predictions. Of course, advanced wake analysis is also critical to accurate power analysis. Finally, an exploration into the effect of second harmonic TEF inputs or even IBC inputs could be made in attempts to optimize power.

One of the limiting factors in the TEF-controlled rotor is the pre-pitch. The pre-pitch value must be selected based primarily on the range in differences between thrust required at different flight speeds. This is reflected directly in the variation of δ_0. However, this design tradeoff in terms of pre-pitch assumes a constant rotational velocity. If the rotational velocity of the rotor could vary by ±10%, as is possible through an engine controller, a significant range in thrust could be achieved. This would likely lower the pre-pitch values required to fly at high speed and further reduce the TEF deflection envelope by minimizing the change in δ_0 across the flight envelope. This feature would likely enable the issue of torsionally stiffening the swashplateless design to be revisited, because the parameter that most immediately prevented an increase in torsional stiffness was the large variation in δ_0 required across the flight envelope. Additionally, when absolute TEF deflections are minimized at any airspeed, power

improves as well. It would also leave greater TEF margin at each airspeed available for maneuver, and it would introduce an element of variable torsional stiffness as well. This flexibility in the means of producing thrust would also better enable a TEF-controlled rotor to deal with varying max gross weights of the helicopter. Once enough variables are added to the control input, a real optimization of the flight against some objective function such as maximum range or maximum endurance is possible.

Once multiple functions of trailing edge flaps are considered, one cannot help but consider the effect of including multiple trailing edge flaps in a spanwise distribution along the rotor blade. These multiple flaps could be designed to perform different missions (primary control for one set and vibration reduction for another), but they could also provide a measure of control redundancy or increased control authority when needed. Additionally, their ability to redistribute lift on the blade may have power savings potential. Another advanced area of research would be to include active feedback and control in the system. This would most naturally lend itself to vibration reduction, but Kaman reports that they have already implemented such a system for active blade track in an effort to eliminate 1/rev vibrations [10]. Such a system could also be added on top of the primary control function of the elevons.

All of the trim analysis included in this thesis was performed on an aircraft with a single gross weight and at a standard sea-level condition. The change in gross weight of an aircraft due to loading or fuel consumption during the course of a flight may have a significant impact in the TEF deflection envelope requirements. These effects must be established. Additionally, changes in air density, as occur with changes in altitude and

temperature, will also have a significant effect on the performance of the rotor. These effects must also be understood and quantified.

Aside from the many analytical studies that need to be documented, this concept must be demonstrated experimentally. Although much work has been done in experimentally demonstrating the effectiveness of TEFs in reducing vibrations, primary control has yet to be demonstrated by a working model. This effort would require solving many practical engineering problems that are not directly addressed in this study to include selecting and implementing a suitable actuator, mounting considerations, and transferring the power and control signals into the rotating frame. Although designers could likely borrow many of the techniques already employed for vibration-reduction TEFs, it still represents an important step in demonstrating this technology. Wind tunnel testing of the system would allow various shaft angles to be set, and the rotor response to various TEF inputs to be tested. Such data would be an invaluable contribution in terms of validation and analysis.

In summary, introducing primary control into the rotating frame opens many possibilities for performance gains. The relative merits and design tradeoffs implicated in utilizing TEFs for multiple functions needs to be further established. However, before such lofty endeavors are undertaken, much more research needs to be done in order to maximize the response of the rotor itself to TEF inputs. Clearly, several techniques exist that have yet to be investigated. An understanding of each of these is vital to the successful implementation of a rotor equipped with trailing edge flaps for primary control.

4.4 Conclusion

This thesis has reviewed the potential performance and operational gains that can be expected from implementing a successful swashplateless rotor. A successful swashplateless rotor promises to reduce the weight and drag of the fuselage, reduce main rotor vibrations, and improve component life and maintenance cost. A conventional rotor incorporates layers of engineering solutions in order to overcome the many unique challenges that the rotor's aerodynamic environment presents. On the other hand, a TEF-controlled swashplateless rotor takes advantage of many of these unique aerodynamic features to yield a responsive, elegant control system. Although several key technological barriers exist before this concept becomes a reality, the concept is worthy of continued research.

This study has also reinforced the veracity of several key principles involved with designing a swashplateless rotor controlled with trailing edge flaps, such as reduced torsional stiffness and proper pitch-indexing. Although pitch indexing varies from airframe to airframe based on the rotor's aeromechanical characteristics, properly selecting this parameter will have a large influence over the required control inputs, maximum forward airspeed, and power required. Low torsional stiffness has also been demonstrated to be a necessary characteristic of swashplateless rotors. Even with the ability to input large forces and moments from the fixed frame, stiff rotors require an unacceptably large flap deflection envelope and yield detrimental vehicle attitudes. Although supplemental means of producing thrust may address this problem, it remains an effective barrier on increasing torsional stiffness of the rotor blades.

Finally, this research effort has demonstrated the benefits of supplementing TEF control with horizontal tail control to create a redundant system capable of finding the most beneficial flight configuration at any airspeed where the helicopter can achieve trim. This study has demonstrated the ability of horizontal tail inputs to reduce elevon deflections to acceptable levels, reduce required power, and modify vehicle attitude. This technique also holds the potential to offer redundant control and improved maneuvering agility. Although much work needs to be done, the concept remains a viable means of achieving the goal of responsive and robust helicopter control without a swashplate.

Bibliography

1. Leishman, J.G., *Principles of Helicopter Aerodynamics*, Cambridge University Press, 2000.

2. Johnson, W., *Helicopter Theory.* Dover Publications, Inc., New York, 1994.

3. Straub, F., Kennedy, D., "Design, Development, Fabrication and Testing of an Active Flap Rotor System," *Proceedings of the 61st Annual Forum of the American Helicopter Society*, Grapevine, TX, June 1-3, 2005.

4 Headquarters, Department of the Army, *Unit and Intermediate Maintenance Manual, TM 1-1520-248-23.* Washington, D.C., 2007.

5. Domke, B., "AH-64A, Paris Airshow," http://www.b-domke.de/AviationImages/Rotorhead/4191.html (June 2001).

6. Kim, J.S., *Design and Analysis of Rotor Systems with Multiple Trailing Edge Flaps and Resonant Actuators.* Ph.D. Thesis, The Pennsylvania State University, Department of Aerospace Engineering, University Park, PA, December 2005.

7. Millot, T, Friedmann, P. "Vibration Reduction in Helicopter Rotors Using an Actively Controlled Partial Span Trailing Edge Flap Located on the Blade," NASA Contractor Report #4611, June 1994.

8. Shen, J. and Chopra, I., "A Parametric Design Study for a Swashplateless Helicopter Rotor with Trailing-Edge Flaps," *Proceedings of the 58th Annual Forum of the American Helicopter Society*, Montreal, Canada, Jun 11-13, 2002.

9. Ormiston, R. A., "Aeroelastic Considerations for Rotorcraft Primary Control with On-Blade Elevons," *Proceedings of the 57th Annual Forum of the American Helicopter Society*, Washington, DC, May 2001.

10. Wei. F. "Design of Soft Torsion Rotor Systems at Kaman Aerospace Corporation," *Proceedings of the 58th Annual Forum of the American Helicopter Society*, Montreal, Canada, Jun 11-13, 2002.

11. Wei, F. "Pitching Moment Control for an Integrated Servo-Flap Rotor," *Proceedings of the 61st Annual Forum of the American Helicopter Society*, Grapevine, TX, June 1-3, 2005.

12. Wei, F. "Design of an Integrated Servo-flap Main Rotor," *Proceedings of the 59th Annual Forum of the American Helicopter Society*, Phoenix, Arizona, May 6-8, 2003.

13. Shen, J. and Chopra, I., "Actuation Requirements for a Swashplateless Helicopter Control System with Trailing-Edge Flaps," *Proceedings of the 43rd AIAA/ASME/ASCE/AHS Structures, Structural Dynamics, and Materials Conference and 10th AIAA/ASME/AHS Adaptive Structures Conference*, AIAA-2002-1444, Denver, Colorado, April 22-25, 2002.

14. Shen, J., Chopra, I., and Johnson, W., "Performance of Swashplateless Ultralight Helicopter Rotor with Trailing-Edge Flaps for Primary Flight Control," *Proceedings of the 59th Annual Forum of the American Helicopter Society*, Phoenix, Arizona, May 6-8, 2003.

15. Shen., J., and Chopra, I., "Swashplateless Helicopter Rotor System with Trailing-Edge Flaps for Flight and Vibration Controls," *Journal of Aircraft*, Vol 43, No. 2, Apr-May 2006, pp. 346-352

16. Shen., J., and Chopra, I., "Aeroelastic Modeling of Trailing-Edge-Flap Helicopter Rotors Including Actuator Dynamics," *Journal of Aircraft*, Vol 41, No. 6, Nov-Dec 2004, pp. 1465-1472.

17. Shen., J., and Chopra, I., "Swashplateless Helicopter Rotor with Trailing-Edge Flaps," *Journal of Aircraft*, Vol 41, No. 2, March-April 2004. pp. 208-214

18. Shen., J., and Chopra, I., "A Parametric Design Study for a Swashplateless Helicopter Rotor with Trailing-Edge Flaps," *Journal of the American Helicopter Society*, Vol. 49, No. 1, January 2004, pp. 43-53

19. Shen, J., *Comprehensive Aeroelastic Analysis of Helicopter Rotor with Trailing Edge Flap for Primary Control and Vibration Control*, PhD Thesis, The University of Maryland, Department of Aerospace Engineering, College Park, MD, 2003.

20. Falls, J., Datta, A., and Chopra, I., "Integrated Trailing-Edge Flaps and Servotabs for Helicopter Primary Control," *Proceedings of the 62nd Annual Forum of the American Helicopter Society*, Phoenix, AZ, May 2006.

21. Falls, J., Datta, A., Chopra, I., "Design and Analysis of Trailing-Edge Flaps and Servotabs for Primary Control." *Proceedings of the 63rd Annual Forum of the American Helicopter Society*, Virginia Beach, Virginia, May 1-3, 2007.

22. Falls, J., Datta, A., Chopra I., "Performance Analysis of Trailing Edge Flaps in Helicopter Primary Control," *Proceedings of the AHS Specialist's Conference on Aeromechanics*, San Francisco, CA, Jan 23-25, 2008.

23. Koratkar, N.A., and Chopra, I., "Analysis And Testing Of Mach-Scaled Rotor With Trailing-Edge Flaps," *AIAA Journal*, Vol. 38, No. 7, July, 2000.

24. Straub, F., "Whirl Tower Test of the SMART Active Flap Rotor," *AHS 4th Decennial Specialist's Conference on Aeromechanics*, San Francisco, Jan 21, 2004.

25. Straub, F. K., et al. "Smart Material-actuated Rotor Technology, 'SMART'." *Journal of Intelligent Material Systems and Structures*, Vol. 15, April 2004.

26. Enenkl, B. , Kloppel, V., and Preibler, D., "Full Scale Rotor with Piezoelectric Actuated Blade Flaps," *28th European Rotorcraft Forum*, Bristol, United Kingdom, Sep 17-19, 2002.

27. Dieterich, O., Enenkl, B., Roth, D., "Trailing Edge Flaps for Active Rotor Control Aeroelastic Characteristics of the ADASYS Rotor System," *Proceedings of the 62nd Annual Forum of the American Helicopter Society*, Phoenix, AZ, May 9-11, 2006.

28. Szefi, J., et al. "Development of a Novel High Authority Piezoelectric Actuator for Rotor Blades with Trailing Edge Flaps." *Proceedings of the 62nd Annual Forum of the American Helicopter Society*, Phoenix, Arizona, May 9-11, 2006.

29. Li, L. Friedmann, P. "Simultaneous Vibration Reduction and Performance Enhancement in Rotorcraft Using Actively Controlled Flaps," *Proceedings of the 62nd Annual Forum of the American Helicopter Society,* Phoenix, AZ, May 9-11, 2006.

30. Patt, D., Li, L., Friedmann, P., "Active Flaps for Noise Reduction: A Computational Study" *Proceedings of the 61st Annual Forum of the American Helicopter Society*, Grapevine, TX, June 1-3, 2005.

31. Milgram, J., *A Comprehensive Aeroelastic Analysis of Helicopter Main Rotor with Trailing Edge Flaps for Vibration Reduction*, PhD Thesis, The University of Maryland, Department of Aerospace Engineering, College Park, MD, 1997.

32. Zhang, J., *Active-Passive Hybrid Optimization of Rotor Blades With Trailing Edge Flaps,* PhD Thesis, The Pennsylvania State University, Department of Aerospace Engineering, May 2001.

33. Liu, L., Friedmann, P., Patt, D., "Simultaneous Vibration and Noise Reduction in Rotorcraft – Practical Implementation Issues," *Proceedings of the 46th AIAA, ASME, AHS/ASC Structures, Structural Dynamics & Materials Conference*, Austin, TX, April 18-21 2005.

34. Theodorsen, T. "General Theory of Aerodynamic Instability and the Mechanism of Flutter," Technical Report No. 496, NACA, 1935.

35. Theodorsen, T., Garrick, I., "Nonstationary Flow About a Wing-Aileron-Tab Combination Including Aerodynamic Balance" Technical Report No. 736, NACA, 1942.

36. Greenberg M., "Airfoil in Sinusoidal Motion in a Pulsating Steam," Technical Report No. 1326, NACA 1947.

37. Hariharan, N., and Leishman, J., "Unsteady Aerodynamics Of A Flapped Airfoil In Subsonic Flow By Indicial Concepts," *Journal of Aircraft*, Vol. 33, No. 5, Sep-October, 1996.

38. Jose, A., Sitaraman, J., Baeder, J. "An Investigation Into the Aerodynamics of Trailing Edge Flap and Flap-Tab Airfoils Using CFD and Analytical Methods." *Proceedings of the 63rd Annual Forum of the American Helicopter Society*, Virginia Beach, Virginia, May 1-3, 2007.

39 Myrtle, T., Friedmann, P., "Application of a New Compressible Time Domain Aerodynamic Model to Vibration Reduction in Helicopters Using an Actively Controlled Flap," *Journal of the American Helicopter Society*, January 2001.

40. Gandhi, F., Sekula, M., "Helicopter Horizontal Tail Incidence Control to Reduce Rotor Cyclic Pitch and Blade Flapping." *Proceedings of the 60th Annual Forum of the American Helicopter Society*, Baltimore, MD, 2004.

41. Gandhi, F., Yoshizaki, Y., "Swashplateless Control of a Rotary-Wing UAV using Variable RPM and a Movable CG," *Proceeding of the 62nd Annual Forum of the American Helicopter Society*, Phoenix, AZ, 2006.

42. Yeo, H., "UH60A_Blade_Property_Ver2_02OCT.xls," *Uh-60a Blade Property Data File for NRTC/RITA Airloads Workshop Participants.* October 2002.

43. Hassan, A., Straub, F., Noonan, K., "Experimental/Numerical Evaluation of Integral Trailing Edge Flaps for Helicopter Rotor Applications," *Journal of the American Helicopter Society*, January 2005.

44. Headquarters, Department of the Army, *Operator's Manual for UH-60A Helicopter, TM 1-1520-237-10*, Washington, D.C., 2003.

45. Howlett, J., "UH-60 Black Hawk Engineering Simulation Program," NASA Contractor Report 166309, December 1981.

46 Yeo, H., Bousman, W., Johnson, W., "Performance Analysis of a Utility Helicopter with Standard and Advanced Rotors," *Journal of the American Helicopter Society*, January 2005.

47 Bousman, W., Kufeld, R., "UH-60 Airloads Catalog," NASA Technical Report No. 2005-212827, August 2005.

48 Cheng, R., Theodore, C., Celi, R., "Effects Of Two/Rev Higher Harmonic Control On Rotor Performance," *Proceedings of the 56th Annual Forum of the American Helicopter Society*, Virginia Beach, Virginia, May 2-4, 2000

49. Hilbert, K., "A Mathematical Model of the UH-60 Helicopter," NASA Technical Memorandum 85890, April 1984.

50 Kaplita, T., "UH-60 Black Hawk Engineering Simulation Model Validation and Proposed Modifications," NASA Contractor Report 177360, July 1985.

51 Cross, J., Brilla, J., Kufeld, R., Balough, D., "The Modern Rotor Aerodynamic Limits Survey: A Report and Data Survey," NASA Technical Memorandum 4446, October 1993.

52 Bousman, W., "Aerodynamic Characteristics of SC1095 and SC1094 R8 Airfoils," NASA Technical Paper 2003-212265, December 2003.

53 Kufeld, R., Bousman, W., "Technical Note UH-60A Airloads Program Azimuth Reference Correction," *Journal of the American Helicopter Society,* April 2005.

Appendix A

UH-60 Helicopter and Rotor Properties

The UH-60 has many unique features that are outlined in any of a number of different publications [40, 42**,** 44, 45, 47, 49, 50, 51, 52, 53]. Many of its properties impart a rather unique response in terms of trim and performance. These include a rear center of gravity, a canted tail rotor, an unusual blade twist, and significant tip sweep. In order to fully model the helicopter, almost every one of these parameters must be properly represented by the simulation model. Therefore this section will detail all of the features that were used for this research effort, and it should hopefully serve as a brief but complete summary of the helicopter's parameters. Values for blade twist and tip sweep can be found in NASA UH-60 Master Database developed by Dr. Yeo for the NRTC/RITA Airloads Workshop [42].

Table A-1: General UH-60 Helicopter Properties

Helicopter Properties			
Weight	W	18300	lbs
Longitudinal CG Offset	x_{cg}	1.525	ft
Lateral CG Offset	y_{cg}	0	ft
Vertical CG Offset	z_{cg}	-5.825	ft
Lon. Stabilator offset	x_{ht}	29.925	ft
Lat. Stabilator offset	y_{ht}	0	ft
Vert. Stabilator offset	z_{ht}	-5.915	ft
Lon. Tail Rotor offset	x_{tr}	32.565	ft
Lat. Tail Rotor offset	y_{tr}	0	ft
Vert. Tail Rotor offset	z_{tr}	0.805	ft
distances with respect to the hub			

Table A-2: General UH-60 Rotor Properties

Rotor Properties			
Number of blades	Nb	4	
Radius	R	26.8	ft
Chord	C	1.73*	ft
twist	θ_{tw}	varies	
angular velocity	Ω	258	RPM
Shaft tilt	α_{Sx}	3° forward	degrees
ref. C_L_a	c_{La}	5.73	/radian
airfoil section		SC1095*	
Lock Numer	γ	6.5344	
Solidity	σ	0.0822	
cd0	c_{d0}	0.0076	
kappa	κ	1.15	
blade mass	M	7.79	slugs
e_B	e_β	1.25	ft
e_Z	e_ζ	1.25	ft
root CU		3.83	ft
	*varies spanwise		
Nondimensional Rotating Frequencies			
1st Flap		υ_β	1.04
1st Lag		υ_ζ	2.71
1st Torsion		υ_θ	4.27
Moments of Inertia (slug-ft^2)			
Flapping		I_β	1861
Lag		I_ζ	1861
torsion		I_f	0.978
inertial flap-torsion coupling		I_x	1.5147

Table A-3: Other UH-60 Properties

Horizontal Tail Properties			
Area	A	45	sq. ft.
Span	S	14	ft
Reference Lift Coefficient Slope	a_{ht}	5.3	/radian
ref drag coefficient, α=0	$c_{d\text{-}ht}$	0.04	
index angle	α_{slew}	varies	
Airfoil Section		NACA0014	
Tail Rotor Properties			
angular velocity	Ωtr	1290	RPM
Radius	R	5.5	ft
Ref. lift curve slope	atr	2π	/radian
Cant Angle	φtr	20	degrees

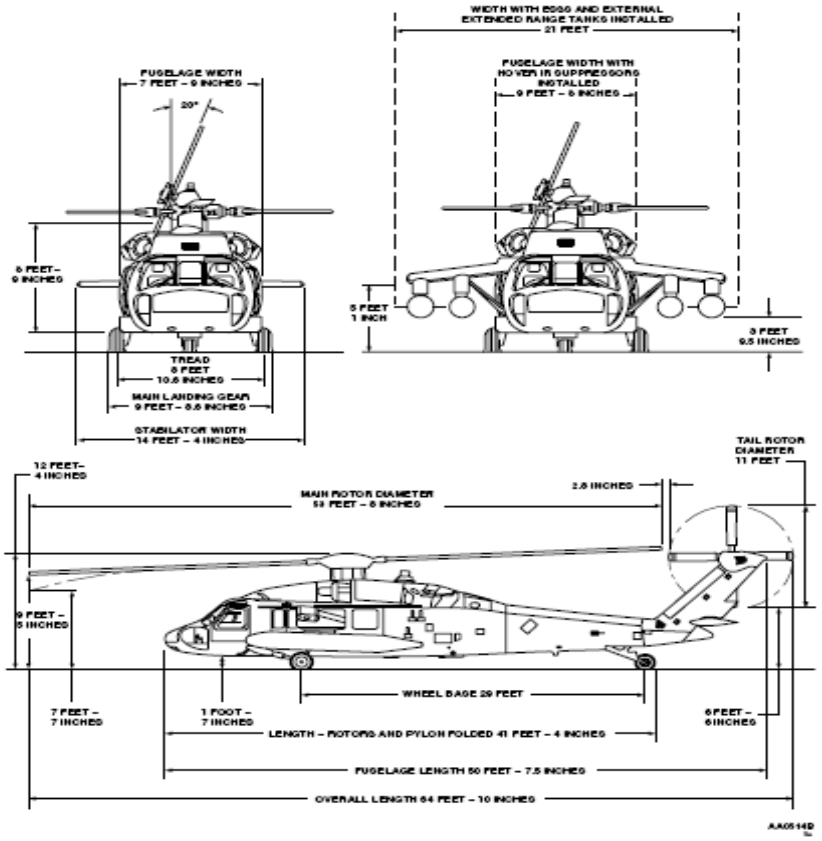

Figure A-1: UH-60 Principle Dimensions [44]

The following plot shows the characteristics of the lag damper attached at the blade root of the UH-60 as given in [42].

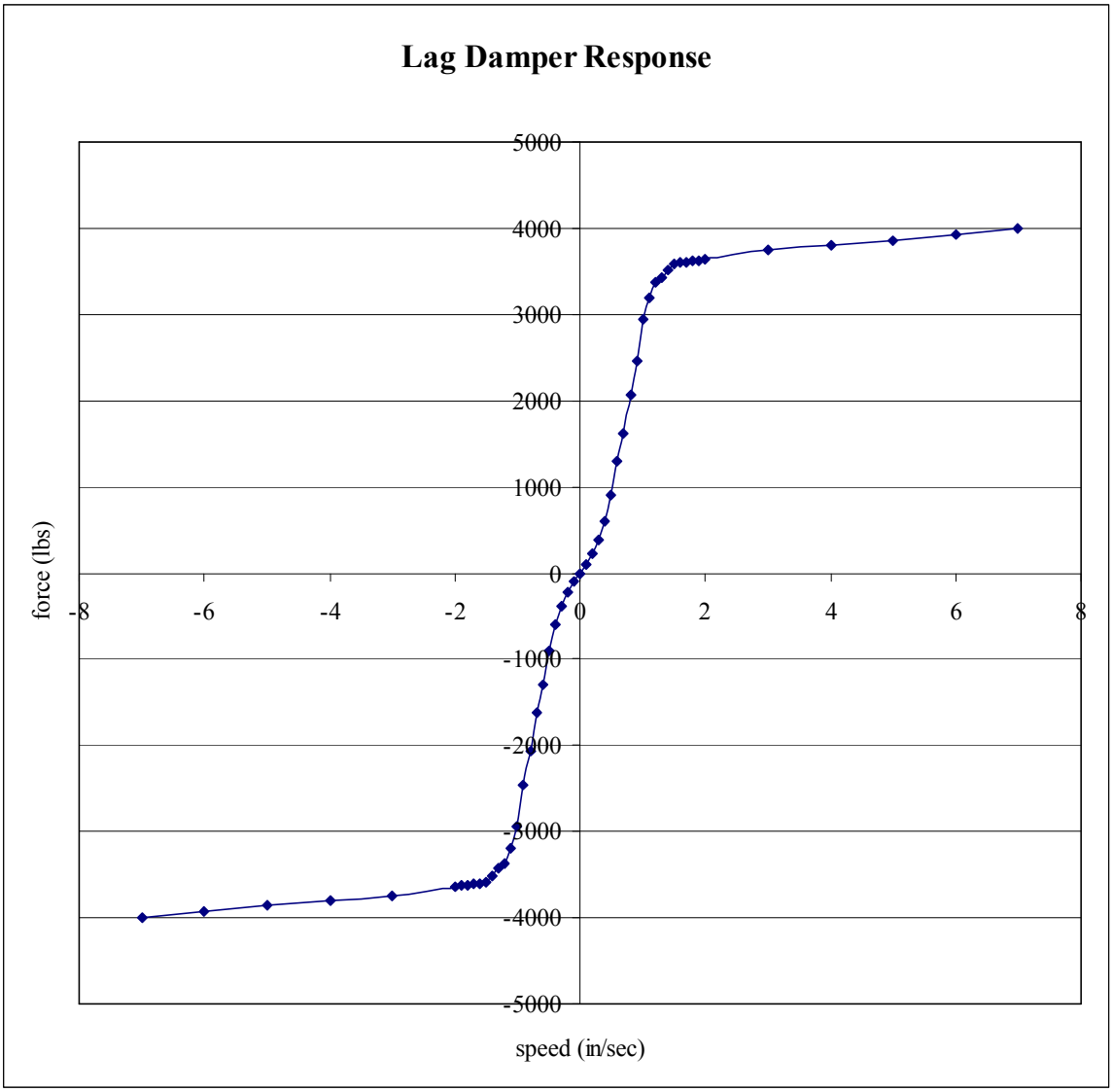

Figure A-2: UH-60 Nonlinear Lag Damper Characteristics [42]

The following plot demonstrates the deviation of the quarter chord, leading edge, and trailing edge of the airfoil from the pitch axis, based on data provided in [42]. The pitch axis is along the x-axis.

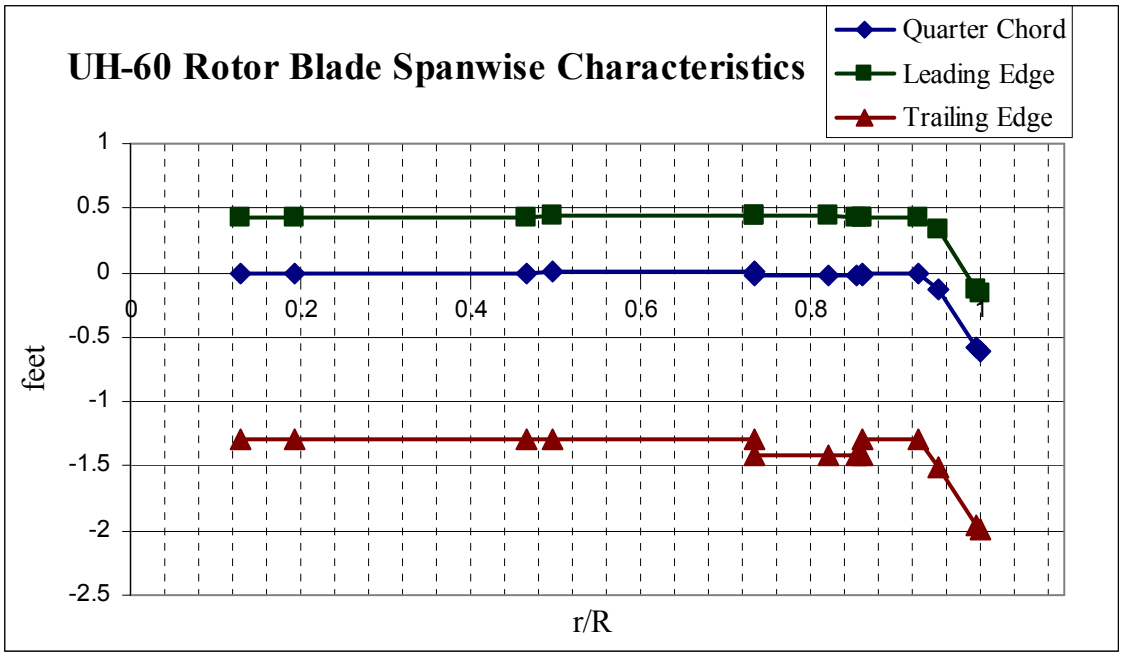

Figure A-3: UH-60 Rotor Blade Geometry [42]

Figure A-4 displays the unusual non-linear twist that the UH-60 rotor blade features as given in [42]. The x-axis represents the $\theta = 0$ location.

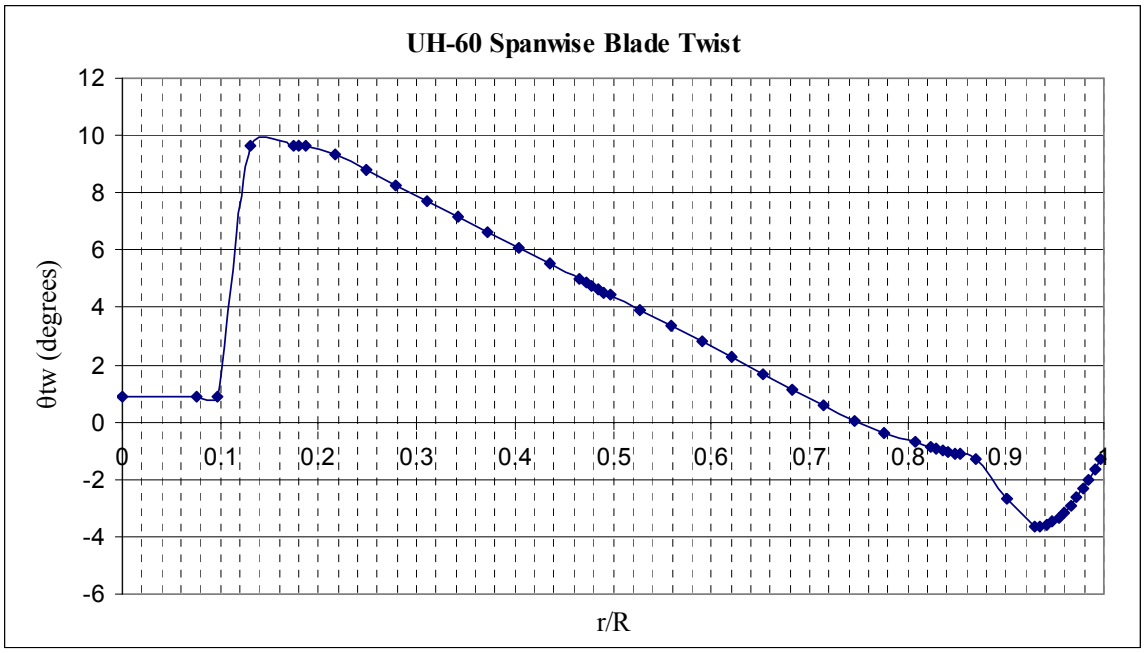

Figure A-4: UH-60 Blade twist distribution [42]

Appendix B

Calculation of Main Rotor Effects on the Horizontal Tail

The main rotor generates significant downwash through lift production. In hover, this is directed directly beneath the rotor. As forward speed increases, the downwash is directed backward and it starts to interact with the empennage. The angle that the resultant inflow begins to make with the vertical is called χ_{ht}. Due to the lack of sophisticated wake data available for horizontal tail calculations, a weighting factor was applied to the main rotor inflow angle in conjunction with the known horizontal tail slew schedule in order to align the vehicle attitude as much as possible with flight test and CAMRAD data. This weighted inflow velocity was then applied to the movable horizontal tail scheme as well. Figure B-1 displays the relative magnitude and direction of both the horizontal tail slew schedule and the main rotor inflow, χ_{ht}. Although the calculation is based solely on trial and error in order to obtain a final simulation results for vehicle attitude coincident with CAMRAD analysis, one can see from the plot that the parameter is closely aligned with the deployment of the horizontal tail—an effect which the original designers of the horizontal tail slew schedule were attempting to achieve.

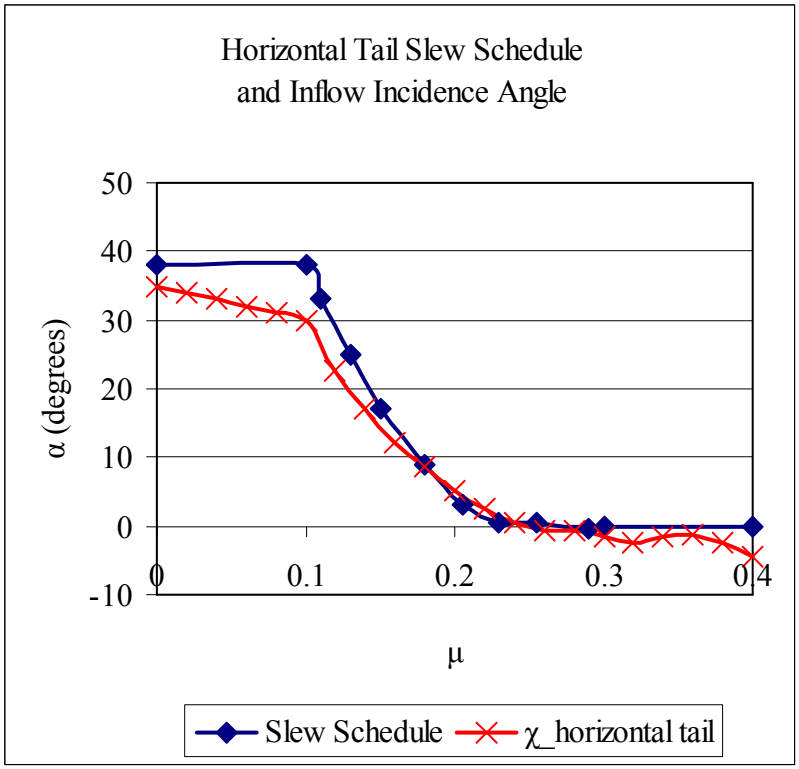

Figure B-1: Horizontal Tail Slew Angle [47] and Main Rotor Inflow Effective Angle

Appendix C

Horizontal Tail Study Plots for Pre-pitch of 20°

Although the following plots were not vital to the discussion in Section 3.7.2 , they are still useful in terms of determining overall response, and to determine the range of effectiveness for tail application. As such, they are presented here. Figure C-1 displays the control (δ_0 and δ_1) and response (β_{1c} and α_{WL}) parameters for μ=0.20. Figure C-2 displays the control (δ_0 and δ_1) and response (β_{1c} and α_{WL}) parameters for μ=0.30. Figure C-3 demonstrates the power implications of this pitch index setting with horizontal tail application. Once again, the black line and square represents the stabilator position as prescribed by the current slew schedule on the UH-60. The blue line represents the solution which provides for minimal cyclic TEF inputs (δ_1). If a third position is plotted, it corresponds to the compromise solution that is meant to moderate vehicle attitude, blade flapping, and TEF inputs simultaneously.

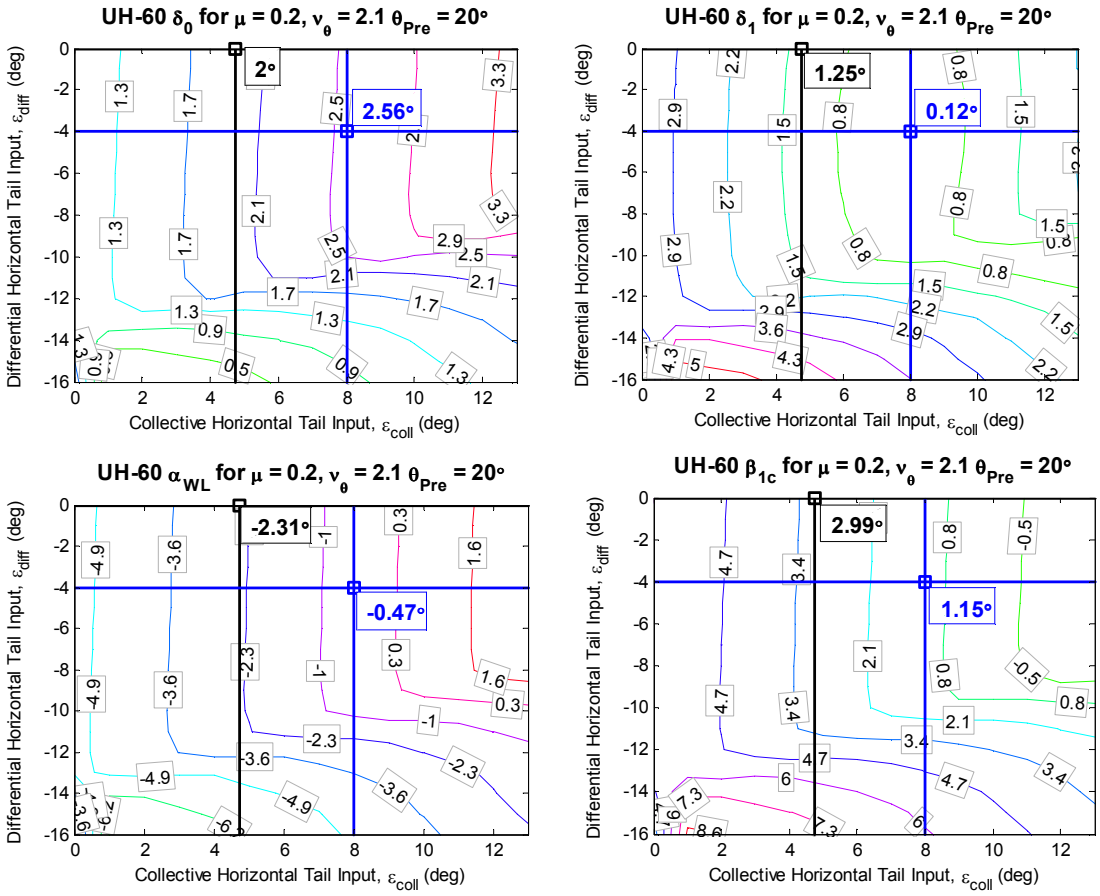

Figure C-1: Control and Response Parameters for θ_{Pre} = 20°, μ=0.20

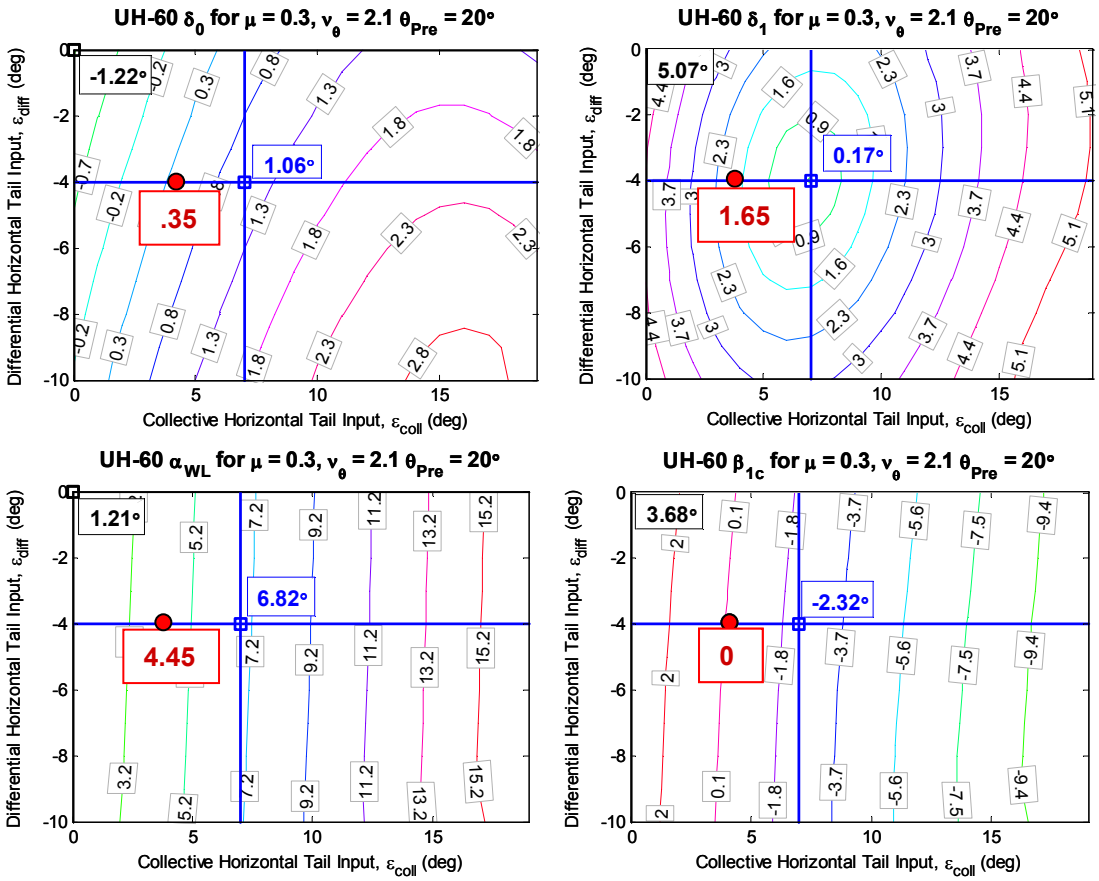

Figure C-2: Control and Response Parameters for $\theta_{Pre} = 20°$, μ=0.30

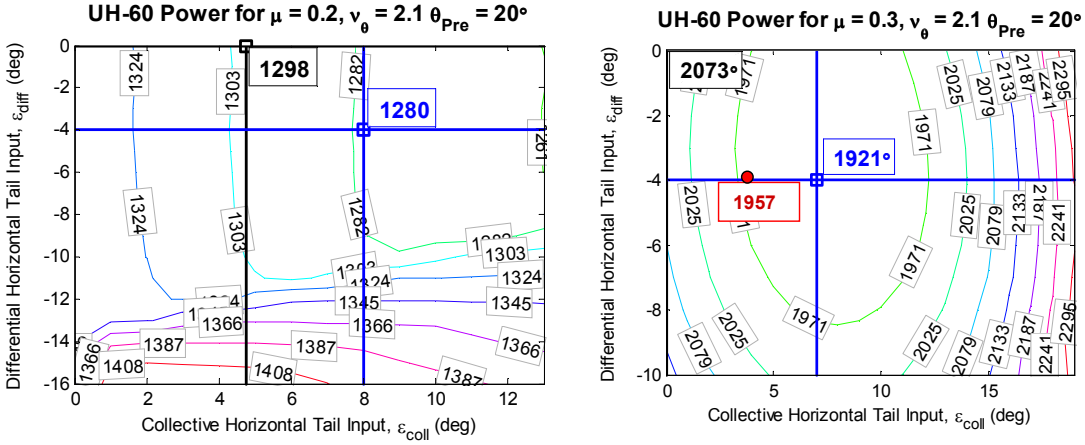

Figure C-3: Power Results for $\theta_{Pre} = 20°$

Appendix D

Horizontal Tail Study Plots for Stiffened Rotor, $v_\theta = 3.0$

Although the following plots were not vital to the discussion in Section 3.7.3 , they are still useful in terms of determining overall system response and to determine the range of effectiveness for tail application. Figure D-1 displays the control (δ_0 and δ_1) and response (β_{1c} and α_{WL}) parameters for μ=0.20.

Once again, the black line intersection represents the stabilator position as prescribed by the current slew schedule on the UH-60. The white line represents the solution which provides for minimal cyclic TEF inputs (δ_1). Since the min-δ_1 solutions offered did not adversely affect vehicle attitude and blade flapping, a compromise solution was not identified.

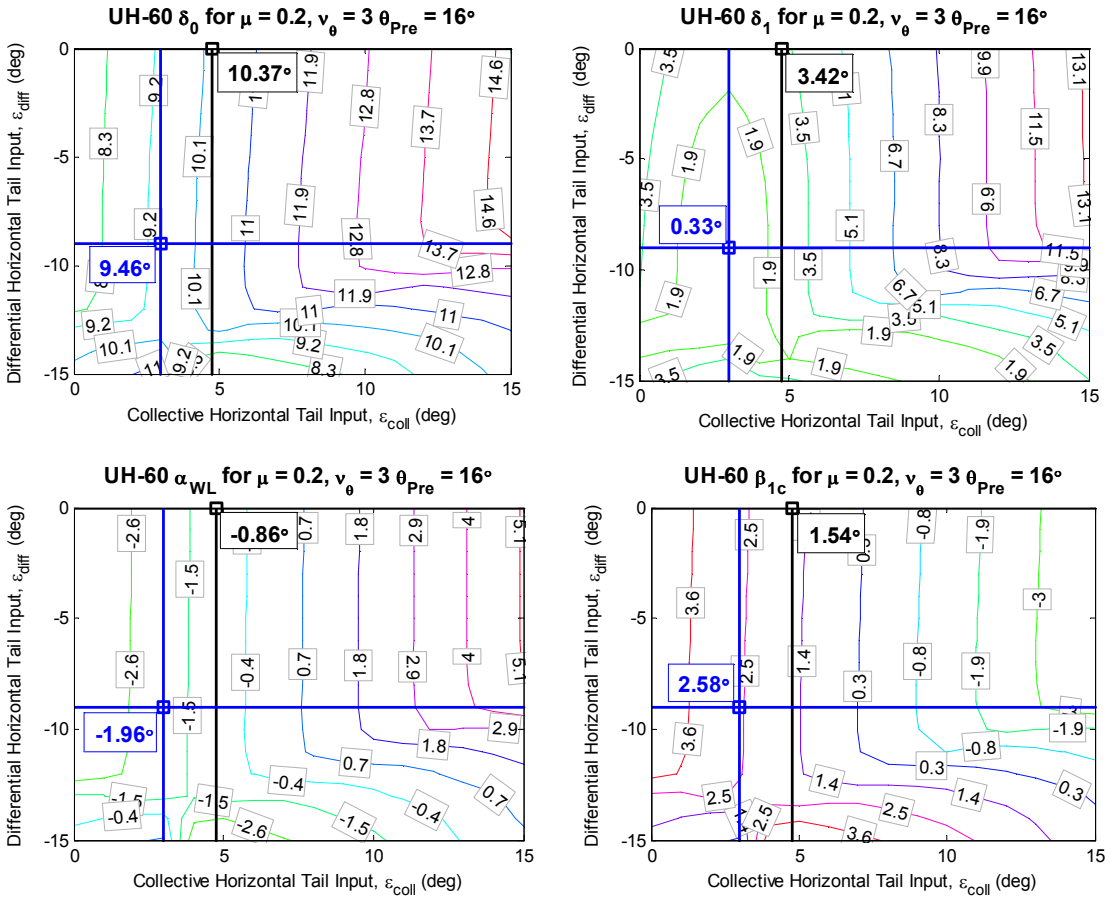

Figure D-1: Control and Response Parameters for $\nu_\theta = 3.0$, θ_{Pre}=16°, μ=0.20

The second group of plots depicted below is for μ=0.29 (124 kts). Figure D-2 displays the standard control inputs and pertinent responses.

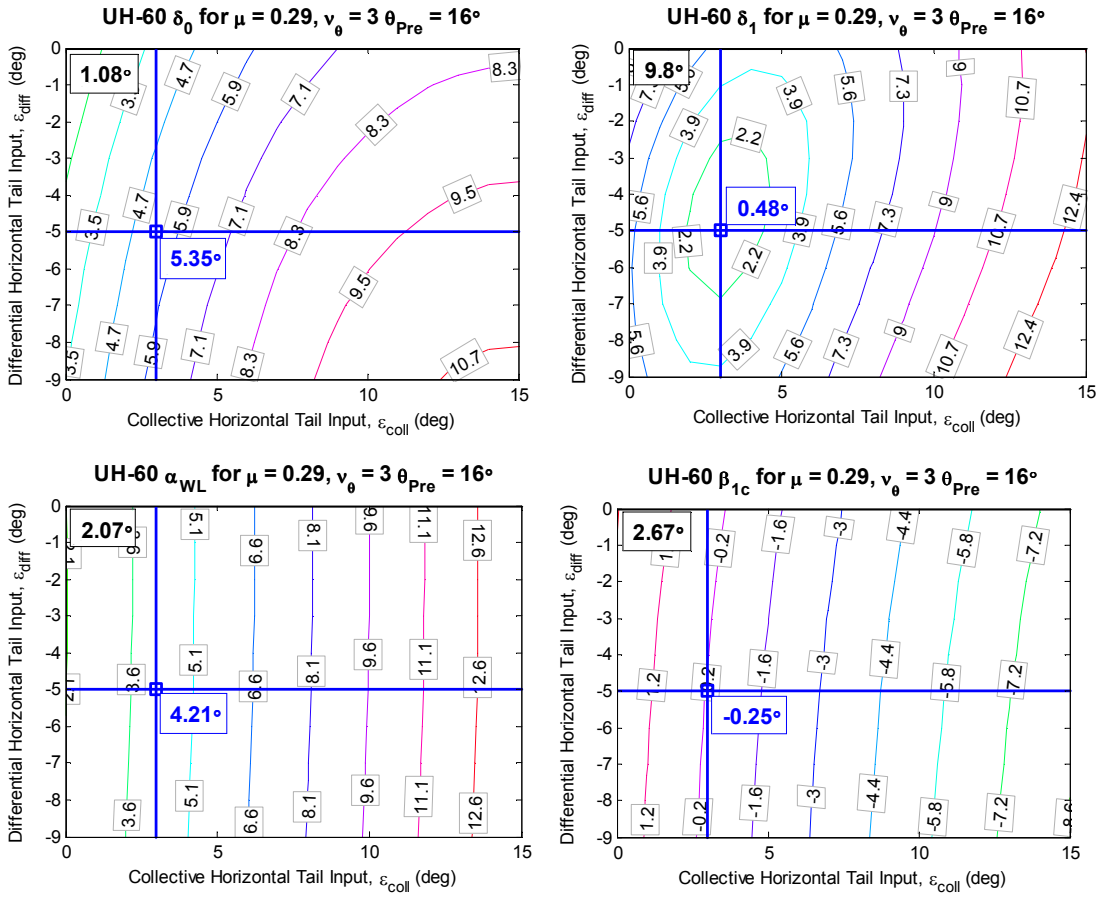

Place Figure Here

Figure D-2: Control and Response Parameters for $\nu_\theta = 3.0$, θ_{Pre}=16°, μ=0.29

Since there are many of the system responses were not directly intuitive from the normal plots, additional plots depicting blade pitch angle (Figure D-3), rotor thrust, and power are also presented (Figure D-4).

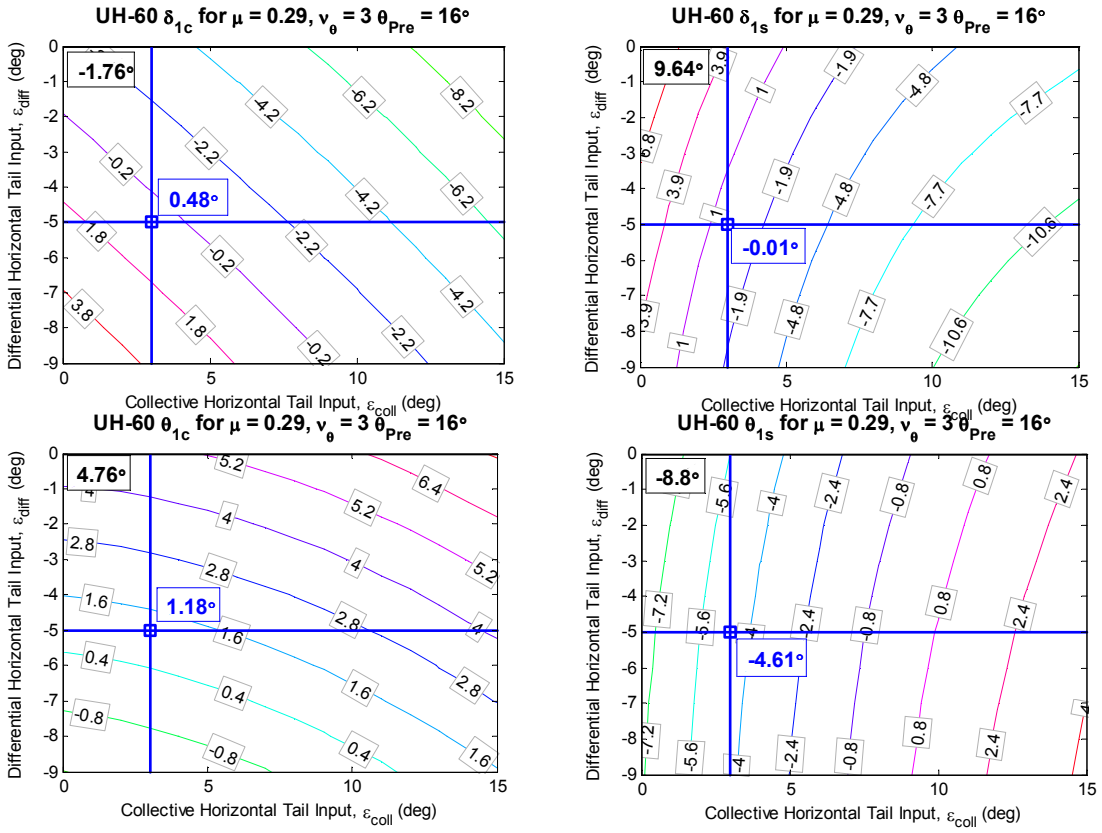

Figure D-3: Blade Pitch Response for Stiffened Rotor, $\nu_\theta = 3.0$, θ_{Pre}=16°

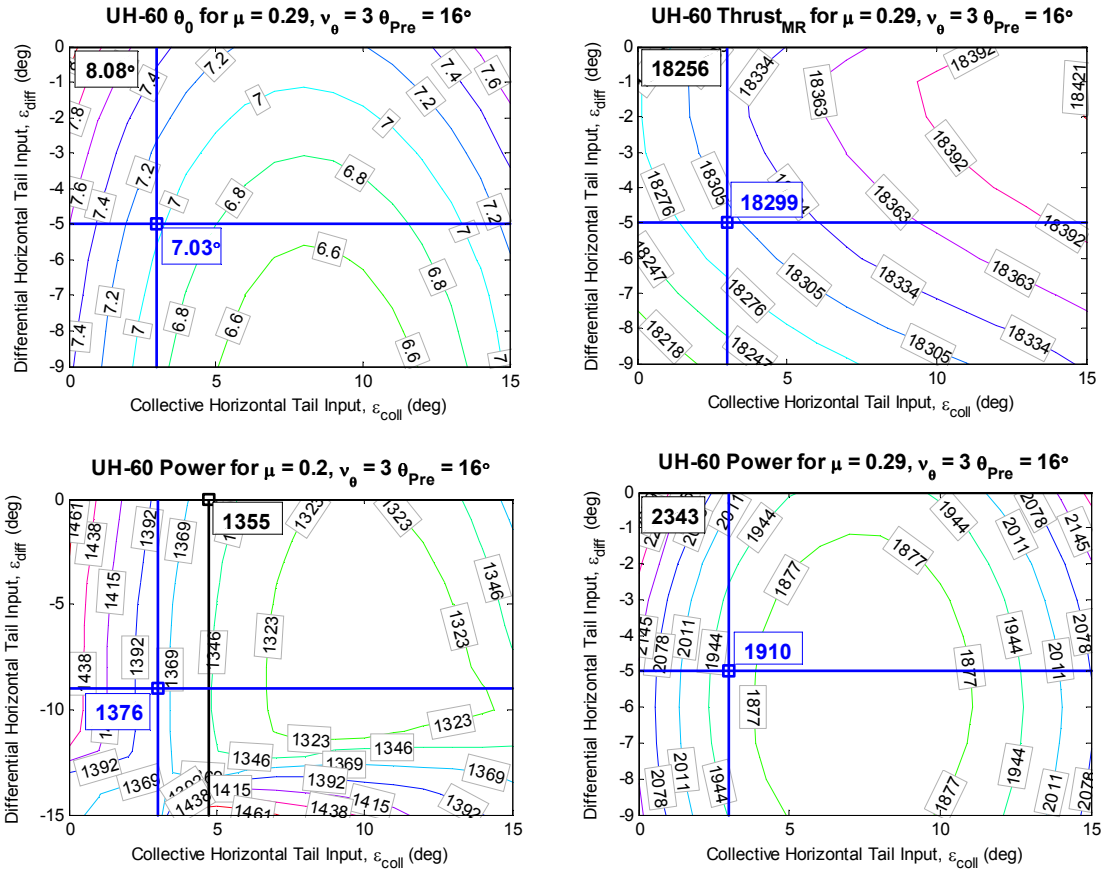

Figure D-4: Main Rotor Thrust and Power for Stiffened Rotor, $\nu_\theta = 3.0$, θ_{Pre}=16°

The values of the TEF deflections that correspond to the pre-pitch value of θ_{Pre}=16° reside outside the capability of existing actuators across all flight speeds due primarily to the large excursions in δ_0. Another value of pre-pitch may be able to move the entire solution set such that it resides within the band of actuator capability (±5°). As described in Section 3.7.3, when a value of θ_{Pre}=12° is analyzed, TEF deflections that reside inside the actuator band of capability are realized, per Figure D-5 for μ=.2 and Figure D-6 for μ=.29.

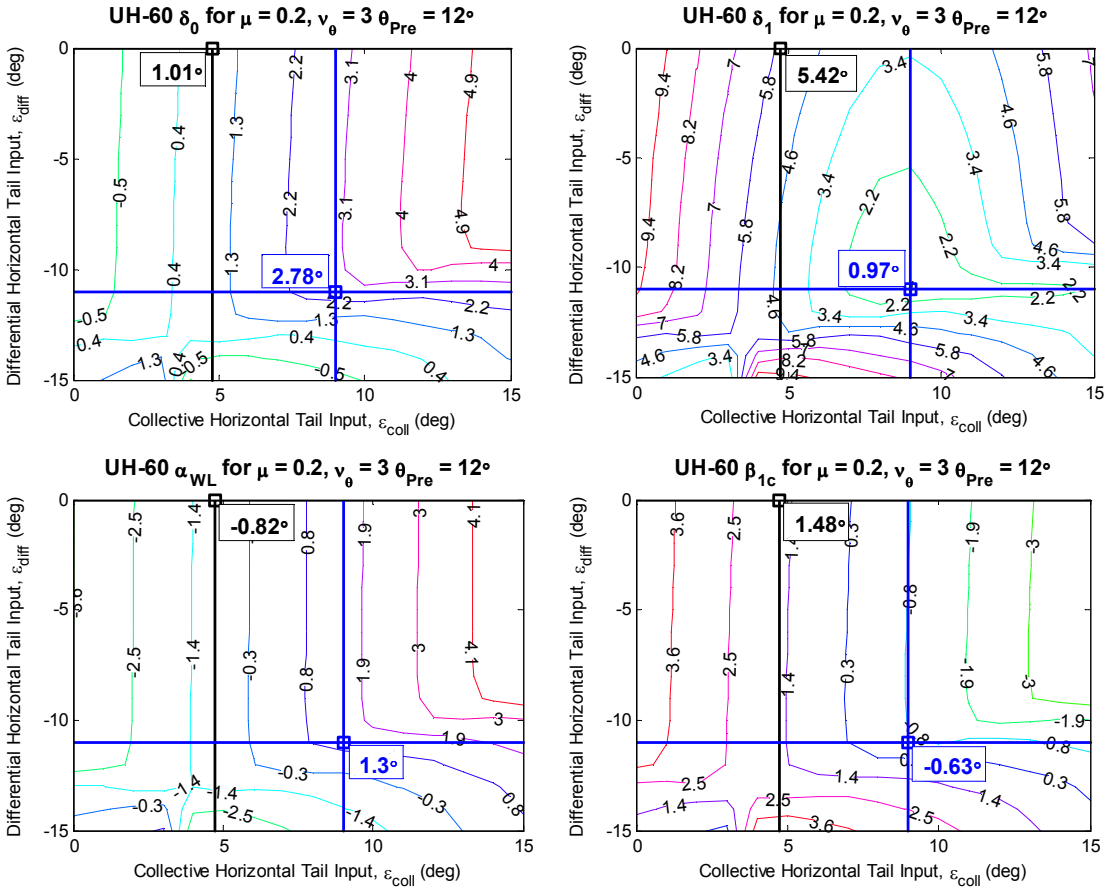

Figure D-5: Control and Response Parameters for $\nu_\theta = 3.0$, $\theta_{Pre}=12°$, $\mu=0.2$

As can be seen, the TEF range at this airspeed is quite favorable, with 1/rev deflection requirements at less than 1° and a slight positive δ0. Additionally, as has been experienced before, this configuration results in an amenable flight attitude and rotor flapping. Therefore, a compromise solution is not needed at this airspeed.

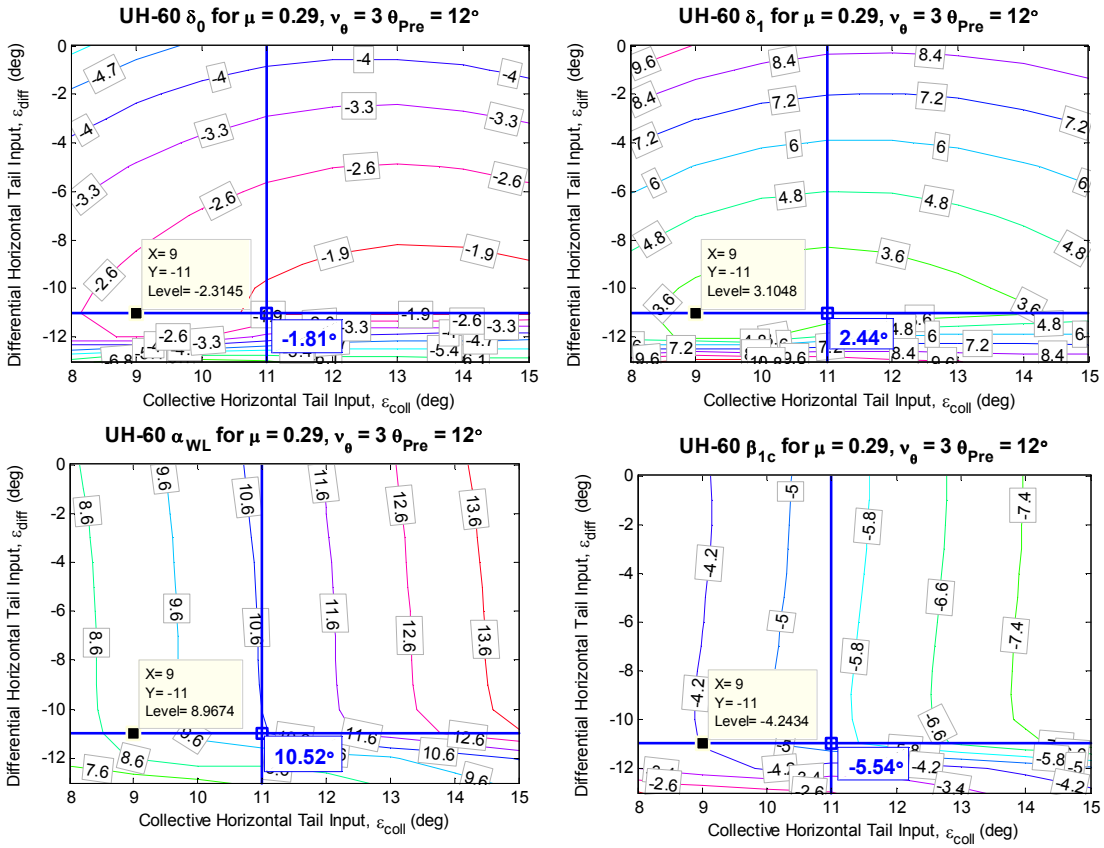

Figure D-6: Control and Response Parameters for $\dot{\nu}_\theta = 3.0$, θ_{Pre}=12°, μ=0.29

As can be seen, the lower pre-pitch value results in the movement of the TEF ranges into the region that current actuators can support. However, these solutions result in vehicle attitude and rotor blowback that is unacceptable and no real compromise solution exists that still appreciably improves the situation. A solution that slightly improves vehicle attitude is highlighted as well, but its improvements are not meaningful. As it stands, this design is not feasible.